Dissecting Transient Protein Interactions Implicated in Cardiovascular Disease: G Protein-Coupled Receptors and Cardiac Myosin-Binding Protein C

A Dissertation

SUBMITTED TO THE FACULTY OF

THE UNIVERSITY OF MINNESOTA

BY

Anja Marie Touma

IN PARTIAL FULFILLMENT OF THE REQUIREMENTS

FOR THE DEGREE OF

DOCTOR OF PHILOSOPHY

Advisor Dr. Sivaraj Sivaramakrishnan

Committee Members: Dr. Aaron Goldstrohm, Dr. Kate Adamala, Dr. Bryce Binstadt

October 2021

ACKNOWLEDGMENTS

Completion of this dissertation would not be possible without the selfless support of my best friend and life partner, Waseem, who became my husband amidst the rigors of graduate school. Thank you also to our daughter, Ilia, for making me a mom. You are a miracle. Your recent arrival has been a joyous reminder to keep life in perspective as I write this dissertation. Thank you to my own “Dr. Mom” for showing me I can be a doctor and a mom. Your enthusiasm for your job has been an inspiration. Thank you to my dad, “Mr. Science”, for introducing me to science; For starting a science fair at my elementary school and helping me make my first poster; And for teaching me about plants, insects, and showing me the stars. Thank you to my grandfather for reminding me to never stop dreaming or looking towards the future, no matter your age. Thank you to the rest of my family, including those who I’ve lost in the past two years. You have each inspired me in different ways and your memory lives on.

Thank you to my advisor, Dr. Sivaraj “Shiv” Sivaramakrishnan for your evolving support and leadership through the COVID-19 pandemic. Thank you to the scientific community and past members of the Shiv Lab for building the scientific foundation on which this research stands. Thank you also to members of the Shiv Lab, past and present, for helpful conversations, companionship, and coffee breaks. Thank you to the Biochemistry, Molecular Biology, and Biochemistry (BMBB) graduate program, as well as my committee, for your guidance, feedback, and for challenging me to become a better scientist. Finally, thank you to the MSTP (MD/PhD) program for providing me the opportunity to become a physician scientist.

DEDICATION

This work is dedicated to my daughter, Ilia. May this serve as an example to you that, with hard work, you can accomplish your dreams. You can be a doctor and a mom. You can do anything you set your mind to.

ABSTRACT

Weak, transient protein-protein interactions in the cell are being increasingly appreciated, yet characterization of these interactions presents a unique challenge. We have used protein engineering techniques, including ER/K α-helical linkers and DNA nanotechnology, to characterize G protein-coupled receptor (GPCR) and cardiac myosin-binding protein C (cMyBP-C) interactions.

The cellular environment can have a significant impact on GPCR signaling and functional selectivity. Our lab has found that GPCR interactions with non-cognate G-proteins can enhance, or 'prime', signaling through the canonical pathway. To investigate the impact of non-cognate interactions on signaling in two promiscuous Gi-coupled receptors, adenosine type 1 (A_1R) and cannabinoid type 1 (CB_1), we utilized a variation of the Systematic Protein Affinity Strength Modulation (SPASM) approach to observe the impact on downstream signaling in live cells. To the C-terminus of intact A_1R or CB_1, we tethered native G-peptides (s-pep, i-pep, and q-pep) derived from the Gα subunit of G-proteins. We found that i-pep and q-pep enhanced Gi signaling while suppressing Gq signaling. This study provides an initial model for the impact of G-peptide interactions in Gi-coupled receptors, and highlights the potential of G-peptide interactions to enhance receptor specificity.

cMyBP-C is an important regulator of cardiac muscle contraction and is commonly implicated in hypertrophic cardiomyopathy (HCM). However, the mechanism of regulation by cMyBP-C remains unclear due to experimental challenges in dissecting these weak, transient interactions. In this study we utilized a nanosurf assay, containing a synthetic β-cardiac myosin thick filament, to systematically probe cMyBP-C interactions with actin and myosin. We recapitulated inhibition of β-cardiac myosin HMM nanotube motility by C0-C2 and C1-C2 N-terminal fragments. Equivalent inhibition of an β-cardiac myosin S1

construct suggests the actin-cMyBP-C interaction dominates this inhibitory mechanism. We found that a C0-C1f fragment lacking the majority of the M-domain did not inhibit β-cardiac myosin nanotube motility, confirming the importance of the M-domain in regulatory interactions. Release of inhibition by phosphomimetic fragments further highlights the importance of the phosphorylatable serines in the regulatory M-domain. These results shed light on the mechanism of cMyBP-C and highlight the utility of the nanosurf assay for precisely manipulating and defining transient protein interactions.

TABLE OF CONTENTS

LIST OF FIGURES

LIST OF ABBREVIATIONS

Abbreviation	Name
2-AG	2-Arachidonoylglycerol
A_1R	Adenosine type 1 receptor
$A_{2A}R$	Adenosine type 2A receptor
$A_{2B}R$	Adenosine type 2B receptor
ATP	Adenosine 5'-triphosphate
β2-AR	β2-adrenergic receptor
BG	Benzyl guanine
BSA	Bovine Serum Albumin
cAMP	Cyclic adenosine monophosphate
CB_1	Cannabinoid type 1 receptor
cDNA	Complementary deoxyribonucleic acid
cMyBP-C	Cardiac myosin-binding protein C
CPA	N^6-Cyclopentyladenosine
D_1R	Dopamine receptor D1
DAG	Diacylglycerol
DMEM	Dulbecco's Modified Eagle Medium
DNA	Deoxyribonucleic acid
DTT	Dithiothreitol
EDTA	Ethylenediaminetetraacetic acid
EGTA	Egtazic acid
F-actin	Filamentous (polymeric) actin

FBS	Fetal Bovine Serum
FRET	Förster or fluorescence resonance energy transfer
GDP	Guanosine diphosphate
GFP	Green fluorescent protein
GPCR	G protein-coupled receptor
G-protein	Guanine nucleotide-binding protein
GTP	Guanosine triphosphate
HCM	Hypertrophic Cardiomyopathy
HEPES	4-(2-hydroxyethyl)-1-piperazineethanesulfonic acid
HMM	Heavy meromyosin
HTRF	Homogeneous Time Resolved Fluorescence
IP_1	Inositol monophosphate
IP_3	Inositol 1,4,5-triphosphate
LMM	Light meromyosin
M-Domain	Myosin-binding protein C motif
NECA	5'-*N*-Ethylcarboxamidoadenosine
N_t	Number of myosin heads available for interaction
NTF	Native thin filament
O.D.	Optical density
PBS	Phosphate buffered saline
PCR	Polymerase chain reaction
PIP_2	Phosphatidylinositol 4,5-bisphosphate
PKC	Protein kinase C

PLC-β	Phospholipase C beta
PMSF	Phenylmethylsulfonyl fluoride
PSB	PSB 1115
PTMs	Post-translational modifications
PTX	Pertussis toxin
RhoGEFs	Rho guanine nucleotide exchange factors
RLC	Myosin regulatory light chain
SCH	SCH 442416
SDS	Sodium dodecyl sulfate
SPASM	Systematic Protein Affinity Strength Modulation
SRX	Super-relaxed state
THC	Tetrahydrocannabinol
TPPI	Transient protein-protein interaction
TRITC	Tetramethylrhodamine
V_1R	V1 vasopressin receptor
WN	WIN 55,212-2 mesylate
WT	Wild-type

CHAPTER 1: Introduction

1.1. Investigating Transient Protein-Protein Interactions:

Despite their transient nature, many weak protein-protein interactions are essential for normal cellular function. Transient protein-protein interactions (TPPIs) are crucial to a wide range of biological processes, especially in the regulation of biochemical pathways and signaling cascades (Acuner Ozbabacan et al. 2011). Cellular processes involved in disease-related pathways are frequently regulated via transient interactions and post-translational modifications that affect these transient interactions (Perkins et al. 2010). The importance of TPPIs as drug targets is also being increasingly appreciated. Therefore, understanding TPPIs may contribute to the discovery and development of therapeutics targeting these transient interactions. However, due to their unstable nature, weak, transient protein-protein interactions can be technically more difficult to study than more stable interactions (Perkins et al. 2010). The identification and analysis of TPPIs generally requires sensitive and high-resolution experimental methods. Using protein engineering techniques, we have worked to identify and characterize diverse TPPIs, refining our understanding of TPPI properties on the structural and cellular level.

Protein complexes have different affinities tailored to their function. Many protein constituents are in equilibrium with protein complexes in the cell and exist in a dynamic association/dissociation process. The strength, or binding affinity, of the protein-protein interaction can be measured with the equilibrium dissociation constant (K_d) (Acuner Ozbabacan et al. 2011). The K_d is defined as the ratio between the rate constant of the complex dissociation reaction (k_d or k_{off}) and the association reaction (k_a or k_{on}). As the name suggests, if the K_d is high, the complex will tend to dissociate. Therefore, a high K_d

describes a weaker protein-protein interaction, while a low K_d is associated with a stronger interaction. Transient protein-protein interactions (TPPIs) are defined as those with K_ds in the millimolar (10^{-3} M) to micromolar (10^{-6} M) range (Acuner Ozbabacan et al. 2011). While they are known to be essential for cellular function, the vast majority of TPPIs are still poorly understood, particularly those with K_ds > 10^{-4} M (Vaynberg et al. 2005).

While transient protein-protein interactions comprise essential functional roles in numerous biological processes, particularly in the dynamic regulation of biological networks, the importance of TPPIs in the cell are still being increasingly recognized. There is an emerging appreciation for the existence of molecular scaffolds close to which biomolecules can be found in high concentrations, making weak interactions between proteins possible despite their low affinity (Gibson 2009). Therefore, we have yet to fully realize the significance of many TPPIs in the complex context of the cell. By definition, the frequency of protein interactions is a function of both the local concentration and the affinity of the constituent proteins for one another (Sivaramakrishnan and Spudich 2011). TPPIs are not easy to detect or investigate experimentally. Therefore, to stabilize these weak interactions and increase our ability to study these TPPIs, one method is to tether the two constituent proteins with a linker. Utilizing an encoded ER/K α-helical linker is one such approach to modify, and systematically vary, the effective concentration of two proteins.

The genetically encoded ER/K α-helical linker is a modular linker with a polypeptide motif composed of repeats of approximately four glutamic acid (E) followed by approximately four arginine (R) or lysine (K) residues. The ER/K helices are derived from *Sus scrofa* myosin VI (10 nm) or the *Trichomonas vaginalis* Kelch-motif protein family (30 nm) (Sivaramakrishnan and Spudich 2011). The single α-helix can be used to regulate the frequency of interaction between two proteins, or between a protein and a peptide at

opposite ends of the helix. Regulation of these interactions is important to gain mechanistic insight into the cellular processes governed by TPPIs and to understand opportunities for pharmacological intervention. In addition, to detect changes in concentration or affinity of interacting proteins, ER/K α-helical FRET (Förster or fluorescence resonance energy transfer) biosensors were developed (Sivaramakrishnan and Spudich 2011; Malik et al. 2013, 2017). FRET is a widely used technique which involves the transfer of energy from a donor fluorophore to an acceptor fluorophore. The efficiency of this energy transfer is inversely proportional to the distance between the fluorophores, which allows one to detect and measure changes in the distance between two interacting proteins (Zadran et al. 2012). This approach in combination with the ER/K α-helix, termed Systematic Protein Affinity Strength Modulation (SPASM) FRET sensor, includes a FRET pair for sensing the frequency of interaction of the protein-protein or protein-peptide interaction at alternate ends of an ER/K α-helical linker. Characterization of the SPASM technique has revealed that the effective concentration of a bimolecular interaction decreases with increasing ER/K α-helix length (Sivaramakrishnan and Spudich 2011).

We have used the SPASM technique in the context of protein and cellular engineering to study TPPIs in both G-protein-coupled-receptor (GPCR) signaling, as well as in the study of molecular motors and cardiac myosin binding-protein C (cMyBP-C) (Sandhu et al. 2019; Touma et al. 2020; Gupte et al. 2017, 2019; Malik et al. 2013, 2017; Semack et al. 2016). TPPIs are frequently found in signaling pathways, as they allow the cell to respond quickly to extracellular stimuli (Acuner Ozbabacan et al. 2011). For example, G-protein interactions with GPCRs are, by nature, examples of strong transient interactions. Activation of G-proteins by GPCRs is vital to the propagation of signaling pathways. In contrast to binary protein-protein interactions, the transient nature of G-

protein-GPCR interactions have evolved to balance between their specificity and promiscuity. We have therefore used SPASM FRET sensors to systematically vary interactions between GPCR and either a G-protein or a G-peptide at alternate ends of an ER/K linker flanked by donor (mCerulean) and acceptor (mCitrine) fluorophores (Sandhu et al. 2019; Touma et al. 2020; Gupte et al. 2017, 2019; Malik et al. 2013, 2017; Semack et al. 2016). SPASM is sensitive to measuring weak and dynamic protein-protein interactions in cellular conditions (Malik et al. 2013). Using this approach, we can probe the stabilization of GPCR conformations that favor interactions with the corresponding G-protein or G-peptide in live cells.

We have also utilized ER/K α-helices to engineer interactions between cardiac myosin binding-protein C (cMyBP-C) and β-cardiac myosin or thin filaments on a synthetic DNA thick filament (Sivaramakrishnan and Spudich 2011; Hariadi et al. 2015). Intrinsically disordered regions of proteins are frequent targets of transient protein binding partners and regulation by post-translational modifications (PTMs) (Acuner Ozbabacan et al. 2011). Cardiac myosin binding-protein C (cMyBP-C) is one such example, containing a less-structured M-domain which serves as a binding partner with myosin and/or actin and is regulated by PTMs including phosphorylation (Gruen and Gautel 1999; Howarth et al. 2012; S. P. Harris et al. 2004; M. Previs et al. 2015). The phosphorylation functions as a "molecular switch", disrupting cMyBP-C interactions with actin and/or myosin (Michael J. Previs et al. 2016; Shaffer, Kensler, and Harris 2009; A. Weith et al. 2012; Gruen, Prinz, and Gautel 1999; Nag et al. 2017). The transient, reversible nature of phosphorylation allows it to play a major role as a regulator in cMyBP-C interactions (Perkins et al. 2010). In order to study these transient cMyBP-C interactions, we re-created sarcomeric architecture by attaching cMyBP-C to β-cardiac myosin synthetic thick filament using ER/K helices to promote interactions with actin and/or myosin.

1.2. G Protein-Coupled Receptor Interactions with G-proteins and G-Peptides:

G-protein-coupled receptors (GPCRs) are transmembrane molecular sensors that are present in nearly all organ systems and mediate a multitude of homeostatic and pathologic processes. GPCRs are the largest family of protein drug targets, comprising upwards of 40% of pharmaceutical targets and constituting the majority of cardiovascular prescriptions (Cherezov, Abola, and Stevens 2010). This is perhaps unsurprising considering the central role GPCRs play in maintaining cardiovascular homeostasis through regulation of blood pressure, cardiovascular contractility, and chronicity (S. R. Foster et al. 2015). Drugs targeting GPCRs, including beta-blockers, are gold-standard therapy for some of the most common maladies presenting in the clinical setting. The clinical efficacy of GPCRs derives from the interaction of the transmembrane receptor with an intracellular cognate G-protein in response to extracellular ligand, which triggers downstream signaling cascades (Oldham and Hamm 2008). Despite a wealth of available pharmaceuticals, heart failure remains a leading cause of morbidity and mortality (J. Wang, Gareri, and Rockman 2018). In part, this can be attributed to poor mechanistic understanding, particularly in the unique pathologic state of heart failure. Signaling in heart failure is complicated by an altered cellular environment and differential expression of proteins, including G-proteins, all of which may have a significant impact on the patient's response to pharmacotherapy (Feldman et al. 1988; Neumann et al. 1988; Eschenhagen et al. 1992; Ping and Hammond 1994). Recent evidence from our lab suggests the non-cognate G-protein environment may have a regulatory role in 'priming' the GPCR to undergo a more efficacious interaction with cognate G-proteins (Gupte et al. 2017, 2019). With further exploration, this priming phenomenon may be harnessed to reduce receptor promiscuity and minimize off-target drug effects. Alternatively, it could be exploited in drug screening to identify biased ligands with functional selectivity for a specific G-protein.

GPCRs are integral membrane proteins and have a characteristic seven-transmembrane domain structure. The fundamental role of GPCRs is to transduce extracellular stimuli into the cell to trigger downstream signaling pathways. GPCRs are a highly diverse superfamily encoded by approximately 800 genes in the human genome (Pierce, Premont, and Lefkowitz 2002). The crystal structure of the bovine rhodopsin GPCR was the first to be resolved (Palczewski et al. 2000) followed by a structure of the β_2-adrenergic receptor (Cherezov et al. 2007). Available GPCR structures show a similar arrangement of the seven transmembrane α-helices, inserted nearly perpendicular to the plasma membrane with an inner pocket where most small-molecule ligands bind (Calebiro et al. 2021). The GPCR superfamily is subdivided into six major families based on structural similarities, including rhodopsin-like (family A), secretin-like (family B), metabotropic glutamate-like (family C), fungal mating pheromone (family D), cAMP (family E), and frizzled/smoothened (family F) receptors (Calebiro et al. 2021). G-proteins (guanine nucleotide-binding proteins) act as transducers and effectors in response to ligand binding. Heterotrimeric G-proteins are composed of Gα, Gβ, and Gγ subunits (Figure 1.1) (Pierce, Premont, and Lefkowitz 2002). The Gα subunit of G-proteins functions as a GTPase. G-proteins are generally grouped into four families based on their Gα subunit: Gs, Gi, Gq, and G12/13. Gs proteins stimulate adenylyl cyclases and cAMP production, while Gi proteins generally inhibit adenylyl cyclases and cAMP (Figure 1.2) (Calebiro et al. 2021). Gq proteins activate PLC-β, which cleaves the membrane phospholipid phosphatidylinositol 4,5-bisphosphate (PIP_2) into inositol 1,4,5-triphosphate (IP_3) and diacylglycerol (DAG). IP_3 then stimulates the release of Ca^{2+} from intracellular stores. Ca^{2+} and DAG then together activate protein kinase C (PKC). Lastly, the family of G12/13 proteins stimulates Rho guanine nucleotide exchange factors (RhoGEFs) (Pierce, Premont, and Lefkowitz 2002).

GPCR signal transduction begins when a ligand binds the GPCR. This promotes a conformational change and reorganization of the cytoplasmic region, inducing coupling with the G-protein. A ternary complex is formed between the receptor, ligand, and G-protein (Figure 1.1a) (Pierce, Premont, and Lefkowitz 2002). The interaction of the G-protein with the activated receptor accelerates the dissociation of GDP from the inactive G-protein and promotes the exchange for GTP, providing energy for dissociation of the α-subunit from the βγ subunits (Figure 1.1b) (Calebiro et al. 2021). The active α-subunit, as well as the βγ subunits, interact with effector proteins which amplify the signal through the production of signal transduction molecules (i.e. cAMP, IP_3) that bind kinases, initiate phosphorylation events, and ultimately regulate target enzymes and resulting physiological

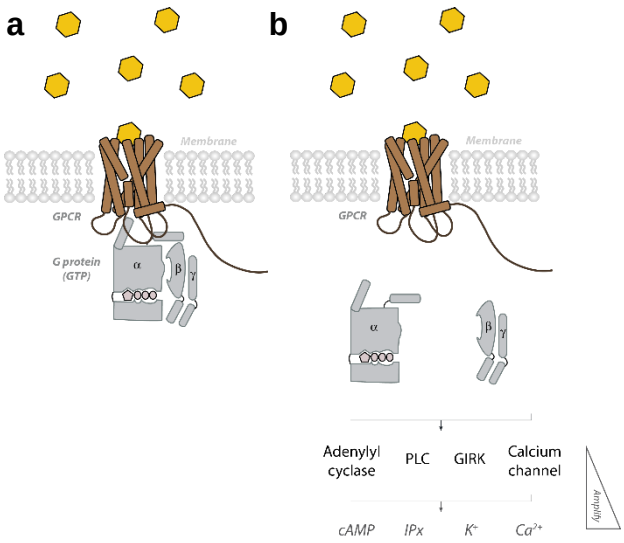

Figure 1.1. GPCR Signal Transduction. ***a,*** Ligand binding to the GPCR induces coupling with the heterotrimeric G-protein containing Gα, Gβ, and Gγ subunits. ***b,*** Upon dissociation from the GPCR, the active α-subunit, as well as the βγ subunits, amplify the signal through interaction with effector proteins, producing signaling molecules (cAMP, IP_3, etc.).

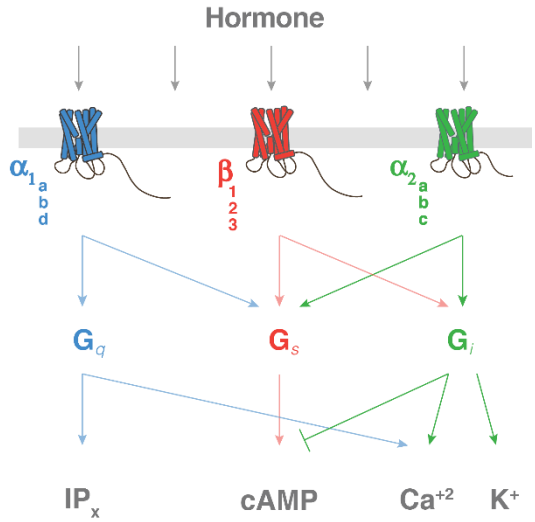

Figure 1.2. Multiplicity of GPCR Signaling. The Gq (canonical α_1) pathway stimulates the production of inositol phosphate (IP_3). The Gs (canonical β-adrenergic) pathway stimulates adenylyl cyclases and cAMP production. The Gi (canonical α_2) pathway inhibits adenylyl cyclases and cAMP. Multiplicity of GPCR signaling is common, where a given receptor can activate multiple different G-protein pathways in a ligand-dependent manner.

responses in the cell. Intrinsic GTPase activity hydrolyzes the GTP to GDP, converting it back to an inactive conformation that dissociates from the effector protein and reassociates with the βγ subunits (Pierce, Premont, and Lefkowitz 2002).

GPCRs have canonical signaling pathways with cognate G-proteins through which they typically couple. However, multiplicity of GPCR signaling (Figure 1.2) is common and promiscuous receptors can activate multiple different G-proteins in a ligand-dependent manner, resulting in a range of outputs. This concept is known as functional selectivity (also known as biased signaling) (Hermans 2003). While GPCRs have been traditionally viewed as linear “on-off” switches, it has become increasingly clear that signaling through GPCRs is complex. Rather, GPCRs should be viewed as highly dynamic systems that exist in a multitude of functionally distinct conformations with a range of outgoing signals (Manglik and Kobilka 2014). Ligands stabilize different subsets of structural conformations, eliciting diverse functional responses (diverse secondary messengers and/or potency) from a given receptor. As a result of this functional selectivity, GPCRs can activate distinct G-proteins or G-protein-independent pathways in a ligand-dependent manner (Hermans 2003). This characteristic of GPCR signaling has been proposed to be the basis for the development of more selective pharmaceuticals. Functional selectivity is also context-dependent, meaning the environment of the cell can influence signaling pathways, either through downstream or proximal effects (Calebiro et al. 2021).

Our lab recently discovered that the G-protein environment can have synergistic effects on the receptor (Gupte et al. 2017). As of yet, the functional consequences of GPCR interactions with non-cognate G-proteins has remained underappreciated since these interactions often do not precipitate G-protein activation (Qin et al. 2011). Further, the presence of a single cognate G-protein binding site on the GPCR suggests non-cognate interactions may competitively suppress canonical signaling. However, in

contrast, what we have observed is that some non-canonical G-protein interactions actually have the capability to influence or enhance signaling through the canonical pathway, a concept which we have termed “GPCR priming” (Gupte et al. 2017, 2019; Touma et al. 2020). Through GPCR priming, individual GPCR-G-protein interactions can reinforce each other to enhance signaling through canonical downstream second messengers. We had previously investigated this phenomenon in Gs-coupled β2-adrenergic (β2-AR) and dopamine (D_1R) receptors, as well as the Gq-coupled V1 vasopressin receptor (V_1R) (Gupte et al. 2017). We have found this priming phenomenon to be receptor-specific. Therefore, we were interested to investigate this phenomenon in Gi-coupled receptors. To examine the influence of the G-protein environment in the promiscuous Gi-coupled adenosine type 1 (A_1R) and cannabinoid type 1 (CB_1) receptors, we utilized a variation of the SPASM technique.

Efforts to link GPCR-G-protein interactions with downstream signaling outcomes in live cells has been difficult due to a range of cellular factors that influence GPCR signaling including variations in expression levels and abundance, stoichiometry, and spatial localization of GPCRs and G-proteins (Hermans 2003). To overcome these limitations, we utilized a variation of the SPASM approach (Figure 1.3) to express receptor-G-protein peptide fusions (Malik et al. 2017; Touma et al. 2020). This provides control over the effective concentration of the interaction and 1:1 stoichiometry inherent in the fusion

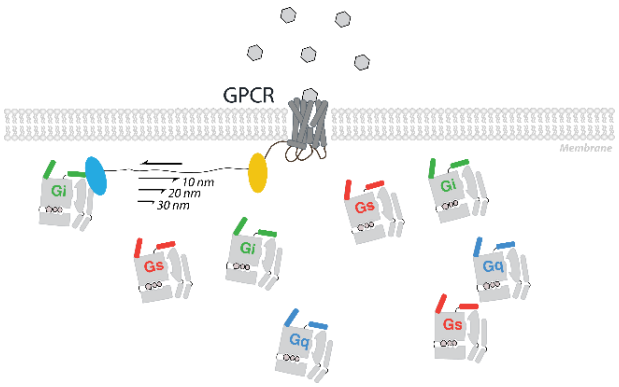

Figure 1.3. Systematic Protein Affinity Strength Modulation (SPASM) Sensor Diagram. Gi protein shown tethered to a GPCR by an ER/K linker (10-30 nm) flanked by mCitrine and mCerulean fluorophores. The sensor localizes to the plasma membrane and can be used to investigate impacts of the G-protein environment.

construct. Importantly, these sensors localize to the plasma membrane and are functional in live HEK293T cells, which allows us to modulate canonical signaling pathways in the cell (Malik et al. 2013). A native G-protein peptide is tethered to the C-terminus of the intact GPCR by an ER/K α-helical linker flanked by fluorophores used in this study to monitor expression and integrity in live cells. G-protein peptides, s-pep, i-pep, and q-pep, are derived from the C-terminal α5 helix of their respective Gα subunits, Gαs, Gαi, and Gαq.

The Gα C-terminus, constituting the G-peptides, has been well characterized and is a critical component of the GPCR-G-protein binding interface, comprising roughly 76% of the atoms making contact at this interface in the β2-AR-Gs crystal structure (Rasmussen et al. 2011). The Gα C-terminus inserts itself into a cytosolic groove formed in the active GPCR (Rasmussen et al. 2011). The C-terminal α5 helix is also a key determinant in G-protein selectivity by GPCRs. The last three residues of this C-terminus have been shown to be particularly important for G-protein selectivity (Conklin et al. 1993). The Gα C-terminus has been found to be both essential and sufficient for G-protein activation by the GPCR (Hamm et al. 1988; Lambright et al. 1994; Rasenick et al. 1994; Yang et al. 1999; Oldham and Hamm 2008). We have previously shown that the C-terminus of either the Gαs or Gαq subunit is sufficient to enhance Gα subunit activation, cAMP levels, and signaling potency, suggesting an altered GPCR conformation (Gupte et al. 2017). However, the C-terminal α5 G-peptide itself is not activated and does not trigger downstream signaling.

While these G-protein peptides constitute the majority of the G-protein interaction with the GPCR, these peptides do not have GTPase activity or bind downstream effectors. This approach allows us to study the effects of the G-protein environment on the canonical GPCR signaling pathways in the cell by isolating the impacts of G-peptides on

endogenous G-protein interactions and downstream signaling. To quantify impacts on downstream signaling, cAMP and IP_1 assays can be used. For Gs and Gi pathways, we use a bioluminescence-based cAMP assay. The Gs pathway enhances cAMP, while cAMP production is inhibited by signaling through Gi (Calebiro et al. 2021). When a decrease in cAMP is observed, to differentiate between a reduction in Gs signaling and enhancement in Gi activity, one can use pertussis toxin (PTX). PTX covalently modifies Gi and prevents its coupling to the GPCR (Calebiro et al. 2021). To characterize impacts on downstream signaling through the Gq pathway, the IP_1 assay can be used. This assay measures the accumulation of IP_1 with an HTRF assay, since the IP_3 lifetime within the cell is very short (less than 30 seconds) before it is transformed into IP_2 and IP_1. Using these downstream assays, we find second messenger signaling is enhanced for select GPCR-G-protein pairs in a receptor-specific manner (Gupte et al. 2017; Touma et al. 2020).

1.3. β-Cardiac Myosin and Cardiac Myosin-Binding Protein C:

Hypertrophic cardiomyopathy (HCM) is the most common inherited cardiovascular disease, affecting one in 500 people worldwide, and is the leading cause of sudden cardiac death in people under 30 (Maron et al. 1995). Clinically, HCM is characterized by a thickened ventricular wall and hyper-contractility, resulting from mutations in sarcomeric proteins. Over 300 HCM mutations have been identified in the *MYH7* gene encoding β-cardiac myosin, which is perhaps unsurprising due to the high degree of coordination required to convert chemical energy from ATP to the mechanical force-generating lever arm swing necessary to propel actin filaments. An additional 350 HCM mutations have been identified in the *MYBPC3* gene encoding cardiac myosin-binding protein C (cMyBP-

C) (Spudich 2015; Carrier et al. 2015), an important regulatory protein in the sarcomere. However, little is known about the effects of these mutations on the muscle sarcomere. Despite much interest in mapping the function of these mutations for pharmaceutical development, existing single molecule and *in-vitro* studies have yielded inconsistent results due to limitations in modeling protein ensembles as they exist in the muscle sarcomere (Witjas-Paalberends et al. 2014; Tyska et al. 2000; Lowey et al. 2008; Palmiter et al. 2000; Nag et al. 2016). Consequently, current therapies for HCM have remained largely empiric, alleviating symptoms but failing to treat or modulate the underlying disease mechanism. To bridge the gap between single molecule and muscle fiber studies we used DNA nanotechnology to reconstitute a DNA nanotube 'thick filament'. The synthetic thick filament transforms our ability to characterize how these mutations impact force production by ensembles of myosin motors.

The sarcomere contains a near-crystalline array of dimeric myosin at 14.3 nm intervals assembled into thick filaments which interdigitate with thin filaments and are responsible for the force production in muscle (Kachur and Pilgrim 2008) (Figure 1.4a). Each myosin molecule has an S1 motor domain containing a nucleotide binding pocket, actin-binding cleft, and a light chain binding region that acts as a swinging lever arm (Figure 1.5). When proteolytically digested by chymotrypsin

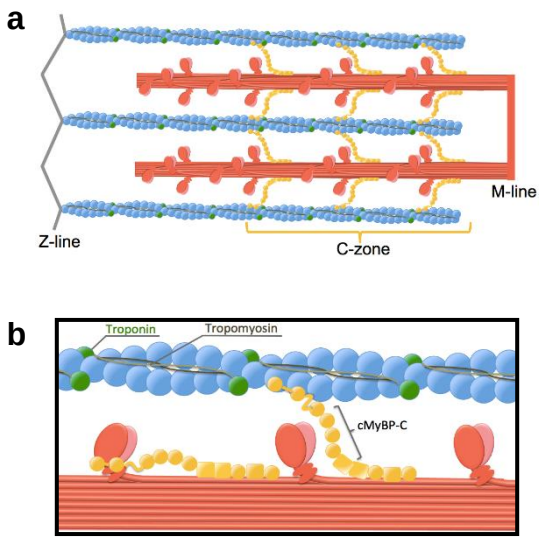

Figure 1.4. Sarcomere Architecture and Models of cMyBP-C Interactions. ***a,*** C-zone of the thick filament in relation to the thin filament. ***b,*** Representation of cMyBP-C anchored to the myosin-containing thick filament by the C-terminus. The cMyBP-C N-terminus interacts with the myosin S1, S2, and/or light chain (*left*). Alternatively (*right*) the cMyBP-C N-terminus can interact with actin.

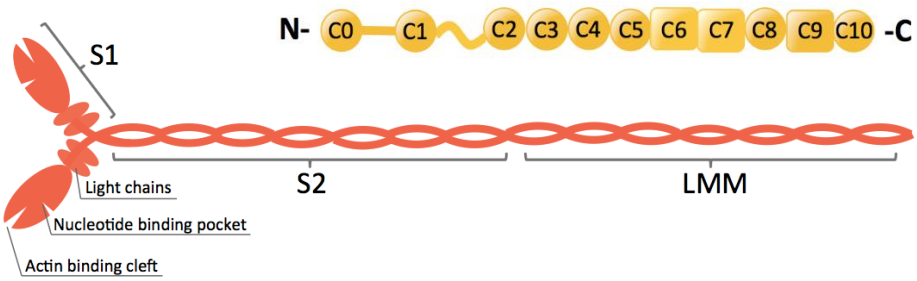

Figure 1.5. Domain Organization of Myosin and cMyBP-C. cMyBP-C (*top*) showing domains C0-C10 from N- to C-terminus. Myosin (*bottom*) features labeled; S1 and S2 domains together compose the myosin HMM.

in the tail region, the myosin molecule yields two fragments: heavy meromyosin (HMM), composed of S1 and S2 subfragments, and light meromyosin (LMM) (Trivedi et al. 2018). A long coiled-coil tail, composed of myosin S2 and LMM regions, is important for incorporation into the native thick filament (Ojima et al. 2015). To generate force, myosin undergoes a mechanochemical cycle wherein ATP hydrolysis is coupled to a power stroke which displaces the thin filament relative to the thick filament (Geeves 2016). In the heart, this cycle begins upon calcium release from the sarcoplasmic reticulum. The calcium binds troponin, displacing tropomyosin and exposing myosin binding sites on the thin filament. The precise structure of the thick filament, coupled with the complex mechanochemical coordination within the myosin molecule, makes this system vulnerable to mutations. β-cardiac myosin is the predominant ventricular myosin isoform in larger mammals, including humans, and is implicated in several inherited cardiovascular diseases including HCM (Machackova, Barta, and Dhalla 2006).

While β-cardiac myosin is commonly implicated in HCM, the largest portion of HCM mutations actually exists in *MYBPC3*, encoding cMyBP-C (Carrier et al. 2015). The cMyBP-C is located in the C-zone of the sarcomere at a ratio of approximately one cMyBP-C to three myosin molecules (Trivedi et al. 2018) (Figure 1.4a). cMyBP-C is a long multi-modular structural protein composed of 11 subdomains labeled C0-C10 from

the N- to C-terminus (Schlossarek, Mearini, and Carrier 2011) (Figure 1.5). The N-terminus is thought to interact with both actin and the myosin S2 domain, while the C-terminus of cMyBP-C is thought to primarily bind to the thick filament backbone (A. Weith et al. 2012) (Figure 1.4b). The region between the C1 and C2 domains is called the M-domain and is thought to be the primary site of interaction for myosin and/or actin. The M-domain contains four serines that are thought to be phosphorylated hierarchically to disrupt cMyBP-C interactions with actin filaments (Michael J. Previs et al. 2016; Shaffer, Kensler, and Harris 2009; A. Weith et al. 2012) or myosin (Gruen, Prinz, and Gautel 1999; Nag et al. 2017). Phosphorylation of the M-domain may be a regulatory mechanism to control the number of active myosin heads in response to β-adrenergic stimulation (Nag et al. 2017). Upwards of 50-60% of β-cardiac myosin exists in a super-relaxed (SRX) folded-back state associated with slow ATP turnover, wherein the proximal myosin S2 tail engages with the myosin S1 motor domain (Hooijman, Stewart, and Cooke 2011; Nag et al. 2017; Nag and Trivedi 2021). It has been hypothesized that cMyBP-C interactions with myosin may stabilize this SRX state. In contrast, cMyBP-C phosphorylation may disrupt this interaction, thereby recruiting active heads from the reserved pool of sequestered SRX myosin and increasing the number of actively cycling myosin heads (Nag et al. 2017; McNamara, Singh, and Sadayappan 2019). Thus cMyBP-C has the capacity to fine-tune muscle contraction, reducing the number of myosin heads available for interaction with actin (N_t) and maintaining an equilibrium between active and inactive heads. This has been hypothesized as a mechanism that is disrupted by HCM mutations in myosin or cMyBP-C, leading to destabilization of the myosin SRX with a resulting increase in Nt and hyper-contractility (Nag et al. 2017).

While it is clear cMyBP-C plays an important role in the pathological phenotype of HCM, the baseline physiological mechanism of contractile regulation by cMyBP-C is

complex and remains largely unknown. cMyBP-C has been shown to buffer the effects of calcium in the sarcomere. At low calcium, it can act as a “gas pedal”, increasing thin filament activation and calcium sensitivity (Michael J. Previs et al. 2016; Mun et al. 2014; M.J. Previs et al. 2012). This “gas pedal” effect has been demonstrated experimentally with a native thick filament motility assay, where actin filament motility is observed in the C-zone of the sarcomere despite low calcium conditions (pCa 9) (M.J. Previs et al. 2012). Activation of the thin filament by cMyBP-C at low calcium was also observed in a negative stain electron microscopy reconstruction. Even under low calcium conditions, the presence of the cMyBP-C N-terminal fragment, C0-C2, appeared to shift the tropomyosin to the high calcium position (Mun et al. 2014). In contrast to the “gas pedal” effects at low calcium, at high calcium cMyBP-C can act as a “brake pedal”, decreasing the velocity of contraction. This “brake pedal” effect is thought to be due to cMyBP-C N-terminus interactions with either myosin or actin, tethering the thick and thin filaments (Figure 1.4b). Therefore it has been hypothesized that loss of wild-type cMyBP-C in HCM may result in loss of this high calcium “brake pedal”, leading to hypercontractility (Michael J. Previs, Michalek, and Warshaw 2014). In order to understand the impacts of HCM on cMyBP-C, we must first understand the role of cMyBP-C in contractile regulation, and through which binding partners (actin and/or myosin) it accomplishes this regulation. To investigate these weak, transient interactions of cMyBP-C, we utilized ER/K linkers with β-cardiac myosin synthetic thick filaments to mimic the interactions of cMyBP-C in the native sarcomere.

Multi-motor assays, such as the *in-vitro* motility assay, have been used to study motor speed and processivity, however the assay has been limited by variability attributed to heterogeneity of the motility surface and motor density. Likewise, single molecule experiments do not capture the unique properties of motor ensembles (S Walcott, Warshaw, and Debold 2012). For instance, a single myosin will experience resistance from other myosin cross-bridges simultaneously bound to actin, resulting in inter-motor interference and altered function (Hariadi et al. 2015). It is therefore essential to study motors in the context of an ensemble to gain a more accurate understanding for the functional properties of myosin within the thick filament. Therefore, we built a synthetic nanotube that would allow systematic dissection of sarcomeric features, yielding a more accurate way to assess ensemble motor function in health and disease (Figure 1.6). We previously used the DNA nanotube assay to characterize ensembles of myosin V, myosin VI, and β-cardiac myosin S1 (Hariadi and Sommese, 2015). However we had not yet utilized DNA nanotubes to characterize β-cardiac myosin HMM or interactions with cMyBP-C fragments. The length (~5 μm) and diameter (~9 nm) of the synthetic nanotube (Figure 1.6) allows us to probe interactions on the scale of a native sarcomere (~ 2 μm long, 6-13 nm in diameter). We can then use the synthetic thick

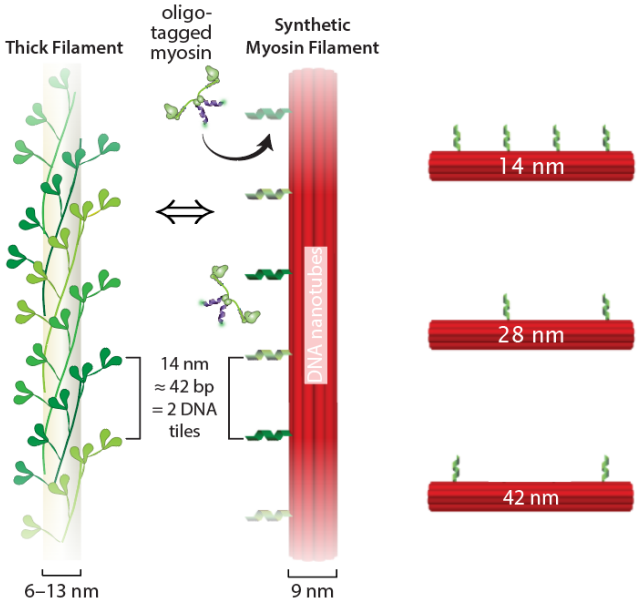

Figure 1.6. Synthetic Nanotube Thick Filament. Protein attachment specificity is achieved by SNAP tags on proteins labeling with unique oligo strands that anneal to oligo handles on the nanotubes (*center*) every 14 nm which corresponds to the 14.3 nm vertical spacing between two adjacent myosin molecules on the native filament (*left*). Inter-protein spacing can be increased to 28 or 42 nm (*right*).

filament to perform gliding assays with precisely controlled motor populations. Nanotubes are attached to a nitrocellulose-coated motility surface in a flow cell by BSA-biotin-neutravidin. Synthetic thick filaments are then decorated with β-cardiac myosin, with or without interdigitated cMyBP-C. Assays are then performed using labeled actin or native thin filaments containing troponin and tropomyosin (NTFs). The velocity by which the motor population propels actin filaments or NTFs serves as a measure of ensemble function. This key method allows us probe protein interactions by precisely controlling protein spacing (14, 28, or 42 nm; Figure 1.6, *right*), type, and stoichiometry on the nanotubes. We can therefore use DNA nanotubes to tease apart individual components of the sarcomere while simultaneously assessing impacts on the overall ensemble. Through this approach, the field will gain much needed insight into the mechanism of cMyBP-C, as well as how HCM may be impacting motor ensembles. This will also inform future pharmaceutical strategies and may support other potential pharmaceutical targets including cMyBP-C interactions.

CHAPTER 2: Allosteric modulation of Adenosine A1 and Cannabinoid 1 Receptor Signaling by G-Peptides

Statement of author contributions: *Anja M. Touma (A.T.) and Rabia U. Malik (R.M.) contributed equally to the work presented in the following chapter. AT. and R.M. both participated in research design, conducted experiments, and performed data analysis. R.M. generated initial drafts for Figures 2.1, 2.4, 2.5, and 2.7. Anja M. Touma wrote the following manuscript.*

2.1. Introduction**:**

G protein coupled receptors (GPCRs) have been the most successful class of drug targets in clinical medicine, due in part to their widespread distribution and important roles in physiology (Insel et al. 2007). The pharmacological success of GPCRs derives from their selective coupling to specific heterotrimeric G-proteins, triggering the corresponding physiological response. Recent drug discovery efforts have focused on the development of allosteric modulators for GPCRs (Conn, Christopoulos, and Lindsley 2009). Allosteric modulators have the potential to increase receptor specificity by targeting sequence motifs unique to receptor family subtypes and isoforms. Further, allosteric modulators require the presence of an orthosteric ligand, providing physiological context-dependent control of GPCR signaling (D. J. Foster and Conn 2017). Therefore, compared to orthosteric ligands, large doses of allosteric modulators can be administered with a lower risk of target-based toxicity (Conn, Christopoulos, and Lindsley 2009). An emerging target site for allosteric modulators is the GPCR-G protein binding interface. The GPCR-G protein binding interface contains sequence divergent structural elements including three intracellular

loops and the GPCR C-tail (Chung 2013). However, the intrinsically disordered nature of the loop and C-tail, combined with the potential for binders in these regions to disrupt GPCR-G protein coupling has limited efforts to rationally design allosteric modulators that target the GPCR-G protein interface (Wakefield et al. 2019).

In this study, we examine the potential for the G protein α subunit C-terminus (G-peptide) to serve as an allosteric modulator of GPCR signaling. The G-peptide is a well-established determinant of GPCR-G protein coupling selectivity (Semack et al. 2016; Okashah et al. 2019). The G-peptide interacts at the cytosolic GPCR-G protein interface, which is distinct from the orthosteric ligand binding pocket. The GPCR interaction with a cognate G-peptide triggers nucleotide exchange in the Gα subunit (GDP to GTP) resulting in G protein activation and downstream signaling. While interactions with non-cognate G-peptides do not precipitate G protein activation, we have recently shown that non-cognate interactions alter receptor conformation resulting in enhanced ligand efficacy (Gupte et al. 2017, 2019). Previous studies show that while the non-cognate G-peptide interactions are transient, the GPCR conformational state persists following dissociation resulting in the allokairic modulation (AKM) of downstream signaling (Gupte et al. 2017, 2019). Allokairic modulators bind asynchronously with the ligand and rely on the temporal persistence of GPCR conformation to exert their influence on orthosteric ligand efficacy (Gupte et al. 2019). Our previous studies focused on the Gs-coupled β2-adrenergic (β2-AR) and dopamine (D_1R) receptors, which show enhanced cyclic AMP generation in the presence of a non-cognate Gq protein. Likewise, the Gq-coupled V1 vasopressin receptor (V_1R) shows enhanced IP_1 levels in the presence of the non-cognate Gs protein (Gupte et al. 2017). In this study, we examine the potential for allokairic modulation of two canonical Gi-coupled receptors, adenosine type 1 (A_1R) and cannabinoid type 1 (CB_1) using G-peptides derived from Gs, Gi, and Gq subtypes.

While β2-AR and D_1R principally signal through Gs, A_1R and CB_1 primarily signal through Gi. However, A_1R and CB_1 display signaling through multiple G-proteins with A_1R signaling through Gi and Gq, and CB_1 signaling through Gi, Gq, and Gs (Bonhaus et al. 1998; Cordeaux, Ijzerman, and Hill 2004; Lauckner, Hille, and Mackie 2005; Chen et al. 2010). CB_1, the most widely expressed GPCR in the central nervous system, primarily signals through Gi producing euphoria and analgesia upon binding tetrahydrocannabinol (THC) in the brain (Agarwal et al. 2007; Ibsen, Connor, and Glass 2017). CB_1 has also been shown to signal through Gq in human embryonic kidney (HEK) 293 cells after treatment with WIN55,212-2 (WN) (Lauckner, Hille, and Mackie 2005) and through Gs in rat globus pallidus, HEK 293, COS-7, CHO, and 3T3 cells after treatment with WN (Bonhaus et al. 1998; Chen et al. 2010; Maneuf and Brotchie 1997). However, the physiological effects of CB_1 signaling through Gs, Gq, and non-G-protein mediated pathways is less clear since there have not been biased ligands identified that specifically target these pathways. A_1R is another example of a promiscuous receptor that can activate different signal transduction pathways in an agonist-dependent manner. A_1R is ubiquitously expressed and most well known for being antagonized by caffeine, producing stimulant effects (Jacobson and Gao 2006). While A_1R canonically signals through Gi, there is evidence that A_1R has a diverse G-protein-activating profile where A_1R can adopt agonist-specific conformations, arising from small changes in ligand structure, which lead to the differential activation of G-proteins including Gi and Gq (Cordeaux, Ijzerman, and Hill 2004). This promiscuity of coupling in these canonical Gi receptors allows us to examine the allosteric effects of the G-peptide on multiple G-protein signaling pathways.

The goal of this focused study is to examine the allosteric effects of G-peptides derived from three distinct Gα C-termini peptides (Gαs, Gαi, and Gαq) on signaling from two promiscuous Gi-coupled receptors (A_1R and CB_1). The C-termini of three G-proteins, Gαs,

Gαi, and Gαq, will be referred to as s-pep, i-pep, and q-pep (or collectively as G-peptides) throughout this manuscript. We expressed A_1R and CB_1 fusions with the s-, i-, or q-pep in HEK 293 cells using systematic protein affinity strength modulation (SPASM) and monitored the impact on downstream signaling in the cell compared to a construct lacking this G-peptide, referred to henceforth as no-pep. We have extensively reported on this SPASM technique, which allows systematic control of the intra-molecular interaction between a GPCR and a G-peptide (Semack et al. 2016; Gupte et al. 2017; Swanson and Sivaramakrishnan 2014; Malik et al. 2017). This technology allows us to directly compare the influence of different G-peptides on the cognate G-protein signaling pathways in cells. While this is a tethered system, we have shown that these engineered GPCR constructs yield similar results to reconstituted systems of GPCR membranes and recombinant G-proteins with regards to allokairic modulation of G protein activation (Gupte et al. 2017; Malik et al. 2017). Hence, despite the synthetic nature of our approach, it provides insight into the impact of receptor interactions with G-peptides on downstream signaling.

To investigate the allosteric effects of G-peptides on Gi-coupled receptors, we used N^6-Cyclopentyladenosine (CPA) and 5'-*N*-Ethylcarboxamidoadenosine (NECA) for A_1R and 2-Arachidonoylglycerol (2-AG) and WIN 55,212-2 mesylate (WN) for CB_1. Our current study confirms what we previously found in Gs-coupled receptors β_2-AR and D_1-R, where s-pep and q-pep positively modulate canonical Gs signaling (Gupte et al. 2017). cAMP response at high concentrations of 2-AG and WN is enhanced by q-pep (~ 30 and 95% increase in cAMP, respectively). Likewise, cAMP stimulation by WN at CB_1 is enhanced by s-pep (~ 40% increase). In contrast, i-pep diminishes cAMP response from CB_1 for both 2-AG and WN (30 and 50% decreases, respectively). At low concentrations of 2-AG, WN, and CPA (nM) we observed inhibition of cAMP, associated with signaling through Gi. We found that the presence of q-pep or i-pep enhanced canonical Gi signaling in A_1R after

activation by CPA (~ 35% increase), and in CB_1 after activation by WN (~ 700% increase) and 2-AG (~ 125% increase), respectively. These findings extend our previously reported allosteric effects of G-peptides to Gi coupled signaling (Gupte et al. 2017, 2019). At high concentrations of 2-AG, WN, CPA, or NECA (μM), stimulation of inositol phosphate (IP_1) is observed, associated with signaling through Gq. We found that the presence of different G-peptides universally inhibits IP_1 signaling through Gq (decreases ranging from 30 to 65%), with the exception of s-pep (~ 50% increase) on CB_1 following activation by WN. Taken together, our data provide an extended model for the allosteric effects of distinct G-peptides on signaling through Gs, Gi, and Gq pathways and highlight the ability of G-peptides to differentially impact signaling in a receptor and ligand-dependent manner.

2.2. Impact of G-Peptides on A_1R and CB_1 Signaling

2.2.1. SPASM Sensor Design:

SPASM sensors were developed for two cognate Gi-coupled receptors, adenosine A_1 receptor (A_1R) and cannabinoid type 1 (CB_1) (Figure 2.1a). From N to C terminus, each SPASM sensor contains a GPCR, mCitrine (to monitor sensor integrity), 10 nm ER/K linker, mCerulean (for matching receptor expression), and a 27-amino acid peptide derived from the α5-helix at the C-terminus of the Gα subunit (s-pep, i-pep, q-pep, or no-pep). We chose the 10 nm linker based on previous work, where we found that a shorter linker corresponded to a higher effective concentration of the protein interaction (Figure 2.2, left) (Sivaramakrishnan and Spudich 2011). We had previously shown that a peptide

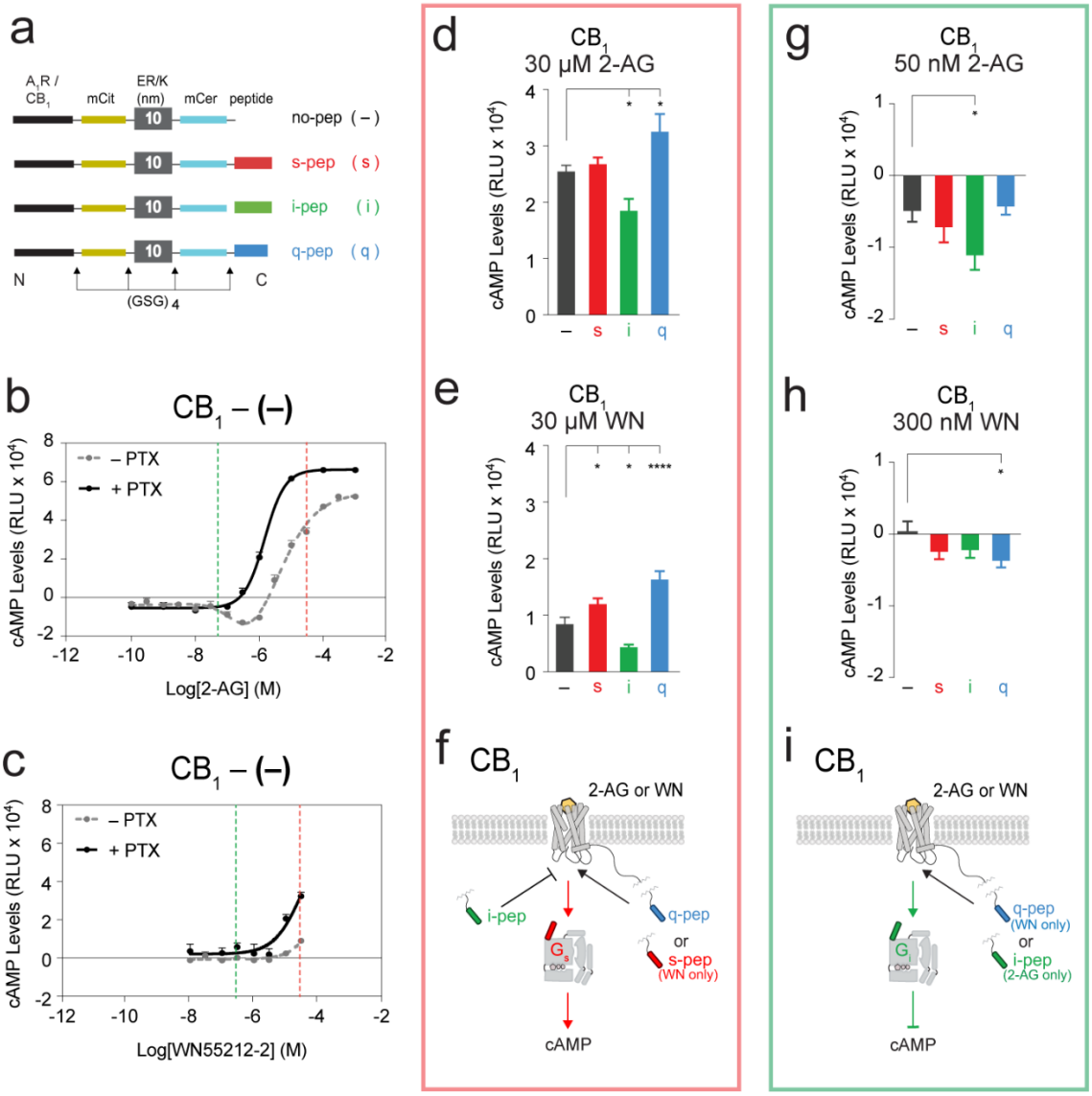

Figure 2.1. Gα peptides differentially impact Gs and Gi signaling in Cannabinoid (CB_1) receptors. ***a*,** SPASM sensors for characterization of second messenger response. Schematics of the A_1R and CB_1 GPCR peptide sensors containing C-terminal Gα peptides corresponding to s-, i-, or q- 5α helices separated with Gly-Ser-Gly $(GSG)_4$ linkers to ensure rotational freedom. The no-pep (-) construct lacks the Gα C-terminal peptide. Forskolin-stimulated cAMP dose response curves of ***b*,** CB_1 agonist, 2-Arachidonoylglycerol (2-AG), and ***c*,** WIN 55,212-2 mesylate (WN55212-2) in a CB_1 no-pep (-) sensor (representative curves from N=2 independent biological replicates composed of ≥3 technical repeats each). cAMP levels shown in the absence (*grey line*) and presence (*black line*) of pertussis toxin (PTX) treatment. Ligands potentiate forskolin-stimulated cAMP accumulation at 30 µM, suggesting Gs bias (*b* and *c*, *red dashed lines*). 2-AG and WIN 55,212-2 mesylate (WN) inhibit forskolin-stimulated cAMP at 50 nM and 300 nM, respectively, suggesting Gi bias (*b* and *c*, *green dashed lines*). cAMP levels of tethered CB_1 sensors after stimulation by forskolin and 30 µM 2-AG (***d***) or WN (***e***) (N=5 independent biological replicates). ***f*,** summary of Gα peptide influence on Gs signaling and cAMP production in CB_1. Inhibition of forskolin-stimulated cAMP by tethered CB_1 sensors after stimulation by 50 nM 2-AG (***g***) (N=8 independent biological replicates) or 300 nM WN (***h***) (N=6 independent biological replicates). ***i*,** summary of Gα peptide influence on Gi signaling and cAMP inhibition in CB_1. GPCR-Gα C-terminal peptide sensors are compared with the no-pep (-) control. Results are expressed as mean ±S.E. ****, p<0.0001; *, p<0.05.

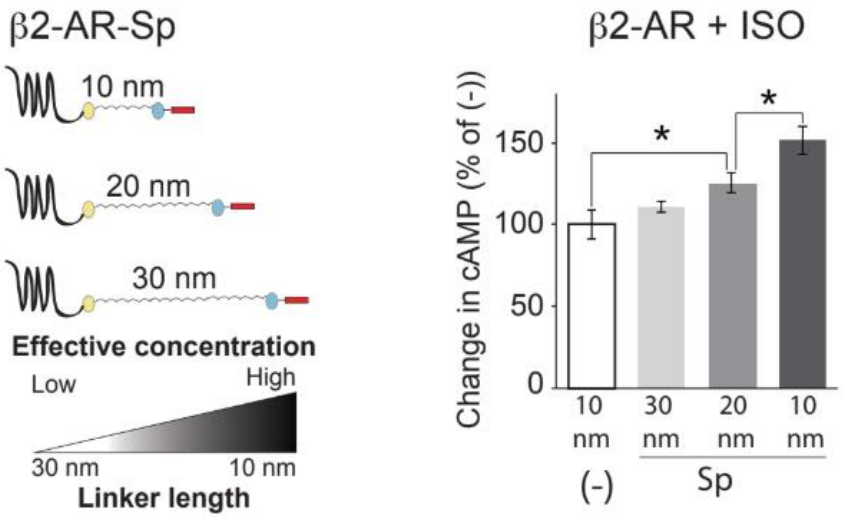

Figure 2.2. Length of Tether and Modulation of Signaling in β2-AR. *Left*, schematic of Gαs C-terminal peptide (*red*) fused to β2-AR via 10, 20, or 30 nm ER/K linkers. Schematic shows effective concentration of protein interaction increasing as linker length decreases. *Right*, relative increase in cAMP production after isoproterenol (ISO) stimulation of 30, 20, and 10 nm β2-AR-s-pep (Sp) sensors compared to a β2-AR sensor lacking peptide (-). Results are represented as percent change from β2-AR no-pep (-) and expressed as mean ±S.E.M. *, $p<0.05$. N=9 technical repeats from 3 independent biological replicates.

derived from Gαs (s-pep) could enhance Gs signaling through β2-AR, and we confirmed this in Figure 2.2 with β2-AR producing a significant increase in cAMP when tethered to the s-pep (Sp) by either a 10 or 20 nm linker (Gupte et al. 2017). However, we observed no significant increase in cAMP production by β2-AR when tethered to s-pep by a 30 nm linker (Figure 2.2). We therefore used a 10 nm linker to tether peptides to GPCRs for subsequent experiments, since it appeared that the effective concentrations enforced by either a 10 or 20 nm linker were required to modulate signaling. The Gα C-terminal peptides have been shown to be essential for activation by the GPCR but do not themselves trigger downstream effectors (Semack et al. 2016; Gupte et al. 2017; Hamm et al. 1988; Lambright et al. 1994; Rasenick et al. 1994; Yang et al. 1999; Oldham and Hamm 2008). In previous studies we have shown the ability of SPASM sensors to be expressed and localized primarily to the plasma membrane in HEK 293 cells (Malik et al. 2013). Our SPASM sensors are therefore designed to modulate the interaction between the attached receptor (A_1R or CB_1) and endogenous G-proteins in cells, allowing one to

study the impact of the tethered Gα peptides on canonical GPCR signaling (Malik et al. 2017). SPASM A_1R and CB_1 constructs lacking a C-terminal peptide (no-pep) were used to measure background cAMP and IP_1 levels and for characterization of ligand dose response.

2.2.2. Impact of Gα C-terminal Peptides on cAMP Response:

Impact of Gα C-terminal peptides on cAMP response in the Cannabinoid (CB_1) Receptor:

Cells expressing the CB_1 sensor display potentiation of forskolin-stimulated cAMP accumulation with signaling dominated by Gs in response to 30 μM of the CB_1 agonists 2-Arachidonoylglycerol (2-AG) (Figure 2.1b, *red dashed line*) or WIN 55,212-2 mesylate (WN) (Figure 2.1c, *red dashed line*) (Bonhaus et al. 1998; Chen et al. 2010). Representative dose response curves with untransfected HEK 293 cells are shown in Figure 2.3 with stimulation by 2-AG (Figure 2.3, *green*) or WN (*purple*). We observed no potentiation of forskolin-stimulated cAMP accumulation in untransfected HEK 293 cells in response to a range of 2-AG and WN concentrations (Figure 2.3), suggesting any potentiation of forskolin-stimulated cAMP accumulation can be attributed to transfected CB_1 receptors rather than endogenous receptors in the HEK 293 cells. CB_1 appeared to inhibit forskolin-stimulated cAMP accumulation with signaling dominated by Gi in response to 50 nM 2-AG (Figure 2.1b, *green dashed line*) or 300 nM WN (Figure 2.1c, *green dashed line*). To characterize Gi signaling in CB_1, dose response curves were performed for both 2-AG and WN (Figure 2.1b and 2.1c, respectively) in the presence (*black lines*) or absence

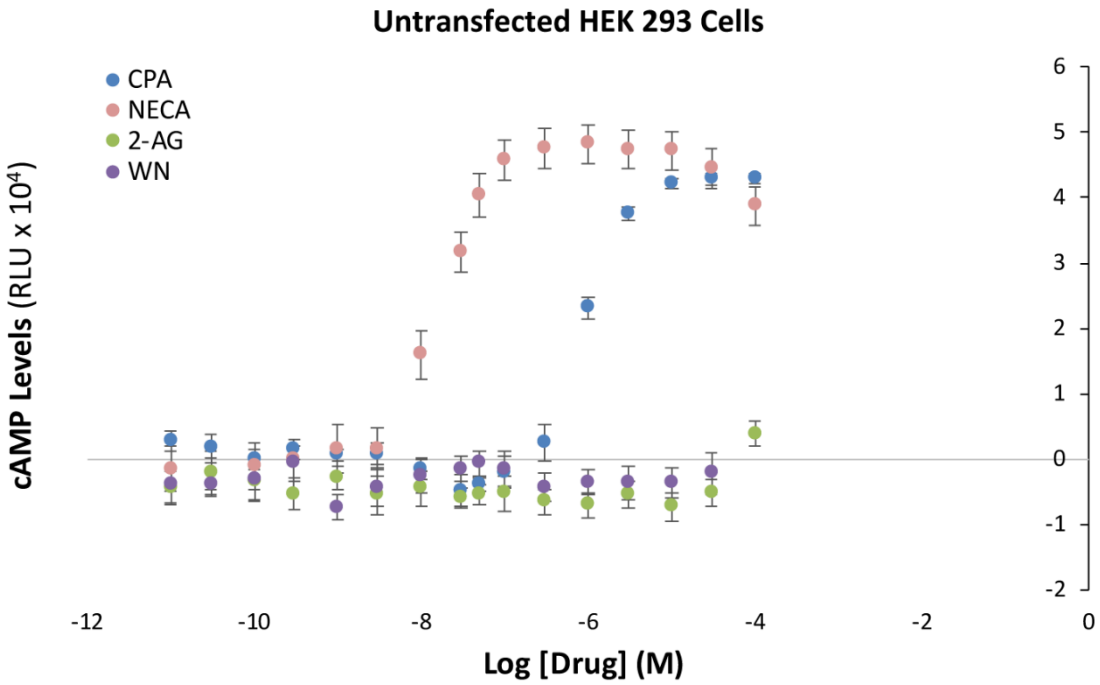

Figure 2.3. cAMP Stimulation by Endogenous HEK 293 Cell Receptors. Representative forskolin-stimulated cAMP dose response curves of untransfected HEK 293 cells shown after stimulation by A1R agonists, CPA (*blue*) and NECA (*pink*), or CB_1 agonists, 2-AG (*green*) and WN (*purple*). Results expressed as ±S.E.M. from 3 technical replicates.

(*gray lines*) of pertussis toxin (PTX). cAMP levels increased in response to PTX treatment in 2-AG-stimulated CB_1 (Figure 2.1b, black line), indicating that cAMP inhibition in the absence of PTX is likely due to signaling through Gi. 2-AG or WN can be used at high concentrations (30 μM, Figure 2.1b and 2.1c, *red dashed lines*) to characterize the impact of peptides on cAMP stimulation and Gs signaling (Figure 2.1d and 2.1e) and at low concentration (50 or 300 nM, Figure 2.1b and 2.1c, *green dashed lines*) to characterize cAMP inhibition and signaling through Gi in CB_1 (Figure 2.1g and 2.1h).

We examined the allosteric modulation of Gαs, Gαi, and Gαq peptides on forskolin-stimulated cAMP accumulation in the promiscuous Gi-coupled receptor, cannabinoid type 1 (CB_1). SPASM sensors with s-, i-, or q-pep fusions, in addition to a no-pep control (-), were expressed in HEK 293 cells as shown previously (Malik et al. 2013). Cells expressing the CB_1 sensors were treated with high concentrations (30 μM) of 2-AG (Figure 2.1d) or

WN (Figure 2.1e) to stimulate cAMP production through the Gs pathway (Figure 2.1b and 2.1c). The q-pep sensor was found to increase signaling through Gs in CB_1, as evidenced by a significant increase in cAMP levels (Figure 2.1d and 2.1e, blue bars). This finding in a Gi-coupled receptor extends our previous results where q-pep exhibited enhanced signaling in the Gs pathway in Gs-coupled receptors (Gupte et al. 2017). S-pep sensors also increased signaling through Gs in CB_1 after stimulation by WN (Figure 2.1e, red bar). In contrast, the presence of i-pep inhibited Gs signaling in CB_1 after stimulation by 2-AG or WN, decreasing cAMP levels (Figure 2.1d and 2.1e, green bars). These findings are also summarized in the schematic (Figure 2.1f) with q-pep (blue) and s-pep (red) stimulating Gs signaling and i-pep (green) inhibiting signaling through Gs.

Gα peptides affected signaling through Gi-mediated inhibition of forskolin-stimulated cAMP accumulation in CB_1. To target Gi signaling, HEK 293 cells expressing CB_1 SPASM sensors were treated with low concentrations of 2-AG (50 nM) or WN (300 nM), conditions resulting in cAMP inhibition (Figure 2.1b and 2.1c). The i-pep increased the inhibition of cAMP production after stimulation by 2-AG (Figure 2.1g, green bar) compared to the no-pep (-) sensor. Treatment with WN leads to an increase in Gi signaling with q-pep but not with i-pep (Figure 2.1h, blue bar). The agonist-dependent enhancement of Gi signaling by both i-pep and q-pep is summarized in the schematic (Figure 2.1i).

Impact of Gα C-terminal peptides on cAMP inhibition in the Adenosine (A_1R) Receptor:

Cells expressing the A_1R no-pep (-) sensor display Gi-mediated inhibition of forskolin-stimulated cAMP accumulation after stimulation by 50 nM of the A_1R agonist, N^6-Cyclopentyladenosine (CPA) (Figure 2.4a, green dashed line). Pertussis toxin (PTX) treatment inhibits Gi signaling, allowing for differentiation between the Gs- and Gi-

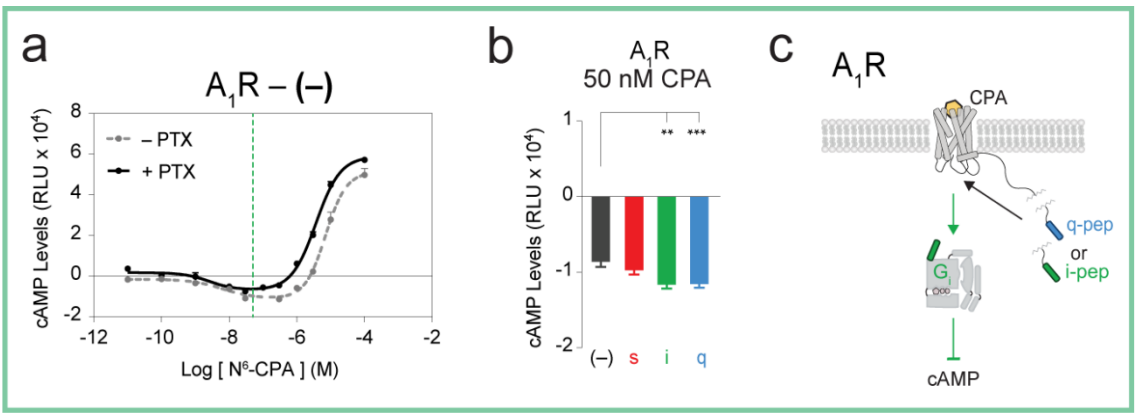

Figure 2.4. Characterization of cAMP Modulation in Adenosine Receptor (A_1R) by SPASM Sensors. Forskolin-stimulated cAMP dose response curves of ***a*,** A_1R agonist, N^6-Cyclopentyladenosine (CPA). cAMP levels shown in the absence (*grey line*) and presence (*black line*) of pertussis toxin (PTX) treatment. 50 nM CPA inhibits forskolin-stimulated cAMP, suggesting Gi bias (*a*, *green dashed line*). ***b*,** Inhibition of forskolin-stimulated cAMP by tethered A_1R peptide sensors after stimulation by 50 nM CPA. ***c*,** Summary of Gα peptide influence on Gi signaling and cAMP inhibition. GPCR-Gα C-terminal peptide sensors are compared with the no-pep (-) control. Results are expressed as mean ±S.E. ***, p<0.001; **, p<0.01. N=8 independent biological replicates.

mediated effects on cAMP (Mangmool and Kurose 2011). cAMP levels increased in response to PTX treatment in CPA-stimulated A_1R (Figure 2.4a, black line), indicating that cAMP inhibition in the absence of PTX is likely due to signaling through Gi. To characterize the impact of different Gα peptides on Gi inhibition of forskolin-stimulated cAMP accumulation in a promiscuous Gi-coupled receptor, cells expressing the different A_1R peptide sensors at equivalent levels were treated with 50 nM of CPA resulting in cAMP inhibition, dominated by Gi (Figure 2.4b). The i-pep and q-pep both increased signaling through Gi in A_1R after stimulation by CPA, as evidenced by a significant increase in cAMP inhibition (Figure 2.4b, *green and blue bars*, respectively). To address potential variability in individual sensor response, for each experiment equivalent sensor expression was verified using fluorescence measurements (see methods) and data for all four peptide sensors were collected together (Figure 2.5). This phenomenon is summarized in a schematic (Figure 2.4c) showing the presence of i-pep (green) and q-pep (blue) increasing signaling through Gi and inhibiting cAMP.

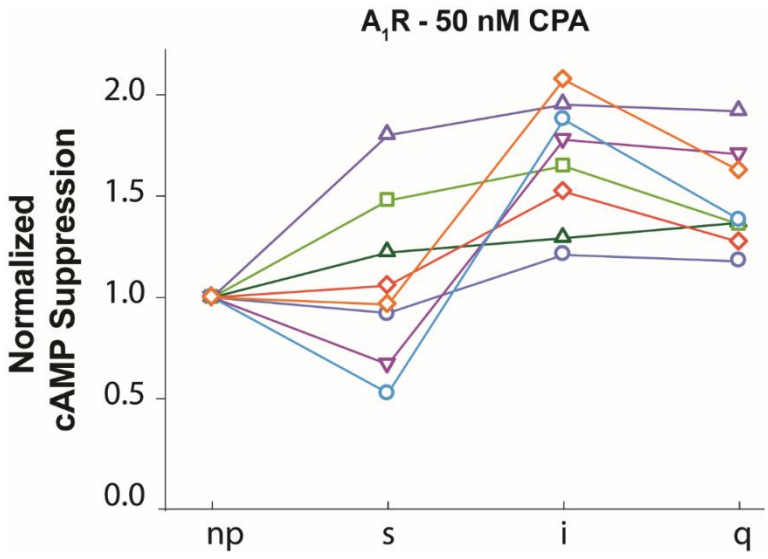

Figure 2.5. Experimental Replicates of cAMP Modulation in Adenosine receptor (A_1R) by SPASM Sensors. Inhibition of forskolin-stimulated cAMP by tethered A_1R peptide sensors, s-, i-, and q-pep, normalized to no-pep (np) control, after stimulation by 50 nM CPA. Each independent experiment (total of n=8 experiments) is represented by a separate color. For each experiment, data for all four peptide sensors were collected together.

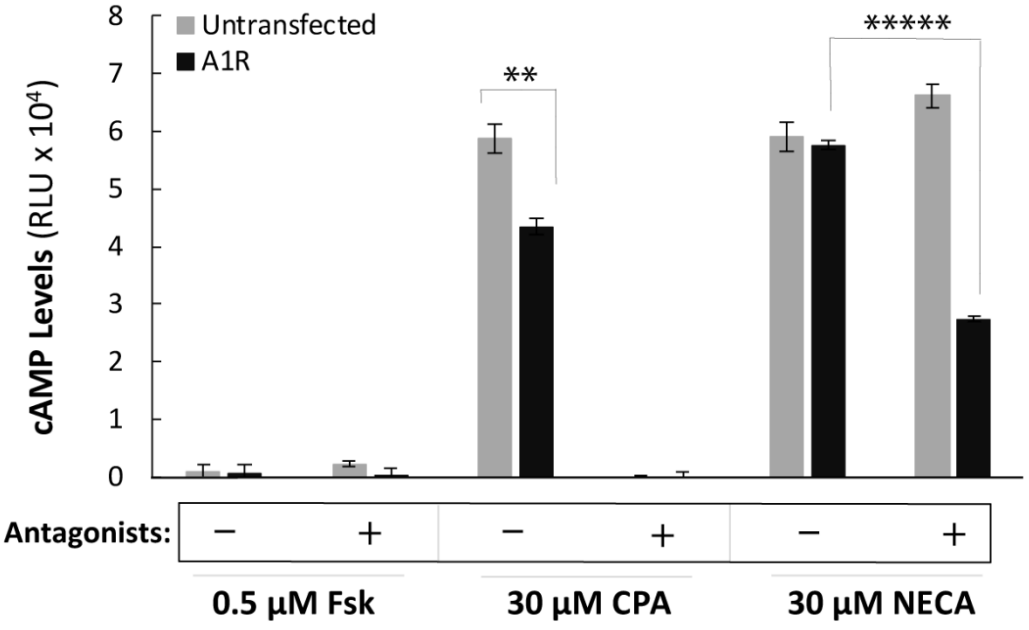

Figure 2.6. cAMP Stimulation by Endogenous HEK 293 Cell Receptors and Adenosine Receptor (A_1R). cAMP levels of untransfected HEK 293 cells (gray bars) and HEK 293 cells transfected with A1R (black bars). cAMP levels shown after stimulation by 0.5 µM forskolin (fsk) alone (*left*), 0.5 µM fsk + 30 µM CPA (*middle*), and 0.5 µM fsk + 30 µM NECA (*right*). Conditions with (+) antagonists were pre-treated with 100 nM of the $A_{2A}R$ selective antagonist, SCH 442416 (SCH), and 1 µM of the $A_{2B}R$ selective antagonist, PSB 1115 (PSB). Results are expressed as mean ±S.E.M. *****, $p<0.00001$; **, $p<0.01$. N=3 independent biological replicates.

Despite the potentiation of forskolin-stimulated cAMP accumulation at high concentrations of CPA (Figure 2.4a), the cAMP accumulation appears to be the result of stimulation of endogenous HEK 293 cell receptors rather than Gs signaling through A_1R receptors. Untransfected HEK 293 cells treated with 30 μM CPA showed higher potentiation of forskolin-stimulated cAMP accumulation than was seen with HEK 293 cells transfected with A_1R (Figure 2.6). Under the same conditions, pre-treatment with 100 nM of the $A_{2A}R$ selective antagonist, SCH 442416 (SCH), and 1 μM of the $A_{2B}R$ selective antagonist, PSB 1115 (PSB), resulted in complete inhibition of cAMP production. The slight decrease in forskolin-stimulated cAMP accumulation in cells transfected with A_1R without antagonist pre-treatment can likely be attributed to increased Gi signaling by transfected A_1R receptors. We performed the same control experiments with untransfected HEK 293 cells treated with 30 uM NECA and found equivalent potentiation of forskolin-stimulated cAMP accumulation as compared to A_1R-transfected cells (Figure 2.6). Pre-treatment with $A_{2A}R$ and $A_{2B}R$ selective antagonists, SCH and PSB, did not change cAMP accumulation in untransfected cells. However, pre-treatment with SCH and PSB in A_1R-transfected cells reduced cAMP accumulation by 50%. In both cases, treatment with either 30 μM CPA or NECA appears to increase forskolin-stimulated cAMP accumulation due to endogenous receptors in the HEK 293 cells. A representative dose-response curve shows potentiation of forskolin-stimulated cAMP accumulation in untransfected HEK 293 cells in response to a range of CPA and NECA concentrations (Figure 2.3). We therefore could not characterize the impact of Gα peptides on Gs signaling in A_1R.

2.2.3. C-terminal Gα Peptides Inhibit IP_1 Signaling in A_1R and CB_1:

C-terminal Gα Peptides Inhibit Gq Signaling from Promiscuous Receptors:

Previous work from our lab suggests that the effect of non-canonical G-proteins on IP_1 signaling are more receptor-specific (Gupte et al. 2017). We found that Gs enhances IP_1 production and signaling through Gq in the vasopressin receptor (V_{1A}-R) but not the α1 adrenergic receptor (α1-AR) (Gupte et al. 2017). In the current study we examined the impact of Gα peptides on Gq signaling and IP_1 production in A_1R and CB_1 receptors. A dose-response study of NECA (Figure 2.7a, *black line*) and CPA (*gray lines*) with A_1R no-pep (-) sensors revealed maximum IP_1 signal at 100 μM ligand (*blue dotted line*). To rule out Gβγ-dependent PLC-β activation, we performed IP_1 dose response assays in the absence (Figure 2.7a, dark *gray line*) and presence (*light gray line*) of pertussis toxin (PTX) treatment. Regardless of CPA concentration, no reduction in IP_1 production was observed in PTX-treated cells compared to untreated cells, suggesting the observed IP_1 production is due to A_1R signaling through the PTX-insensitive Gq pathway. Additionally, to rule out Gq signaling through endogenous HEK 293 $A_{2B}R$ receptors, IP_1 levels were assessed in untransfected HEK 293 cells after stimulation by 100 μM CPA or NECA (Figure 2.8). Regardless of pre-treatment with 1 μM of the $A_{2B}R$ selective antagonist PSB 1115 (PSB), significant IP_1 production occured in A_1R transfected cells but not in untransfected HEK 293 cells, suggesting IP_1 production resulted from Gq signaling through A_1R and not endogenous $A_{2B}R$ (Figure 2.8). A_1R SPASM sensors with tethered s-, i-, or q-pep, in addition to a no-pep (-) sensor lacking a peptide, were expressed in HEK 293 cells to equivalent levels. IP_1 assays were performed with each of the A_1R sensor constructs after stimulation by 100 μM CPA (Figure 2.7b, left) or NECA (right). Constructs containing the

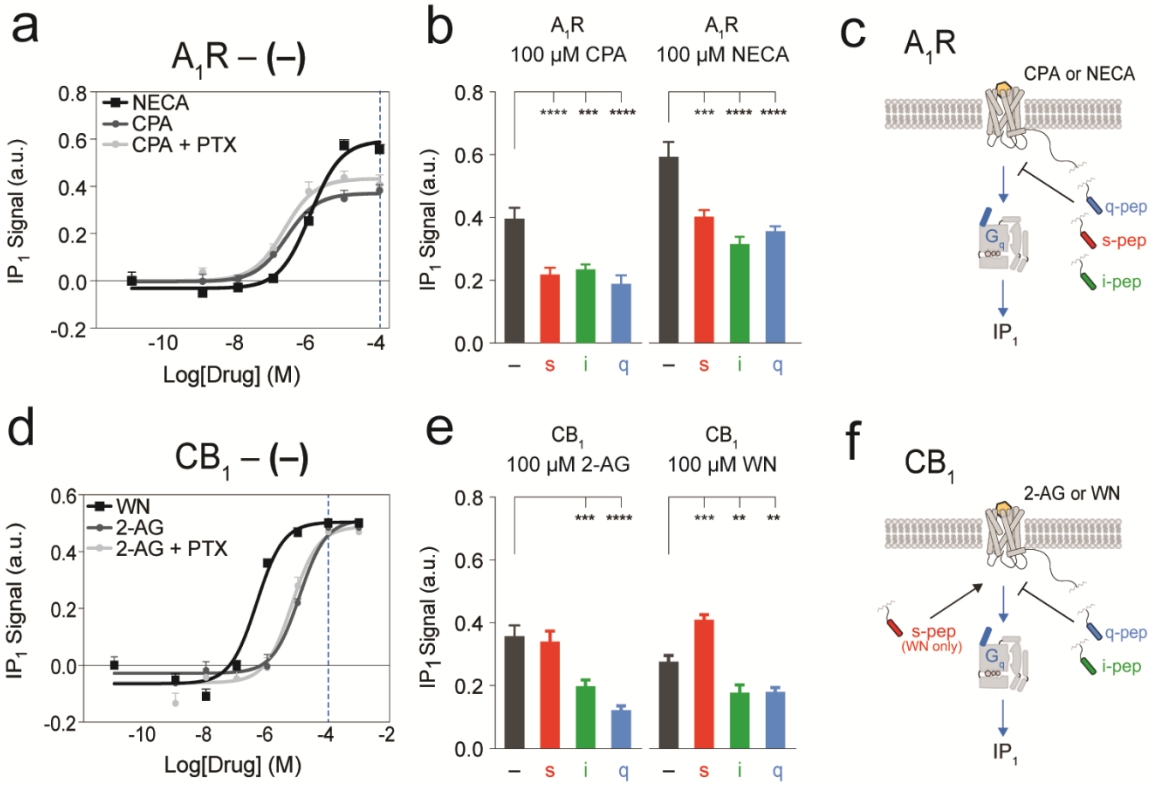

Figure 2.7. Gαq and Gαi Peptides Inhibit Signaling through Gq. ***a*,** IP_1 dose response curve of A_1R agonists, CPA (*gray lines*) (representative curves from N=2 independent biological replicates composed of ≥3 technical repeats each) and NECA (*black line*) (N=3 technical repeats), with A_1R-no-pep (-) sensor. IP_1 levels shown in the absence (dark *gray line*) and presence (*light gray line*) of pertussis toxin (PTX) treatment. 100 µM CPA or NECA stimulate IP_1 (*a*, *blue dashed line*). ***b*,** IP_1 signal from A_1R after stimulation by 100 µM CPA (left) (N=3 independent biological replicates) or NECA (right) (N=4 independent biological replicates) in the presence of different Gα C terminal peptides compared to no-pep (-) control. **c,** summary of Gα peptide influence on Gq signaling and IP_1 production in A_1R. ***d*,** IP_1 dose response curve of CB_1 agonists, 2-AG (*gray lines*) (N=5 independent biological replicates) and WN (*black line*) (N=4 independent biological replicates), with CB_1-no-pep (-) sensor. IP_1 levels shown in the absence (dark *gray line*) and presence (*light gray line*) of pertussis toxin (PTX) treatment. 100 µM 2-AG or WN stimulate IP_1 (*d*, *blue dashed line*). ***e*,** IP_1 signal from CB_1 Gα C terminal peptide sensors after stimulation by 100 µM 2-AG (left) or WN (right) compared to no-pep (-) control (N=3 technical repeats). ***f*,** summary of Gα peptide influence on Gq signaling and IP_1 production in CB_1. Results are expressed as mean ±S.E. ****, p<0.0001; ***, p<0.001; **, p<0.01.

s-pep, i-pep, or q-pep inhibited IP_1 production regardless of ligand, as summarized in the schematic (Figure 2.7c).

To examine the impact of the Gα peptides on Gq signaling in a second promiscuous receptor, CB_1, we first performed assays to identify the optimal concentration of ligand to use for characterization. A dose-response study of WN (Figure 2.7d, *black line*) and 2-AG (*gray lines*) on CB_1 no-pep (-) sensors revealed maximum IP_1 signal at

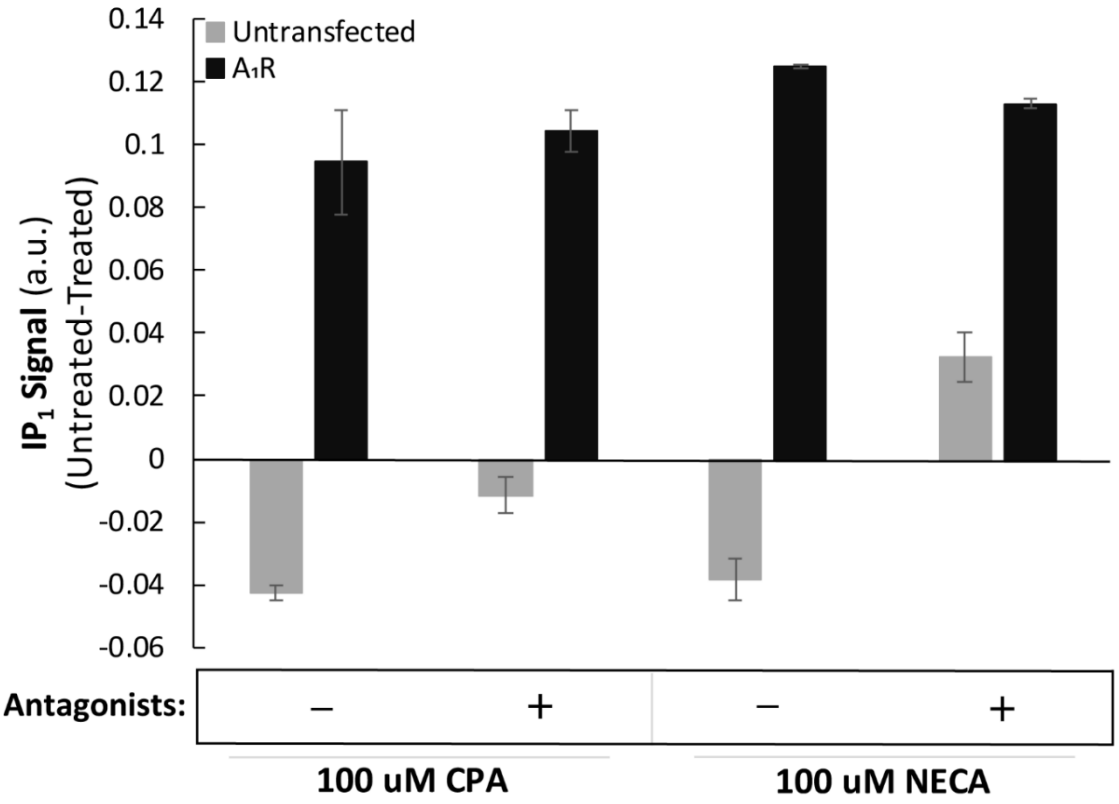

Figure 2.8. IP_1 Production by Endogenous HEK 293 Cell Receptors and Adenosine Receptor (A_1R). IP_1 levels of untransfected HEK 293 cells (gray bars) and HEK 293 cells transfected with A_1R (black bars). IP_1 levels shown after stimulation by 100 μM CPA (*left*), and 100 μM NECA (*right*). Conditions with (+) antagonist were pre-treated with 1 μM of the $A_{2B}R$ selective antagonist, PSB 1115 (PSB). Results are expressed as mean ±S.E.M. N=9 independent biological replicates.

100μM ligand (*blue dotted line*). To rule out Gβγ-dependent PLC-β activation, we performed IP_1 dose response assays in the absence (Figure 2.7d, dark *gray line*) and presence (*light gray line*) of pertussis toxin (PTX) treatment. Regardless of 2-AG concentration, no reduction in IP_1 production was observed in PTX-treated cells compared to untreated cells, suggesting the observed IP_1 production is due to CB_1 signaling through the PTX-insensitive Gq pathway. An IP_1 assay was performed on HEK 293 cells expressing SPASM sensors with s-, i-, or q-pep fusions, in addition to a sensor lacking a peptide no-pep (-), after stimulation by 100 μM 2-AG (Figure 2.7e, *left*) or WN (*right*). Consistent with A_1R, the i-pep and q-pep inhibited signaling through Gq in CB_1, as evidenced by reduction of IP_1 signal (Figure 2.7e, green and blue bars, respectively). The

s-pep significantly enhanced signaling through Gq after stimulation by 100 μM WN (Figure 2.7e, right, red bar). The influence of i-pep, q-pep, and s-pep on Gq signaling and subsequent IP_1 production in CB_1 is summarized in the schematic (Figure 2.7f). We have summarized these findings in a model in Figure 2.9, highlighting how Gα C-terminal peptides differentially influence signaling in each of these promiscuous receptors.

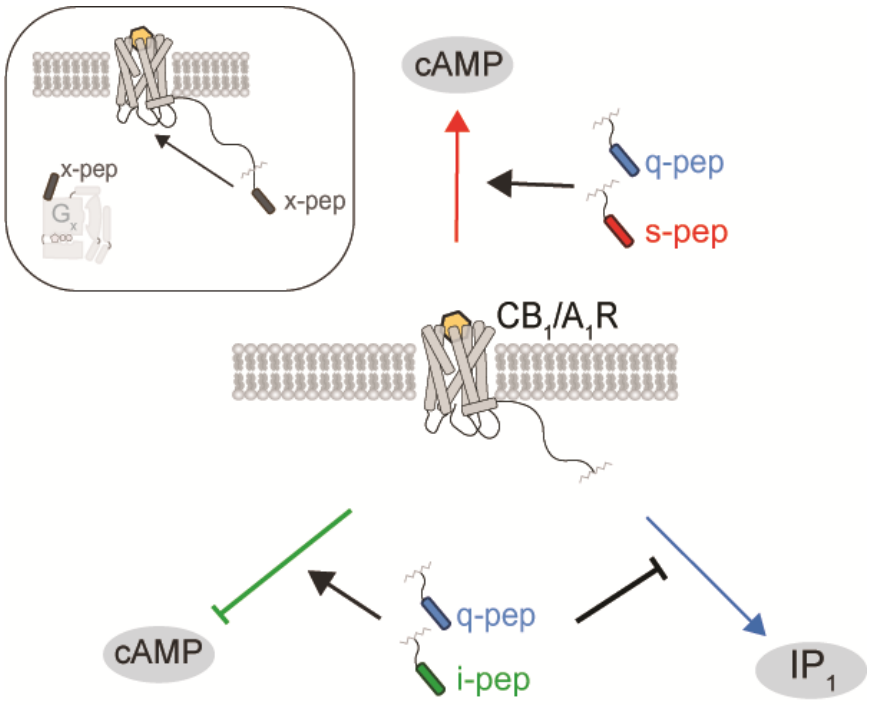

Figure 2.9. Model of Gα Peptide Influence on GPCR-G Protein Signaling. *Inset*, SPASM sensor with attached peptide (x-pep) shown next to G-protein containing C-terminal Gα peptide (x-pep). *Above*, model of Gα peptides (s-pep, i-pep, or q-pep) that modulate Gs (*red arrow*), Gi (*green inhibitory arrow*), or Gq (*blue arrow*) signaling pathways in CB_1 or A_1R receptors after stimulation by different agonists. Q-pep and s-pep enhance Gs signaling. Q-pep and i-pep enhance Gi signaling while inhibiting Gq signaling.

2.3. Summary and Discussion:

In this study we demonstrate the allosteric modulation of two Gi-coupled receptors, A_1R and CB_1, using peptides derived from the C-terminus of the Gα subunit (G-peptides). G-peptides derived from Gαi and Gαq (i-pep and q-pep) enhance agonist-dependent cAMP inhibition, demonstrating their function as positive allosteric modulators of Gi-coupled signaling. In contrast, i-pep and q-pep suppress agonist-dependent IP_1 levels suggesting that they function as negative allosteric modulators of Gq-coupled signaling. Taken together with our previous studies focused on Gs-coupled receptors, our findings reinforce the potential of G-peptides to allosterically modulate signaling from class A GPCRs (Gupte et al. 2017, 2019). While allosteric modulation of GPCR signaling has gained prominence to address the need for receptor specificity, efforts have mainly focused on allosteric sites adjacent to the orthosteric ligand binding pocket and lipophilic molecules that target transmembrane helices (Conn, Christopoulos, and Lindsley 2009). In contrast, here we use as G-peptides as probe molecules to demonstrate allosteric modulation through the GPCR-G protein binding interface.

The two Gi coupled receptors (CB_1 and A_1R) examined in this study have also been reported to signal to varying degrees through other G proteins (Bonhaus et al. 1998; Cordeaux, Ijzerman, and Hill 2004; Lauckner, Hille, and Mackie 2005; Chen et al. 2010; Maneuf and Brotchie 1997). While traditionally described as a Gi-coupled receptor, it has been demonstrated that A_1R can couple to Gs and Gq in response to CPA or NECA, suggesting A_1R can adopt agonist-specific conformations arising from small differences in ligand structure leading to differential G-protein activation (Cordeaux, Ijzerman, and Hill 2004). However, previous studies emphasize A_1R signaling through Gi and contradict signaling through Gs (Freissmuth, Schutz, and Linder 1991; Jockers et al. 1994). Our data

suggest any apparent Gs signaling by A_1R, measured by potentiation of forskolin-induced cAMP production, cannot be distinguished from activation of endogenous $A_{2A}R$ or $A_{2B}R$ receptors by A_1R agonists. We saw significantly higher potentiation of forskolin-induced cAMP production in untransfected HEK 293 cells compared to A_1R-transfected HEK 293 cells in response to CPA, suggesting CPA is likely stimulating endogenous Gs-coupled receptors (Figure 2.6). Further investigation revealed $A_{2A}R$ and $A_{2B}R$ specific antagonists could inhibit this potentiation of cAMP in untransfected cells, suggesting any potentiation of forskolin-induced cAMP production likely resulted from stimulation of endogenous $A_{2A}R$ or $A_{2B}R$ receptors. Therefore, we could not independently examine A_1R signaling through the Gs pathway. The $A_{2B}R$ receptor is also known for signaling through Gq, however control experiments confirmed Gq signaling likely occurred through A_1R and not $A_{2B}R$ since no significant IP_1 production was seen in untransfected HEK 293 cells (Figure 2.8). In accordance with a previous studies, we confirmed CB_1 did indeed signal through Gs, as no significant potentiation of forskolin-induced cAMP production was observed in untransfected HEK 293 cells stimulated by the CB_1 agonists 2-AG or WN (Figure 2.3) (Bonhaus et al. 1998; Chen et al. 2010; Maneuf and Brotchie 1997). We therefore used CB_1 to examine the impact of G-peptides on Gs signaling, with findings consistent with our previous report for the Gs selective β2-AR receptor (Figure 2.1 d-f) (Gupte et al. 2017).

Our data contrast with previous studies that report inhibition of GPCR signaling by native cognate G-peptides (Gilchrist et al. 1999, 2001; Gilchrist, Li, and Hamm 2002). In these studies, minigene vectors were used to overexpress cognate G-peptides in cells at arbitrarily high concentrations, in order to identify and selectively inhibit cognate G protein engagement with the receptor. Accordingly, we have previously shown that high concentrations of cognate G-peptides (100 μM s-pep) can competitively inhibit signaling from Gs-coupled receptors (Gupte et al. 2017, 2019). In contrast, we find that non-cognate

G-peptides can bind weakly to the receptor and serve as positive allosteric modulators (Gupte et al. 2017, 2019). While no significant positive allosteric effects were noted in studies with minigene vectors encoding non-cognate G-peptides, these could be attributed to the variation and/or lack of control in expression since saturating levels would result in inhibition (Gilchrist et al. 1999, 2001; Gilchrist, Li, and Hamm 2002). To alleviate the confounding effects of G-peptide concentration, we used the SPASM constructs to provide equivalent effective concentrations of distinct G-peptides across different receptor-ligand-pathway combinations. Further, the ER/K linker in the SPASM sensors provides an effective concentration of approximately 10 μM (Swanson and Sivaramakrishnan 2014), which is significantly lower than our previously reported threshold for competitive inhibition by cognate G-peptides. Using this technology, we observe differential effects of G-peptides on distinct pathways emerging from the same receptor. Specifically, while both i-pep and q-pep augment Gi mediated cAMP inhibition, they suppress IP_1 accumulation downstream of Gq activation. Given that sensor expression levels were matched between cAMP and IP_1 assays and the ER/K linked G-peptides (i-pep and q-pep) are presented at equal effective concentrations, it is unlikely that inhibition of Gq signaling stems from a simple competitive inhibition mechanism. Instead, the differential effects of G-peptides likely stem from the dynamic conformational landscape of GPCRs (Nygaard et al. 2013; Sandhu et al. 2019).

We propose a model wherein transient interactions with G-peptides alter receptor conformation. The receptor does not form a stable ternary complex with the G-peptide and therefore at low concentrations (10 μM) does not interfere with the kinetics of the receptor-cognate G protein interaction (Gupte et al. 2019). However, the altered receptor conformation triggered by G-peptide binding impacts ligand efficacy for cognate G protein activation, resulting in positive or negative allosteric modulation of downstream responses.

The inability of the G-peptides, especially those derived from non-cognate G proteins, to form stable interactions with the receptor has been previously observed in A_1R-Gi fusions (Waldhoer et al. 1999). The lack of stable ternary complex formation with non-cognate G proteins has been suggested as a kinetic proofreading mechanism to prevent non-cognate GPCR-G protein coupling (Waldhoer et al. 1999). Nonetheless, we have previously shown that both cognate and non-cognate G-peptide interactions influence receptor conformation (Gupte et al. 2019). Transient interactions of the G-peptide at the cognate G protein binding site on the receptor stabilize a distinct receptor conformational state. This conformational state persists following G-peptide dissociation enabling increased efficacy of subsequent cognate G protein coupling and enhanced downstream signaling (Gupte et al. 2019). Given that the G-peptide and cognate G protein share the same binding site, albeit staggered in time, we propose that the G-peptides function as allokairic modulators (AKMs) of cognate GPCR signaling. Allokairy is an established concept in enzymatic reactions, wherein increased substrate concentrations can increase maximal reaction rates, especially if the substrate stabilizes a distinct active enzyme conformation (Hilser, Anderson, and Motlagh 2015). AKMs can bind asynchronously with the orthosteric ligand and rely on temporally persistent conformational states of the enzyme to exert their effects (Gupte et al. 2019). G peptides as AKMs provide access to the entire GPCR-G protein interaction interface for allosteric modulation, without necessarily competing with cognate G protein coupling. Targeting the GPCR-G protein interface offers the potential to enhance receptor specificity, especially given the three intrinsically disordered loop regions with considerable isoform specific sequence homogeneity.

2.4. Materials and Methods:

Reagents and buffers:

5'-*N*-Ethylcarboxamidoadenosine (NECA), pertussis toxin (PTX), and forskolin were purchased from Sigma-Aldrich. 2-Arachidonoylglycerol (2-AG), N^6-Cyclopentyladenosine (CPA), WIN 55,212-2 mesylate (WN), SCH 442416 (SCH), and PSB 1115 (PSB) were purchased from Tocris. cDNA encoding $G\alpha i_2$ isoform 1, Gαq, and the long splice variant of Gαs were acquired from GE (Open Biosystems). Human A_1R was acquired from DNASU Plasmid Repository. *Mus musculus* CB_1 was acquired from transOMIC technologies. DNA transfection reagents X-tremeGENE HP and Mirus-LT DNA were purchased from Roche and Mirus, respectively. Buffer A is Phosphate Buffered Saline (PBS pH 7.4; Gibco™), 800 μM ascorbic acid, and 0.2% dextrose (w/v). Buffer B (Stimulation Buffer 2; Cisbio) is 10 mM HEPES, 1 mM $CaCl_2$, 0.5 mM $MgCl_2$, 4.2 mM KCl, 146 mM NaCl, 5.5 mM glucose, 50 mM $LiCl_2$, pH 7.4.

Molecular cloning:

For mammalian HEK 293 expression, all GPCR and Gα constructs were cloned into a PCDNA5/FRT vector (ThermoFisher). GPCR sensors were cloned with a modular scheme. Each GPCR sensor contained (from N- to C-terminus): a full length GPCR (A_1R or CB_1), mCitrine, 10 nm ER/K linker, mCerulean, and a Gα subunit C-terminal peptide corresponding to Gαs, Gαi, Gαq, (s-pep, i-pep, or q-pep, respectively) or a control peptide (no-pep), consisting of repeating $(Gly\text{-}Ser\text{-}Gly)_4$ residues. A $(Gly\text{-}Ser\text{-}Gly)_4$ linker was inserted between all protein domains as part of the primer sequence to allow for free rotation between domains. All sensors also contained either an N-terminal HA-tag or a His-tag. All constructs were confirmed by sequencing.

Mammalian cell preparation and sensor expression:

HEK293T-Flp-In (HEK293T, ThermoFisher) cells were cultured in DMEM media (ThermoFisher) supplemented with 10% FBS (v/v) (Millipore Sigma), 4.5 gL^{-1} D-glucose, 1% Glutamax (ThermoFisher), 20 mM HEPES, pH 7.5 at 37 °C in a humidified atmosphere at 5% CO_2. HEK293T cells were plated onto 6-well tissue culture treated plates at ~30% confluence. Cells were transfected 16–20 h later with X-tremeGENE HP DNA transfection reagent. Transfection conditions including the amount of DNA (1.4–4 µg DNA + 4.2–6 µl reagent) and the length of transfection (control no-pep sensors: 18–24 h; sensors containing s-, i-, or q-pep: 22–32 h) were optimized to consistently yield equivalent levels of sensor expression across different conditions. Where indicated, 12 h after transfection, cells were incubated with 100 ng ml^{-1} PTX for 16 h. Experiments were conducted at 60–80% transfection efficiency (evaluated on a Nikon tissue-culture microscope enabled with fluorescence detection using 20x and 40x magnification). At the time of the experiment, 60–90% of transfected cells expressed predominantly plasma membrane localized sensor with minimal localization to the intracellular compartments. Sensor integrity, localization, and sensor expression were tracked for all experiments to ensure consistency. Each experiment was performed at equivalent sensor expression and matched O.D. of the cell suspension using the following steps. Cells were first resuspended by gentle pipetting into their original media, spun down (350 g, 3 min), and washed once with Buffer A or B for cAMP or IP_1 assays, respectively. Subsequently, cells were resuspended in an appropriate volume of the same buffer to reach a 0.3 O.D. measured at $A_{600\,nm}$. Sensor expression was measured by mCitrine fluorescence. mCitrine fluorescence was held within 1.6–2.4 × 10^6 counts-per-second (cps) for a cell O.D. of 0.3. Sensor integrity was confirmed by measuring the mCitrine (Horiba Fluoromax-4; excitation 490 bandpass 8 nm; emission range 500–600 bandpass

4 nm; emission maximum 525 nm) to mCerulean fluorescence ratio (excitation 430 bandpass 8 nm; emission range 450–600 bandpass 4 nm; emission maximum 475 nm). Experiments were conducted at mCitrine to mCerulean fluorescence ratio of 1.7–2.1.

cAMP assays:

HEK293T cells expressing indicated sensor were harvested 28–32 h post transfection (XtremeGENE HP) to assess cAMP levels using the bioluminescent cAMP Glo assay (Promega). Cells were gently suspended in their original media, counted using a hemocytometer, and spun down (350 g, 3 min). Cells were resuspended in an appropriate volume of Buffer A to reach 4×10^6 cells mL^{-1} density. Cell suspensions were aliquoted into 384-well opaque plates (5 µL per well). Where indicated, cells were pre-incubated with 100 nM of the adenosine type 2A receptor ($A_{2A}R$) selective antagonist, SCH 442416 (SCH), and 1 µM of the adenosine type 2B receptor ($A_{2B}R$) selective antagonist, PSB 1115 (PSB) in 10 µM forskolin for 15 min at 37 °C. Cells were incubated with CPA or NECA (for A_1R) or 2-AG or WN (for CB_1) for 15 min with 10 µM forskolin at 37 °C. Subsequently, cells were lysed and the protocol was followed according to the manufacturer's recommendation (Promega). Luminescence was measured using a microplate reader (SpectraMax M5e, Molecular Devices). cAMP levels were evaluated by subtracting relative luminescence units (RLUs) in the absence and presence of agonists. Each experiment was performed in quadruplicate and independently repeated at least three times ($N > 3$). For experiments involving comparisons between multiple sensors, equivalent sensor expression was first verified using fluorescence measurements (see previous section) and data for all four sensors were collected together (Figure 2.5).

IP_1 assays:

HEK293T cells expressing the indicated sensor were harvested 28–32 h post transfection (XtremeGENE HP) to assess IP_1 levels using the IP-One HTRF assay kit (Cisbio). Cells were gently suspended in their original media, counted using a hemocytometer, and spun down (350 g, 3min). An appropriate volume of Buffer B (StimB buffer) was added to reach 3×10^6 cells mL^{-1} density. Where indicated, cells were pre-incubated with 1 μM of the $A_{2B}R$ selective antagonist, PSB 1115 (PSB) for 30 min at 37 °C. Cells were incubated with 100 μM of CPA or NECA (for A_1R) or 100 μM of 2-AG or WN (for CB_1) at 37 °C for a total incubation time of 30 or 120 min. The manufacturer's protocol was modified to achieve a high signal to noise ratio as follows: 70 μL of suspension was incubated for one hour with 2 μL IP_1 conjugated to d2 dye diluted in 13 μL of lysis buffer (Cisbio) and 2 μL terbium cryptate-labeled anti-IP_1 monoclonal antibody also diluted in 13 μL of lysis buffer. 80 μL of each reaction suspension was then transferred and split between 4 wells (20 μL/well) on a 384-well opaque plate. IP_1 spectra were collected by exciting samples at 340 nm (bandpass 15 nm). Emission counts were recorded from 600–700 nm using a long pass 475 nm filter (FSQ GG475, Newport). Raw IP_1 signal was calculated as the ratio of fluorescence emissions at 665nm and 620nm. Data were corrected by subtracting the untransfected IP_1 ratio from cells expressing transfected sensor. Data are presented as a change in IP_1 ratio following drug treatment. Each experiment included four repeats per condition and was independently repeated at least three times (N>3).

Statistical Analysis:

Data are represented as mean values ±S.E.M. All experiments were repeated for at least three independent trials, with 3–6 technical repeats per condition (N>3). Statistical analysis was performed using GraphPad Prism 7.0c (Graphpad Software, Inc.). To assess significance across experimental repeats, pooled or un-pooled data underwent subsequent pairwise ANOVA analysis. Tukey's post hoc test was performed to assess significance when evaluating comparisons between multiple conditions with p-values *p≤0.05; **p≤0.01; ***p≤0.001; ****p≤0.0001; *****p≤0.00001.

CHAPTER 3: Dissecting β-Cardiac Myosin and Cardiac Myosin-Binding Protein C Interactions using a Nanosurf Assay

3.1. Introduction:

Cardiac myosin-binding protein C (cMyBP-C) is a large, multidomain thick filament-associated sarcomeric protein that modulates cardiac muscle contractility by tuning the speed and efficiency of contraction and relaxation (M.J. Previs et al. 2012; Moss, Fitzsimons, and Ralphe 2015; S. P. Harris, Lyons, and Bezold 2011). Despite almost 50 years since its discovery (Starr and Offer 1971; Offer, Moos, and Starr 1973), the mechanisms by which cMyBP-C modulates contractility, including its binding partners and the associated regulatory mechanisms, are not completely understood. The importance of cMyBP-C in regulating contraction was first appreciated in the 1990s when two mutations in *MYBPC3*, the gene encoding cMyBP-C, were shown to cause hypertrophic cardiomyopathy (HCM), a heritable heart condition characterized by left ventricular hypertrophy and diastolic dysfunction (Bonne et al. 1995; Watkins et al. 1995). Since then, over 350 *MYBPC3* mutations have been identified in HCM patients, and it has become the most prominent gene linked to HCM (Carrier et al. 2015). The discovery of these mutations- including nonsense, frameshift, and missense mutations distributed across the protein- have provided substantial motivation towards understanding the role of cMyBP-C in the sarcomere (S. P. Harris, Lyons, and Bezold 2011). However, despite this increased interest and established importance of cMyBP-C in regulating contraction, the mechanisms by which cMyBP-C regulates contraction have largely remained elusive due to experimental challenges in studying the complex, transient, weak interactions of cMyBP-C within the sarcomere.

Existing studies suggest that cMyBP-C modulates cardiac muscle contractility by sensitizing the thin filament to calcium, while slowing shortening velocity through interactions with actin and/or myosin (M.J. Previs et al. 2012; Mun et al. 2014; Heling, Geeves, and Kad 2020; S. P. Harris 2021). cMyBP-C exists in two regions of the muscle sarcomere A-band, in 7-9 stripes spaced 43 nm apart. This aligns with the 43 nm helical myosin head repeat on the thick filament (Flashman et al. 2004; Luther et al. 2008; M.J. Previs et al. 2012; Lee et al. 2015). cMyBP-C contains 11 subdomains, named sequentially C0-C10, and is anchored to the thick filament backbone at its C-terminus by a high-affinity LMM myosin binding site in C10 (Figure 3.1a) (Okagaki et al. 1993; Alyonycheva et al. 1997). The N-terminus extends away from the thick filament and engages in regulatory interactions with myosin and/or actin (M.J. Previs et al. 2012; Heling, Geeves, and Kad 2020; Luther et al. 2011; Rahmanseresht et al. 2021). The cardiac isoform contains a regulatory cMyBP-C motif or M-domain between C1 and C2 domains, which co-sedimentation assays have established to be the primary interacting region for myosin S2 (Gruen and Gautel 1999; Howarth et al. 2012; S. P. Harris et al. 2004; Ratti et al. 2011; Pfuhl and Gautel 2012). Studies with actin have found that the M-domain, as well as the C0, C1, and C2 domains, interact with actin (S. P. Harris et al. 2004; Kensler, Shaffer, and Harris 2011; S. P. Harris et al. 2016; M. Previs et al. 2015; Risi et al. 2021). The N- and C-terminal cMyBP-C interactions to the thin and thick filaments, respectively, may tether the two filaments thus functioning as a brake on shortening velocity at high calcium concentrations (M.J. Previs et al. 2012; Luther et al. 2011). In contrast, at low calcium concentrations, cMyBP-C appears to enhance contractility by sensitizing the thin filament to calcium (M.J. Previs et al. 2012; Michael J. Previs et al. 2016; Mun et al. 2014). While these studies have established multiple modes of cMyBP-C regulation of muscle function, their relative significance in regulating actomyosin motility is still a matter of debate. Additionally, cMyBP-C function itself may

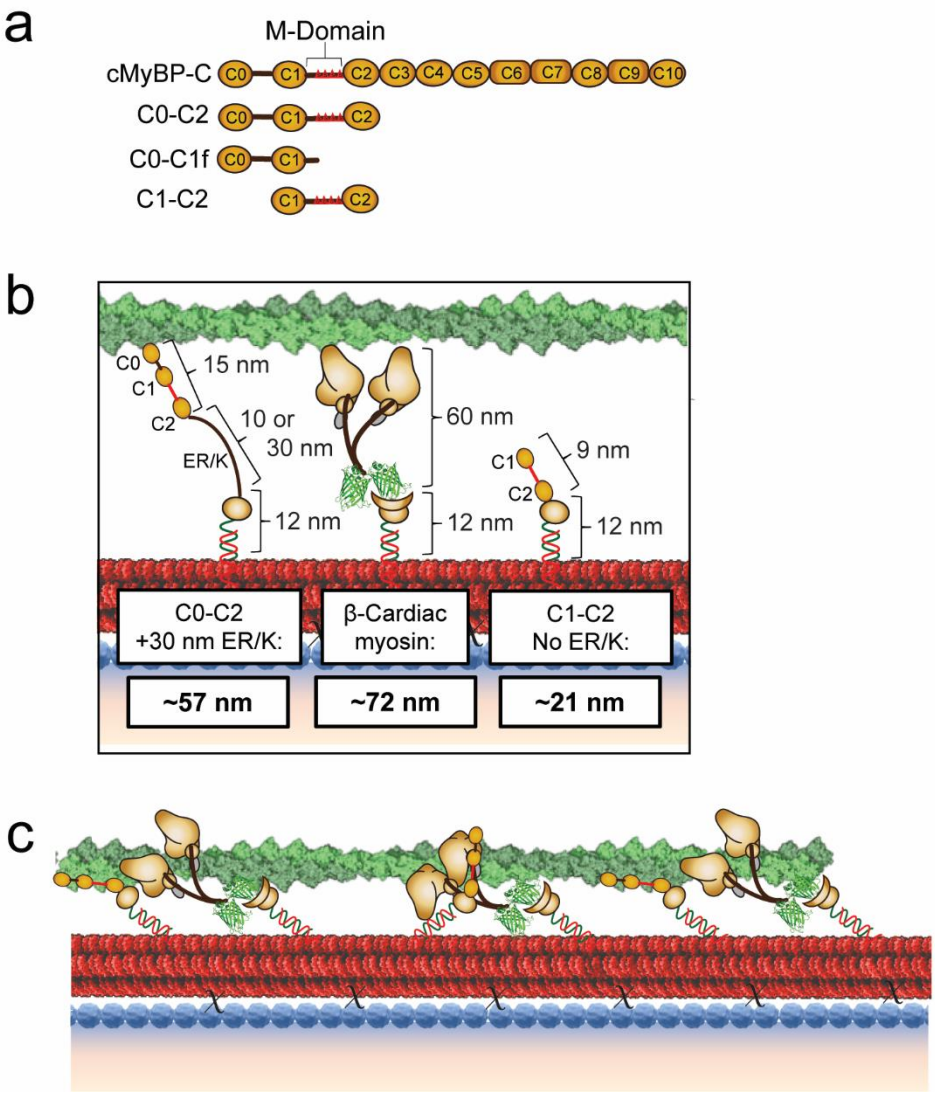

Figure 3.1. Flexibility in the Nanosurf Assay allows cMyBP-C Interactions with Actin and/or Myosin. a, Schematic of cMyBP-C domains C0-C10 containing the M-domain in the linker region between the C1 and C2 domains and the N-terminal fragments used, including C0-C2, C0-C1f, and C1-C2. **b**, Diagram showing lengths of representative cMyBP-C N-terminal fragments, C0-C2 (left, *yellow;* ~15 nm) and C1-C2 (right, *yellow;* ~9 nm) and recombinant human β-Cardiac myosin HMM (center, *brown;* ~60 nm) with C-terminal GFP attached to the nanotube (*red*) via GFP nanobody-SNAP. All proteins are attached to the nanotube via a SNAP protein labeled with oligo (~12 nm) complementary to the nanotube DNA handle. C0-C2 is shown with an encoded ER/K linker (left; 10 or 30 nm). Total approximate lengths of bound proteins are listed: C0-C2 + 30 nm ER/K (~57 nm), β-Cardiac myosin (~72 nm), and C1-C2 without an ER/K (~21 nm). **c**, Diagram depicting spatially staggered interaction sites on the actin filament (*green*) and possible cMyBP-C interactions with both actin (left, right C0-C2 fragments) and myosin S2 (center C0-C2 fragment).

be regulated as the M-domain contains four serines that are thought to be phosphorylated hierarchically to disrupt cMyBP-C interactions with actin filaments (Michael J. Previs et al. 2016; Shaffer, Kensler, and Harris 2009; A. Weith et al. 2012) or myosin (Gruen, Prinz, and Gautel 1999; Nag et al. 2017). Thus, phosphorylation of the M-domain may be a regulatory mechanism to control the number of active myosin heads in response to β-adrenergic stimulation (Nag et al. 2017).

The complex interactions of cMyBP-C with actin and myosin have made *in vitro* assessment of cMyBP-C challenging. Some *in vitro* motility studies have demonstrated inhibition of actomyosin motility by a variety of cMyBP-C N-terminal fragments (A. Weith et al. 2012; M.J. Previs et al. 2012; Razumova et al. 2006). However, mechanistic interpretation of these assays is limited by a lack of control over protein stoichiometry and orientation. Likewise, single molecule and solution assays do not capture the unique architecture of motor ensembles or cMyBP-C interactions as they exist in the sarcomere. To overcome these limitations, we utilized DNA nanotechnology to build a synthetic nanostructure that would allow systematic *in vitro* dissection of sarcomeric interactions, with control over protein type, stoichiometry, and spacing (Hariadi et al. 2015). Ten-helix DNA nanotubes were engineered with protein attachment strands every 14 nm corresponding to the 14.3 nm vertical spacing between two adjacent myosin molecules on the native thick filament as in the sarcomere (Figure 3.2a) (Hariadi et al. 2015). With expressed myosin linked to the nanotube, these nanotubes can then be attached to a surface so that actin filament gliding assays can be performed with precisely controlled molecular motor populations, yielding a more accurate and interpretable way to assess ensemble motor function in health and disease. We have validated this approach with high duty-ratio myosins V and VI, which spend a large portion of their ATPase cycle strongly bound to actin in the force generating state (Hariadi et al. 2015). However, using

the S1 fragment of β-cardiac myosin on DNA nanotubes (Hariadi et al. 2015), due to its very low duty ratio (~0.05) (Uyeda, Kron, and Spudich 1990; D. E. Harris and Warshaw 1993), very low actin-landing rates were observed, thus limiting the utility of this assay to compare and contrast the impact of different cMyBP-C domains or sarcomeric mutations on actomyosin motility.

In this study, we overcame the low duty ratio limitation by combining the DNA nanotube assay with the standard *in vitro* motility surface assay into one, which we refer to as the "nanosurf" assay. We used this assay to examine the potential binding partner and mechanical interactions between β-cardiac myosin and cMyBP-C when placed in spatially defined patterns on DNA nanotubes. By this approach, we initially characterized the motile properties of β-cardiac myosin HMM and S1 fragments using both actin and calcium-activated regulated thin filaments. Consistent with our previous results for myosin V, VI, and β-cardiac myosin S1, we found no significant differences in mean actin or regulated thin filament velocities when β-cardiac myosin HMM or S1 was spaced at 14 nm versus 28 nm on the nanotube (Hariadi et al. 2015). Using β-cardiac myosin HMM spaced at 28 nm intervals, cMyBP-C N-terminal fragments were interdigitated on the nanotube. We found that the incorporation of C0-C2 or C1-C2 fragments (Figure 3.1a) significantly inhibited actin or regulated thin-filament velocity 4-6 fold. Interestingly, we saw similar inhibition using a β-cardiac myosin S1 construct lacking the S2 region thought to interact with cMyBP-C. These results suggest that the interaction between cMyBP-C and actin may have a greater contribution to the inhibitory effects of cMyBP-C compared to the myosin interaction. In addition, we found a 3-fold proportional reduction in this inhibition using a phosphomimetic C0-C2 fragment, where the four phosphorylatable serines in the M-domain were replaced with aspartic acids, highlighting the regulatory importance of this domain. Further, we did not see inhibition of

actomyosin motility with a C0-C1f fragment lacking the majority of the M-domain (Figure 3.1a), further establishing the importance of this domain. Taken together, the nanosurf assay recapitulates the slowing of actomyosin motility by cMyBP-C. We have therefore established the β-cardiac myosin synthetic thick filament as a tool for precisely manipulating the spatially dependent interactions of cMyBP-C, thereby helping define the dynamic equilibrium of binding partner interactions that are critical to the modulatory capacity of cMyBP-C within the muscle sarcomere.

3.2. Nanosurf Assay

3.2.1. Characterization of Nanosurf Motility Assay**:**

We previously highlighted the use of synthetic nanotube thick filaments as a tool to characterize the behavior of ensembles of myosin motor proteins (Hariadi et al. 2015). Our previous study primarily utilized two different highly processive unconventional myosins, V and VI. We did report an initial characterization of nanotube motility with recombinant β-cardiac myosin S1, demonstrating proof-of-concept of this assay for muscle myosins. However, the broader application of this assay to cardiac myosin was limited by the infrequent actin gliding events, consistent with the low duty ratio of cardiac myosins (Figure 3.2b). Therefore, in this study we developed the ‘nanosurf’ assay, with myosin present on both the nanotube and the surrounding coverslip surface (Figure 3.2c). The presence of myosin on the coverslip surface recruits actin filaments to the surface and greatly increases the probability that a motile actin filament will encounter and travel onto a nanotube. The previous format of the assay, with myosin restricted to the nanotube,

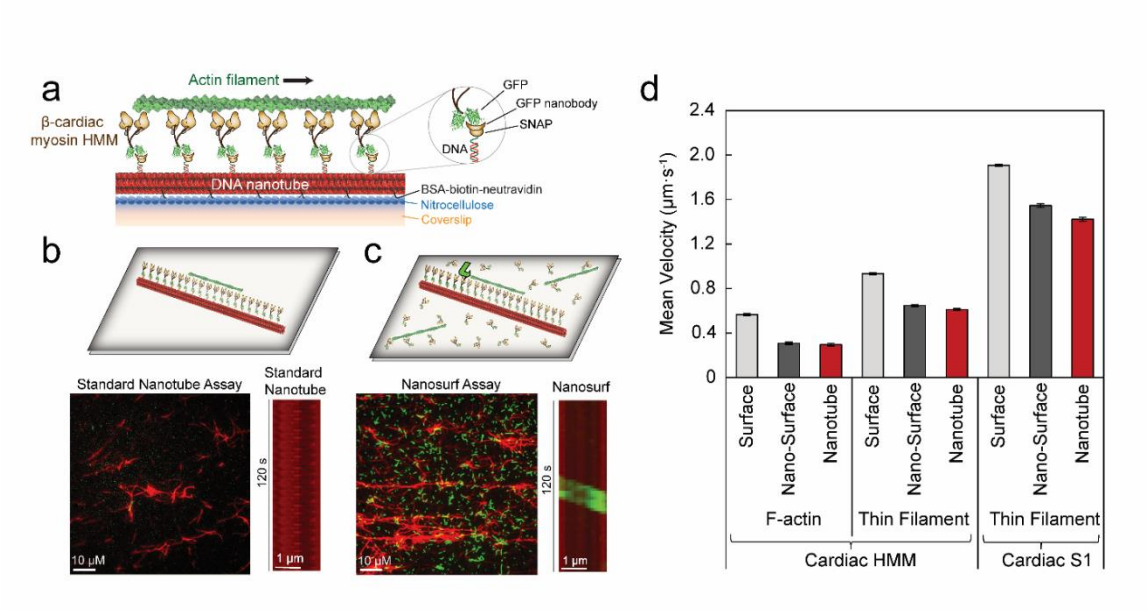

Figure 3.2. Optimization of Human β-Cardiac Myosin HMM Nanosurf Assay. a, Schematic of the β-cardiac myosin synthetic thick filament assay with recombinant human β-Cardiac myosin HMM (*brown*) with C-terminal GFP attached to the nanotube (*red*) via GFP nanobody-SNAP labeled with complementary oligo to the nanotube DNA handle (*inset*). Nanotubes are attached to the nitrocellulose-coated (*blue*) coverslip (*orange*) via BSA-biotin-neutravidin (*black X's*) **b**, Schematic of standard nanotube assay within a flow cell with motor bound to nanotubes only and nanotubes attached to a coverslip surface blocked with BSA (*top*). Field of view at 1000x (*bottom left*) and kymograph (*bottom right*) for standard nanotube assay with β-cardiac myosin HMM showing the low landing rate of actin filaments on the nanotube surface. **c**, Schematic (*top*) of nanosurf assay with motor bound to both the nanotubes and the coverslip surface and actin (*green*) can be observed gliding from the coverslip surface onto the nanotube (*green arrow*). Field of view at 1000x (*bottom left*) and kymograph (*bottom right*) for nanosurf assay with β-cardiac myosin HMM showing a higher landing rate for actin filaments on the nanotube surface. **d**, Velocities of F-actin (*left*) and regulated thin filaments (*middle*) with β-cardiac myosin HMM and regulated thin filaments with β-cardiac myosin S1 (*right*) on a standard *in vitro* motility surface (*light grey*), on the coverslip surface in the nanosurf assay (nano-surface; *dark grey*), and on the nanotubes in the nanosurf assay (*red*). Mean velocities represented as $\mu m \cdot s^{-1}$ ± SE. N = 132-390 filaments from 3-5 independent protein preparations per condition.

exhibited only a few actin filaments per camera field-of-view (Figure 3.2b). In contrast, the nanosurf assay provides about a two order-of-magnitude increase in motile events along DNA nanotubes during the ~2 min data acquisition time (Figure 3.2c). To distinguish motility surface filaments from those gliding on the DNA nanotube (i.e. nanotube motility), analysis of nanotube motility events were limited to actin filaments that travel across the coverslip surface and then turn sharply to glide across the nanotube (Figure 3.2c schematic, *green arrow*). In comparison, analysis of actin filament movement solely on the motility surface (i.e., nano-surface motility) was limited to that not in the vicinity of a

nanotube. In the nanosurf assay, the velocity of an F-actin filament traveling along a nanotube, with an ensemble of human β-cardiac myosin HMM spaced at 14 nm intervals (0.30 ± 0.01 μm·s^{-1}; n=132 pooled filaments from four independent protein preparations), is similar to the velocity of an F-actin filament traveling across the human β-cardiac myosin HMM coated coverslip surface (nano-surface; 0.31 ± 0.01 μm·s^{-1}; n=139 filaments from four protein preparations). However, these velocities were significantly lower than those obtained, using matched β-cardiac myosin preparations, using a standard *in vitro* motility surface gliding assay (Figure 3.2d "surface", *light grey*; 0.57 ± 0.01 μm·s^{-1}; n=390 filaments). Hence, to account for any surface effects on actin gliding speeds, all future comparisons are made using matched nanosurf assays with equivalent assay conditions. These trends were also observed with fully activated (pCa 5), calcium-regulated, native thin filaments with either β-cardiac myosin HMM and or β-cardiac S1 (data from three independent protein preparations of each subfragment) (Figure 3.2d). With β-cardiac myosin HMM, thin filaments had an *in vitro* motility surface velocity of 0.93 ± 0.01 μm·s^{-1} (n=300 filaments), a nano-surface velocity of 0.65 ± 0.01 μm·s^{-1} (n=206 filaments), and a nanotube velocity of 0.61 ± 0.01 μm·s^{-1} (n=206 filaments). The increased velocity for thin filaments when compared to F-actin (Figure 3.2d), regardless of the myosin subfragment, has been described previously (Fraser and Marston 1995). With β-cardiac myosin S1, the regulated thin filaments had an *in vitro* motility surface velocity of 1.91 ± 0.01 μm·s^{-1} (n=359 filaments), a nano-surface velocity of 1.55 ± 0.02 μm·s^{-1} (n=270 filaments), and a nanotube velocity of 1.42 ± 0.02 μm·s^{-1} (n=270 filaments). In contrast, the average velocity of F-actin filaments in a standard *in vitro* motility surface assay with β-cardiac myosin S1 was 1.24 ± 0.01 μm·s^{-1} (n=360 filaments), once again demonstrating slower velocities associated with F-actin when compared to activated thin filaments. Taken together, these data provide baseline motility conditions for the nanosurf assay and establish the nanosurf assay as a robust method to study β-cardiac myosin ensembles.

3.2.2. Motor Spacing Does Not Impact β-Cardiac HMM Motility**:**

Next, we examined the impact of β-cardiac myosin motor spacing on actin gliding speeds. In our previous study with myosin V, myosin VI, and β-cardiac myosin S1, in a standard nanotube assay, we found no significant differences in nanotube ensemble velocity when myosin was spaced at 14 nm compared to 28 nm (Hariadi et al. 2015). Using the nanosurf assay with human β-cardiac myosin HMM or S1 spaced at either 14 nm or 28 nm intervals (Figure 3.3a,b), the velocities of either F-actin or regulated thin filaments traveling on nanotubes were quantified (Figure 3.3c). With HMM, we found no significant difference between F-actin velocities (data from five independent protein preparations) at 14 nm (0.30 ± 0.01 μm·s^{-1}; n=162 filaments) versus 28 nm (0.32 ± 0.01 μm·s^{-1}; n=143 filaments), as visually represented in the kymographs in Figure 3.3d. Similarly, there was no significant difference in regulated thin filament velocities at pCa 5 with human β-cardiac myosin HMM or S1 (data from three independent protein preparations of each

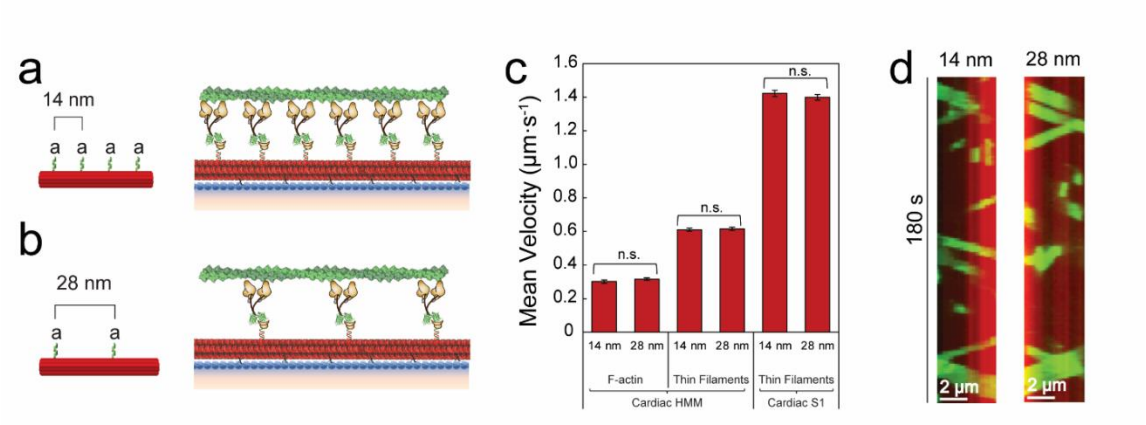

Figure 3.3. Motor Spacing Does Not Impact β-Cardiac HMM Motility. Schematic of the synthetic thick filament with nanotube motor spacing of 14 nm (**a**) or 28 nm (**b**). **c,** Velocities of F-actin (left) and regulated thin filaments (middle) on nanotubes decorated with β-cardiac myosin HMM or regulated thin filaments on nanotubes decorated with β-cardiac myosin S1 (right) at 14 or 28 nm spacing in the nanosurf assay. **d,** Kymographs of F-actin filaments (green) traveling on a nanotube (red) with β-cardiac myosin HMM at 14 nm (left) or 28 nm (right) spacing. Mean velocities represented as μm·s-1 ± SE. N = 143-270 filaments from 3-5 independent protein preparations per condition. Comparisons were performed using Student's t-test. n.s. = not significant.

subfragment). With the HMM spaced at 14 nm versus 28 nm, regulated thin filament velocities were 0.61 ± 0.01 μm·s^{-1} (n=206 filaments) and 0.62 ± 0.01 μm·s^{-1} (n=175 filaments), respectively. With S1 spaced at 14 nm versus 28 nm, regulated thin filament velocities were 1.42 ± 0.02 μm·s^{-1} (n=270 filaments) and 1.40 ± 0.02 μm·s^{-1} (n=240 filaments), respectively. These data indicate that 28 nm spaced myosins on nanotubes can be used with interdigitated cMyBP-C so that any effects of cMyBP-C on actin filament velocities cannot be attributed to myosin density/spacing on the nanotube.

3.2.3. C0-C2 Inhibits β-Cardiac HMM and S1 Nanotube Motility**:**

We used the nanosurf assay as a tool to investigate the possible role of cMyBP-C in the sarcomere. The cMyBP-C protein contains 11 domains, C0-C10, with the N-terminal domains C0-C2 thought to be most critical for its regulatory interactions with actin and myosin (Figure 3.4a) (M.J. Previs et al. 2012; Heling, Geeves, and Kad 2020; Luther et al. 2011; Rahmanseresht et al. 2021). Further, the M-domain linker between the C1 and C2 domains contains 4 phosphorylatable serines that, once phosphorylated in response to adrenergic stimuli, may modulate cMyBP-C's impact on cardiac contractility (Michael J. Previs et al. 2016; Shaffer, Kensler, and Harris 2009; A. Weith et al. 2012; Gruen, Prinz, and Gautel 1999; Nag et al. 2017). Hence, the C0-C2 N-terminal fragment was used to simulate the influence of the full-length cMyBP-C. Human β-cardiac myosin spaced at 28 nm intervals (Figure 3.4b, *myosin only*) on the nanotube was interdigitated with C0-C2, also at 28 nm intervals, (Figure 3.4b, +*C0-C2*) containing either no ER/K α-helical linker, a 10 nm ER/K α-helical linker, or a longer 30 nm ER/K α-helical linker to potentially facilitate cMyBP-C interactions with both actin and myosin (Figure 3.1b,c). As shown in

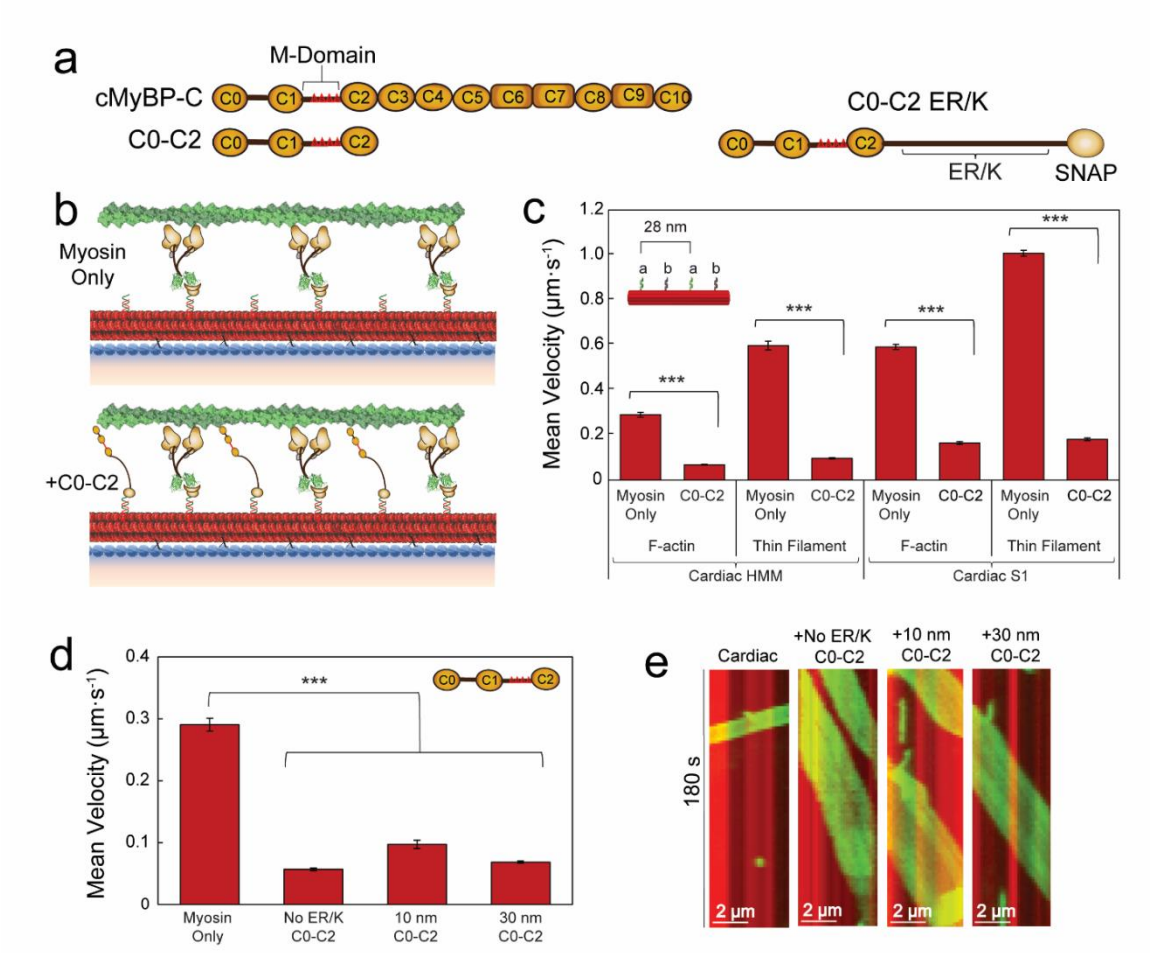

Figure 3.4. C0-C2 Inhibits β-Cardiac HMM and S1 Nanotube Motility. a, Schematic of cMyBP-C domains C0-C10 with the M-domain (red triangles) containing 4 phosphorylatable serines in the linker region between the C1 and C2 domains and the N-terminal fragment used, C0-C2. C0-C2 schematic (right) shown with the encoded ER/K linker and SNAP tag. **b,** Schematics of synthetic thick filaments with β-cardiac myosin HMM bound to oligo a' at 28 nm intervals (myosin only, top) and interdigitated C0-C2 containing M-domain, bound to oligo b' (bottom). **c,** Velocities of F-actin and regulated thin filaments on nanotubes decorated with β-cardiac myosin HMM (left) or β-cardiac myosin S1 (right) bound to oligo a' alone versus myosin +C0-C2 containing a 30 nm ER/K bound to oligo b' in the pattern shown (inset). **d,** Mean velocities of F-actin filaments on nanotubes decorated with β-cardiac myosin HMM only versus β-cardiac HMM nanotubes with interdigitated C0-C2 (inset) containing no ER/K helix, a 10 nm ER/K helix, or a 30 nm ER/K helix. **e,** Kymographs of F-actin filaments (green) traveling on a nanotube (red) with β-cardiac myosin HMM only versus cardiac nanotubes with interdigitating C0-C2 containing no ER/K helix, a 10 nm ER/K helix, or a 30 nm ER/K helix. Mean velocities represented as μm·s-1 ± SE. N = 82-514 filaments from 3-8 independent protein preparations per condition. Significance calculated using Student's t-test or one-way ANOVA where appropriate. Significance is denoted as ***P ≤ 0.001.

Figure 3.4c, when C0-C2 with a 30 nm ER/K linker was present on a nanotube decorated with β-cardiac myosin HMM (data from eight independent protein preparations), ensemble velocity of F-actin was reduced 4-fold from 0.29 ± 0.01 μm·s^{-1} (n=211 filaments) to 0.07 ± 0.002 μm·s^{-1} (n=389 filaments). Likewise, with the presence of C0-C2, regulated thin filament velocity at pCa 5 on β-cardiac myosin HMM nanotubes (data from three independent protein preparations) was reduced 6-fold from 0.60 ± 0.02 μm·s^{-1} (n=171 filaments) to 0.10 ± 0.003 μm·s^{-1} (n=223 filaments). These effects are comparable to a previously reported ~ 5-fold decrease in actin gliding speeds in a standard *in vitro* motility assay with chicken skeletal muscle myosin and cMyBP-C adsorbed at high concentrations (0.4 μM) (A. Weith et al. 2012). We found no significant impact of the ER/K linker or linker length on the inhibitory capacity of C0-C2, as all C0-C2 ER/K constructs inhibited F-actin nanotube motility ~4-fold (Figure 3.4d; data from n=82-389 filaments pooled from 3-8 independent protein preparations), as visually represented in the kymographs in Figure 3.4e. Together, these studies demonstrate the robust use of the nanosurf assay to recapitulate the effects of cMyBP-C on actomyosin motility.

To distinguish between cMyBP-C effects being imparted through its interaction with actin and/or myosin, we utilized nanotubes decorated with β-cardiac myosin S1, which lacks the S2 domain that has been implicated as the primary cMyBP-C interacting region in myosin (Gruen and Gautel 1999; Howarth et al. 2012; S. P. Harris et al. 2004; Ratti et al. 2011; Pfuhl and Gautel 2012). β-cardiac S1 and HMM displayed similar velocity inhibition with the C0-C2 fragment (Figure 3.4c). Specifically, the presence of C0-C2 with β-cardiac S1 (data from three independent protein preparations) reduced F-actin velocity almost 4-fold (0.59 ± 0.01 μm·s^{-1} to 0.16 ± 0.01 μm·s^{-1}; n=180 and 267, respectively) and regulated thin filament velocity almost 6-fold (1.01 ± 0.01 μm·s^{-1} to 0.18 ± 0.01 μm·s^{-1}; n=450 and 514, respectively). These data suggest that C0-C2 interactions with actin,

rather than myosin S2, are the primary determinant of its effects on actin gliding speed in the nanosurf assay. The significance of C0-C2-actin interactions is also evident in the extent of actin recruitment to nanotubes. When the C0-C2 fragment was attached to the nanotubes without motor, it pulled more F-actin filaments (237.0 filaments per field of view ± 37 standard deviation; Figure 3.5a) onto nanotubes than motor in the absence of C0-C2 (146.7 filaments per field of view ± 22 standard deviation; Figure 3.5b). In contrast, undecorated nanotubes alone did not pull down actin filaments. The presence of both C0-C2 and β-cardiac myosin HMM on nanotubes yielded greater actin recruitment on nanotubes than either of them alone (326.7 filaments per field of view ± 116 standard deviation; Figure 3.5c). Robust actin recruitment to nanotubes was still seen by C0-C2, even when the surface was blocked in the standard nanotube assay (Figure 3.5d).

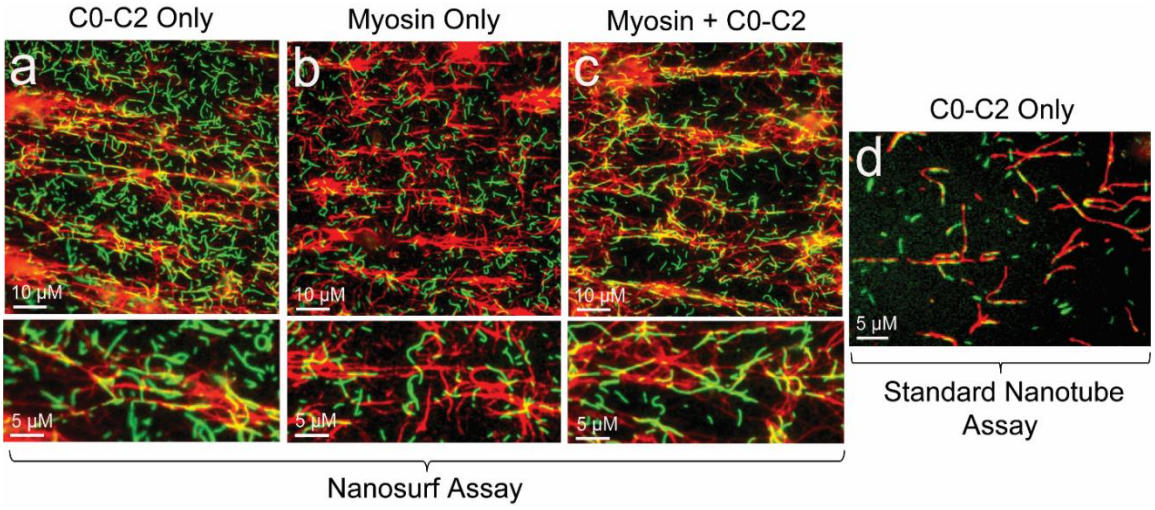

Figure 3.5. cMyBP-C C0-C2 N-terminal Fragment Recruits Actin onto Nanotubes. a-c, We examined actin (*green*) recruitment onto nanotubes (*red*) in the nanosurf assay. Nanotubes were labeled with **a,** C0-C2 only (containing 30 nm ER/K, with fragments spaced at 28 nm intervals), **b,** β-cardiac myosin HMM only (myosin spaced at 28 nm intervals), or **c,** β-cardiac myosin HMM + C0-C2 (C0-C2 contained 30 nm ER/K; myosin was spaced at 28 nm intervals and interdigitated with C0-C2 for a final spacing of 14 nm between myosin and C0-C2 proteins). The top panels in **a-c** show the field of view at 1000x with selected enlargements shown in the bottom panels. **d**, Actin recruitment was also examined using standard nanotube assay blocking conditions and nanotubes labeled with C0-C2 + 30 nm ER/K.

3.2.4. cMyBP-C M-Domain Essential for Inhibition

cMyBP-C M-domain Phosphorylation and Structurally Dependent Inhibition of β-Cardiac Myosin HMM and S1 Nanotube Motility:

To investigate the role of individual cMyBP-C domains in the inhibition of actomyosin motility, we examined alternative N-terminal fragments, C0-C1f and C1-C2 in our nanosurf assay (Figure 3.6a). The C0-C1f fragment contains the C0 and C1 domains, as well as the first 17 amino acids of the M-domain (Figure 3.6a). This segment of the M-domain contains several arginine residues proposed to be essential for cMyBP-C interaction(s) resulting in actomyosin inhibition (Figure 3.6b, *left, inset*) (A. Weith et al. 2012; Bhuiyan et al. 2012). However, it lacks the four phosphorylatable serines found in the M-domain (Figure 3.6a) (A. Weith et al. 2012; A. E. Weith et al. 2012). The C1-C2 fragment contains the C1 and C2 domains, as well as the entire M-domain linker region between C1 and C2. Using the nanosurf assay, human β-cardiac myosin spaced at 28 nm intervals on the nanotube was interdigitated with either C0-C1f (Figure 3.6b, *left*), C1-C2 (Figure 3.6b, *right*), or C0-C2, each spaced at 28 nm. The presence of C0-C1f did not significantly impact F-actin or thin filament motility driven by either β-cardiac myosin HMM or S1 (Figure 3.6c; data from n=100-274 filaments pooled from 3-4 independent protein preparations). In contrast to C0-C1f, the C1-C2 fragment was as inhibitory of F-actin and thin filament motility as C0-C2 (Figure 3.6d). Specifically, both C1-C2 and C0-C2 reduced F-actin velocity on β-cardiac myosin HMM nanotubes ~ 4-fold, and reduced thin filament velocity on β-cardiac myosin S1 nanotubes ~8-fold (Figure 3.6d, e; data from n=90-270 filaments pooled from 3-4 independent protein preparations). These data are consistent with similar inhibitory effects observed with the addition of C1-C2 or C0-C2 to a standard *in vitro* motility assay (A. Weith et al. 2012; Razumova et al. 2006).

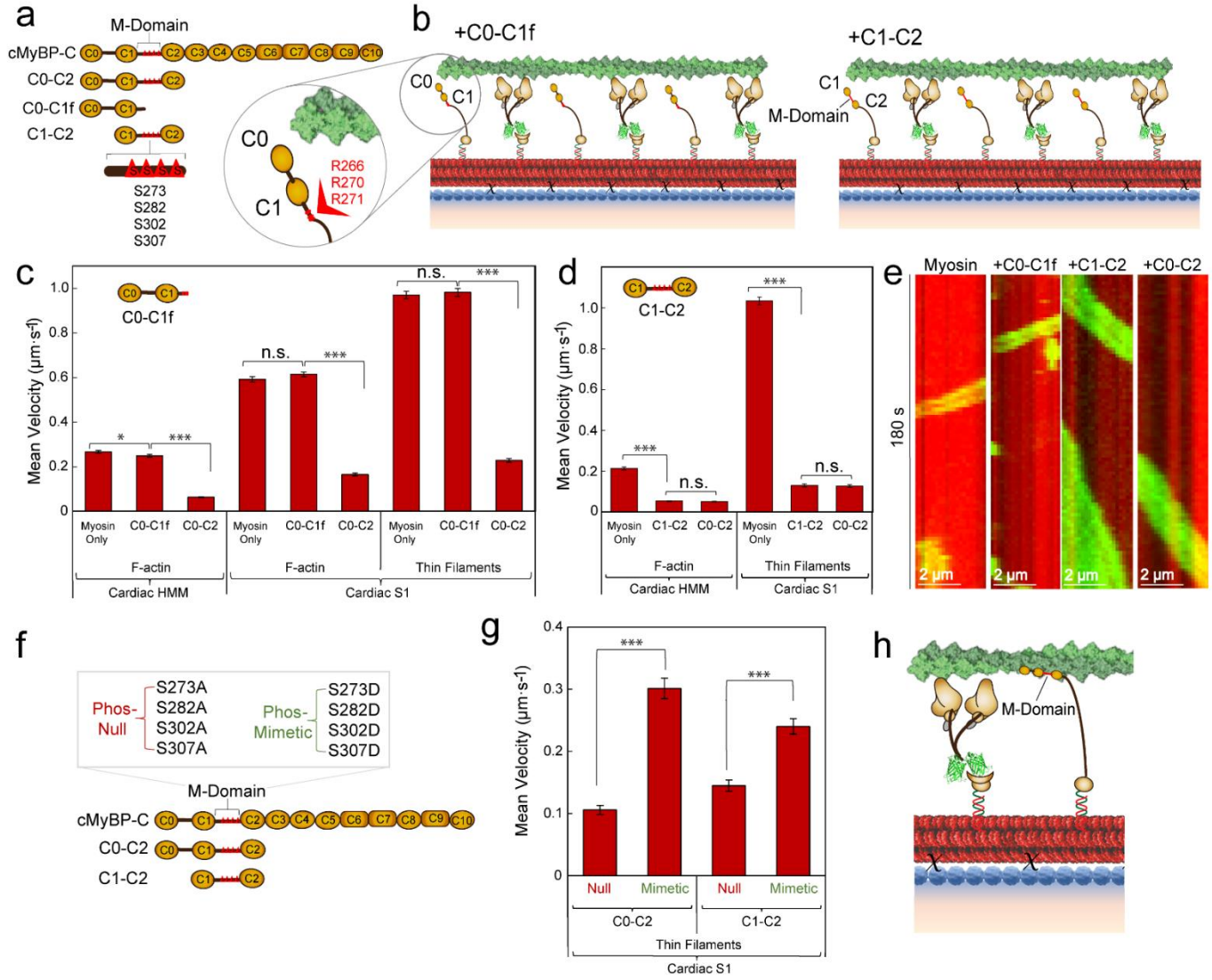
a
M-Domain
cMyBP-C
C0-C2
C0-C1f
C1-C2
S273
S282
S302
S307
C0
C1
R266
R270
R271
b
+C0-C1f
+C1-C2
M-Domain
c
C0-C1f
Mean Velocity (μm·s-1)
n.s.
***
*
Myosin Only
C0-C1f
C0-C2
F-actin
Cardiac HMM
Cardiac S1
Thin Filaments
d
C1-C2
e
Myosin
+C0-C1f
+C1-C2
+C0-C2
180 s
2 μm
f
Phos-Null
S273A
S282A
S302A
S307A
Phos-Mimetic
S273D
S282D
S302D
S307D
g
Null
Mimetic
h

Figure 3.6. cMyBP-C M-domain Essential for Inhibition of β-Cardiac Myosin HMM and S1 Nanotube Motility. a, Schematic of cMyBP-C domains C0-C10 containing the M-domain (*red triangles*) in the linker region between the C1 and C2 domains and the N-terminal fragments used, including C0-C2, C0-C1f, and C1-C2. The four phosphorylatable serines in the M-domain are represented by red triangles (S273, S282, S302, S307). **b,** Schematics of synthetic thick filaments with β-cardiac myosin HMM bound to oligo a' at 28 nm intervals and interdigitated C0-C1f (*left*) or C1-C2 (*right*) containing the entire M-domain, bound to oligo b'. C0-C1f (*inset*) contains the first 17 amino acids of the M-domain including several arginine residues (R266, R270, R271) oriented away from the actin filament. **c**, Velocities of F-actin on nanotubes decorated with β-cardiac myosin HMM (*left*) and either F-actin (*middle*) or regulated thin filaments (*right*) on nanotubes decorated with β-cardiac myosin S1. β-cardiac nanotubes were either labeled with the motor alone or interdigitated with C0-C1f or C0-C2 containing 30 nm ER/K helices. **d**, Velocities of F-actin on nanotubes decorated with β-cardiac myosin HMM (*left*) and regulated thin filaments on nanotubes decorated with β-cardiac myosin S1 (*right*) versus β-cardiac nanotubes with interdigitated C1-C2 or C0-C2 containing 30 nm ER/K helices. **e**, Kymographs of F-actin filaments (*green*) traveling on a nanotube (*red*) with β-cardiac myosin HMM alone versus cardiac nanotubes with interdigitating C0-C1f, C1-C2, or C0-C2. **f,** Schematic of cMyBP-C domains C0-C10 with the M-domain (*red triangles*) containing 4 phosphorylatable serines in the linker region between the C1 and C2 domains mutated to alanines (phospho-null) or aspartic acids (phospho-mimetic) within the C0-C2 and C1-C2 N-terminal fragments. **g**, Mean nanotube velocities of regulated thin filaments on nanotubes decorated with β-cardiac myosin S1 and interdigitating phospho-null or phospho-mimetic C0-C2 (*left*) or C1-C2 (*right*) containing 30 nm ER/K helices. **h,** Schematic of β-cardiac myosin (brown) synthetic thick filament with cMyBP-C N-terminal fragment (yellow) bound to actin (green), functioning as a tether between thick and thin filaments and reducing velocity. Mean velocities represented as $\mu m \cdot s^{-1}$ ± SE. N = 90-410 filaments from 3-4 independent protein preparations per condition. Significance was calculated using Student's t-test. Significance is denoted as $*P \leq 0.05$, $***P \leq 0.001$.

The C1-C2 fragment contains the entire M-domain, including the phosphorylatable serines (S273, S282, S302, S307) that regulate cardiac contractility. Hence, we generated phospho-null (Ser to Ala) and phospho-mimetic (Ser to Asp) C0-C2 and C1-C2 N-terminal fragments (Figure 3.6f), as previously reported for the C0-C3 fragment (M.J. Previs et al. 2012; A. E. Weith et al. 2012). Mass spectrometry suggests that our insect-cell expressed N-terminal fragments are not phosphorylated (*data not shown*). The phospho-null C0-C2 and C1-C2 fragments inhibited thin filament velocity over β-cardiac myosin S1 nanotubes to a similar extent as unmodified fragments (Figure 3.6g; data from n=240-270 filaments pooled from three independent protein preparations). However, the phospho-mimetic C0-C2 and C1-C2 mutants exhibited less inhibition (Figure 3.6g), as previously reported for the identical phosphomimetic substitutions in the C0-C3 fragment used in the *in vitro* motility assay (M.J. Previs et al. 2012; A. E. Weith et al. 2012). These results highlight the

importance of the phospho-serines in regulating cMyBP-C mediated inhibition of β-cardiac myosin function.

3.3. Summary and Discussion**:**

In this study, we utilized DNA nanotechnology to recapitulate the sub-structure of the cardiac sarcomere, by creating an artificial myosin thick filament with incorporated cMyBP-C. Using nanotube thick filaments comprised of spatially-defined recombinant human β-cardiac myosin subfragments with and without interdigitated cMyBP-C N-terminal fragments, we characterized the velocity of either F-actin or regulated thin filaments as a means of defining the mechanical effect of actomyosin/cMyBP-C interactions. Using an assortment of cMyBP-C N-terminal fragments, our results suggest that the binding of cMyBP-C to actin may underly the inhibitory effect of cMyBP-C on actomyosin motility over nanotubes (Figure 3.6h) and that the cMyBP-C M-domain is crucial to this inhibition. Further, phosphomimetic cMyBP-C fragments, displaying diminished inhibition of thin filament velocity on nanotubes, demonstrate the established modulatory role of M-domain phosphorylation on cMyBP-C function (M.J. Previs et al. 2012; Shaffer, Kensler, and Harris 2009; Barefield and Sadayappan 2010; Michael J. Previs et al. 2016). Together, these results establish the nanosurf technology as a model system for dissecting protein interactions in the sarcomere.

The Nanosurf Assay:

The nanosurf assay described here overcomes a key limitation of our previously reported standard nanotube assay, where only myosin-labeled nanotubes exist on the

coverslip surface (Hariadi et al. 2015). While the standard nanotube assay is well suited to study high duty ratio motors, which readily recruit actin filaments from solution and display abundant motility, the use of low duty ratio, β-cardiac myosin nanotubes is limited by infrequent engagement of actin filaments from the surrounding solution (Figure 3.2b). To overcome this challenge, we seeded β-cardiac myosin subfragments at a sufficient density on the surface to which the nanotubes were attached (see Methods) so that the coverslip surface myosin recruited actin filaments from solution, which then encountered the neighboring nanotubes, substantially enhancing the frequency of nanotube motile events (Figure 3.2c). The actin gliding speeds on nanotubes and the surrounding surface are indistinguishable, however, these speeds are significantly reduced compared to that observed in the standard *in vitro* motility assay (Figure 3.2d). These data suggest that the surface conditions and/or the mode of myosin attachment likely contribute to the lower speeds in the nanosurf assay. Specifically, the addition of flexible joints, associated with the myosin attachment strategy (see Methods), may reduce the efficient transfer of myosin displacements to the actin filament, leading to slower velocities. Hence, we focused on motility comparisons between conditions only within the nanosurf assay. In addition, similar flexibility by the addition of a variable length ER/K α-helical linker to the cMyBP-C fragment ensured that cMyBP-C on the nanotube was spatially free to interact with β-cardiac myosin and/or actin filaments (Figure 3.1b,c). Interestingly, the ER/K α-helical linker was not essential for the observed cMyBP-C effects on actin filament motility, as constructs lacking the ER/K α-helical linker demonstrated equivalent inhibition. Overall, the multiple rotational elements in the myosin and cMyBP-C attachment, combined with myosin's access to numerous sites along the actin filament (Figure 3.1c), yields significant conformational freedom without limiting protein-protein interactions.

cMyBP-C Modulates Actin Filament Motility on Cardiac Myosin Nanotubes:

The molecular basis for cMyBP-C's role in modulating cardiac contractility *in vivo* has relied on *in vitro* solution and motility studies that defined the capacity of cMyBP-C to slow thin filament velocity and to sensitize the thin filament to calcium (M.J. Previs et al. 2012; A. Weith et al. 2012; Razumova et al. 2006; Inchingolo et al. 2019; Michael J. Previs et al. 2016; Mun et al. 2014). More importantly, the cMyBP-C N-terminal domains encompassing C0-C2 within these assays were sufficient to recapitulate the function of whole cMyBP-C (M.J. Previs et al. 2012; A. Weith et al. 2012; Shaffer, Kensler, and Harris 2009; Kensler, Shaffer, and Harris 2011). However, the importance of stoichiometries and spatial relations between myosin and cMyBP-C within the native thick filament are lost in the standard *in vitro* motility assay, where monomeric myosin is non-specifically adhered to the motility surface with free floating cMyBP-C or its fragments in solution. Therefore, the use of native thick filaments from mouse cardiac tissue that maintained the myosin to cMyBP-C stoichiometry and spatial relations was critical to confirming that both thin filament slowing and calcium sensitization are mediated by cMyBP-C, but only within the thick filament C-zone where cMyBP-C resides. However, the native thick filament assay does not lend itself to systematic perturbations to the myosin or cMyBP-C for molecular structure-function studies due to the high cost of animal model design. The nanosurf assay fills this need by allowing the stoichiometry and spatial relations between myosin and cMyBP-C to be defined and by the relative ease in expression of human β-cardiac myosin and cMyBP-C fragments that decorate the nanotube surface. In fact, here we report a 1:1 ratio of human β-cardiac myosin HMM or S1 to various cMyBP-C N-terminal fragments spaced 14 nm apart and that the cMyBP-C N-terminus does inhibit thin filament motility on the nanotube surface.

We observed that slowing of F-actin or fully activated thin filament velocity by the C0-C2 N- terminal fragment was structurally localized to the C1-C2 domains, with the M-domain linker between C1 and C2 being a critical component (Figure 3.6d). The importance of the M-domain is emphasized by phosphomimetic replacement of four serines within the M-domain that reduce the observed slowing of thin filament velocity, as reported previously (M.J. Previs et al. 2012; A. E. Weith et al. 2012). To further characterize this regulatory domain, we utilized the C0-C1f fragment, which contains only the first 17 amino acids of the M-domain but lacks the four phosphorylatable serines (A. Weith et al. 2012; A. E. Weith et al. 2012). Interestingly, a previous study showed inhibition of thin filament velocity by C0-C1f in a standard *in vitro* motility assay, and it was proposed that several C-terminal arginine residues in this fragment may be particularly important for this inhibition (Figure 3.6b, *inset*) (Bhuiyan et al. 2012; A. Weith et al. 2012). The inability of the C0-C1f to slow thin filament velocity in our nanosurf assay (Figure 3.6c), despite the presence of several C-terminal arginine residues (Figure 3.6b, *inset*), further supports the importance of the entire M-domain. A potential source for this discrepancy is the weaker binding of C0-C1f to actin that manifests only when high concentrations of this fragment are used in the standard *in vitro* motility assay (A. Weith et al. 2012).

In vitro, both actin and myosin-binding have been described for the cMyBP-C N-terminus (Luther et al. 2011; Rahmanseresht et al. 2021; Gruen and Gautel 1999; S. P. Harris et al. 2004; Ratti et al. 2011; Kensler, Shaffer, and Harris 2011; S. P. Harris et al. 2016; M. Previs et al. 2015; Risi et al. 2021). Whether one or both of these binding partner interactions is responsible for the modulatory capacity of cMyBP-C is still a matter of debate. The myosin S2 domain was the first structural element identified in cMyBP-C binding (Gruen and Gautel 1999). Using the β-cardiac S1 fragment, which is

devoid of the S2 segment, on the nanotubes, substantial slowing of actin gliding speeds in the presence of the C0-C2 and C1-C2 fragments remained (Figure 3.6d). Although we cannot rule out binding of these fragments to the myosin regulatory light chain (Ratti et al. 2011) or to a yet defined region of the motor domain (Nag et al. 2017), the preponderance of data both here and in the literature (Rahmanseresht et al. 2021; M.J. Previs et al. 2012; Mun et al. 2014; Luther et al. 2011; Kensler, Shaffer, and Harris 2011; S. P. Harris et al. 2016; M. Previs et al. 2015; Risi et al. 2021; Michael J. Previs et al. 2016; Shaffer, Kensler, and Harris 2009) suggest that the cMyBP-C inhibitory effect *in vitro* may in large part be due to its interaction with actin. In fact, recent *in vivo* super-resolution data suggest that the cMyBP-C N-terminus in mouse myocardium resides predominantly near the thin filament regardless of the muscle's active state and that only when activated would the myosin head domain being in close enough proximity to interact with the cMyBP-C terminus (Rahmanseresht et al. 2021). The slowing of thin filament velocity may arise, in part, due to drag forces imposed by cMyBP-C binding and tethering the thin filament to the nanotube (Colson 2019), thereby slowing actomyosin kinetics (Greenberg, Shuman, and Ostap 2014; Sung et al. 2015). In addition, cMyBP-C may be competing with myosin for binding sites on actin, thus reducing the number of force generating motors, as suggested previously (Sam Walcott, Docken, and Harris 2015; S. P. Harris et al. 2016; Inchingolo et al. 2019; Saber et al. 2008).

Conclusion:

In conclusion, we have established the DNA synthetic thick filament nanosurf assay as a robust tool for the characterization of β-cardiac myosin and cMyBP-C interactions, mimicking sarcomeric architecture. We have recapitulated actomyosin inhibition by cMyBP-C N-terminal fragments on recombinant human β-cardiac myosin

DNA nanotubes and begun to dissect the mechanisms underlying contractile regulation by cMyBP-C. Our results emphasize the importance of the M-domain and its phosphorylation in regulating actomyosin motility. Our study also highlights the role of cMyBP-C N-terminal interactions with actin in regulating motility and suggests the actin-cMyBP-C interaction is the dominant interaction underlying actomyosin inhibition by cMyBP-C. Taken together, our results support a model where cMyBP-C tethers the thick and thin filaments at high calcium, imposing drag, and slowing thin filament velocity. Future studies can build on this foundation to examine other aspects of contractile regulation, including external load, on cMyBP-C function.

3.4. Materials and Methods:

DNA Nanotube and Benzyl-Guanine Oligonucleotide Preparation:

Cy5-labeled ten-helix DNA nanotubes composed of 40 single-stranded DNA tiles with 14 or 28 nm spacing between single-stranded protein binding handles were prepared with biotin strands for surface attachment using an annealing protocol as previously described (Hariadi et al. 2015). The nanotube DNA handles at 14 or 28 nm are designed to anneal to DNA strands bound to a SNAP protein encoded with the GFP nanobody. The SNAP protein binds benzyl-guanine treated DNA oligos. To prepare the benzyl-guanine oligo, benzyl-guanine NHS ester (BG-GLA-NHS; New England Biolabs, Ipswich, MA) was covalently linked to C6-amine oligonucleotides (with or without Cy3 modification, C6-amine-Cy3-a' or C6-amine-a'). This was accomplished by incubating 0.17 mM C6-amine-a' or C6-amine-b' with 11.6 mM BG-GLA-NHS in 0.1 M sodium

borate, pH 8.5 at 37°C for ~4 hours with rotation. The BG-labeled oligonucleotide was then purified twice through Illustra G-50 micro columns (GE Healthcare, Buckinghamshire, UK) equilibrated in 2 mM Tris, pH 8.5 since the primary amine reacts with any unreacted benzyl guanine. The final BG-labeled oligonucleotide concentration was determined by measuring Cy3 absorbance (for BG-Cy3-a' or BG-Cy3-b') or by estimating the concentration of single-stranded DNA (for BG-a' or BG-b') using a NanoDrop spectrophotometer (NanoDrop One^{C}, ThermoFisher, Waltham, MA).

GFP Nanobody–SNAP and Cardiac Myosin Binding-Protein C (cMyBP-C)-SNAP Preparation:

The DNA sequence for the GFP-nanobody was generated and synthesized by Genewiz (South Plainfield, NJ) as previously described (Sommese et al. 2016). The SNAP-tagged GFP nanobody construct contained from N- to C-terminus: the GFP nanobody, a flexible $(Gly\text{-}Ser\text{-}Gly)_2$ linker, the SNAP tag for oligonucleotide labeling, and both FLAG and 6xHis purification tags. N-terminal fragments (C0-C2, C0-C1f, or C1-C2) of the *Mus musculus* cardiac myosin-binding protein C cDNA were cloned into pBiex-1 and engineered with a C-terminal SNAP-FLAG-6xHis. C0-C2 and C1-C2 phospho-null or phospho-mimetic constructs were created by mutating S273, S282, S302, and S307 to alanines or aspartic acids, respectively. For cMyBP-C constructs containing a linker, either a 10 nm ER/K α-helical linker (derived from *Sus scrofa's* Myosin VI) or a 30 nm linker (derived from the Kelch-motif family protein, *Trichomonas vaginalis*), as previously characterized and described, were inserted between the cMyBP-C C-terminus and the N-terminus of the SNAP (Sivaramakrishnan and Spudich 2011; Swanson and Sivaramakrishnan 2014; Malik et al. 2017). Gly-Ser-Gly repeats were inserted between each element to ensure rotational flexibility. The C0-C2 and C1-C2 fragments contained

all structural elements within and including their respective domains, notably including the M-domain between C1 and C2. The C0-C1f fragment contained the C0 and C1 domains with the respective unstructured pro-ala rich linker region, as well as the first 17 amino acids of the M-domain, as described previously (A. Weith et al. 2012). The proteins were then transiently transfected (pBiex-1; Escort IV, Sigma-Aldrich, St. Louis, MO) into Sf9 cells, expressed, and affinity purified similarly to previously published protocols (Rai et al. 2021; Sommese et al. 2016). Briefly, cells were lysed at 72 h in lysis buffer: 0.5% IGEPAL, 4 mM $MgCl_2$, 200 mM NaCl, 7% sucrose, 20 mM Imidazole (pH 7.5), 0.5 mM EDTA, 1 mM EGTA, 1 mM dithiothreitol (DTT), 1 µg/ml phenylmethylsulfonyl fluoride (PMSF), 10 µg/ml aprotinin, and 10 µg/ml leupeptin. Lysates were centrifuged (176,000*g*, 4°C, 25 min) in a TLA 100.4 rotor (Beckman Coulter, Brea, CA) and bound to anti-FLAG M2 affinity resin (Sigma-Aldrich, St. Louis, MO) at 4°C. The FLAG resin was washed with wash buffer: 20 mM imidazole, 150 mM KCl, 5 mM $MgCl_2$,1 mM EDTA, 1 mM EGTA, 1 mM DTT, 1 µg/mL PMSF, 10 µg/mL aprotinin, and 10 µg/mL leupeptin, pH 7.4. To label the SNAP tag, GFP nanobody or cMyBP-C fragments bound to anti-FLAG resin were incubated with excess (>10 µM) BG-oligonucleotide in wash buffer overnight at 4°C with rotation. BG-oligonucleotide-labeled SNAP proteins bound to resin were again washed with wash buffer and eluted using 0.2 mg/mL FLAG peptide (Sigma-Aldrich, St. Louis, MO) overnight at 4°C with rotation. To confirm labeling, proteins were loaded onto a 10% SDS gel followed by Coomassie staining. The protein was stored in 50% glycerol (v/v) at -20°C.

Recombinant Human β-cardiac Myosin Preparation:

The human β-cardiac myosin cDNA (AAA51837.1) was purchased from Thermo Fisher Scientific, Waltham, MA. PCR amplification was used to subclone the M2β-HMM

fragment containing the first 25-heptads of the proximal S2 region (1-1016) into a pshuttle vector (a gift from Dr. Don Winkelmann). A GCN4 leucine zipper was added after the S2 region to promote dimerization which was followed by an eGFP tag at the C-terminus. An N-terminal FLAG tag was also included for purification. Similarly, an M2β-S1 (1-842) construct with a C-terminal eGFP tag and N-terminal FLAG tag was generated and subcloned into a shuttle vector provided by Vector Laboratories, Burlingame, CA. Recombinant adenovirus was generated as previously described to express M2β-HMM-eGFP in C_2C_{12} cells (Swenson et al. 2017). Vector Laboratories produced the initial recombinant adenovirus of M2β-S1-eGFP. High-titer adenovirus was produced by a method developed in the Winkelmann laboratory (Liu et al. 2015; Q. Wang, Moncman, and Winkelmann 2003) and as previously described (Swenson et al. 2017; Winkelmann et al. 2015). For expression of β-cardiac myosin eGFP, C_2C_{12} cells (typically 20-30, 145 mm diameter plates) were differentiated and infected with recombinant adenovirus (5×10^8 PFU/ml) diluted into differentiation media as described previously (Swenson et al. 2017). The cells were harvested on day 10 and myosin eGFP was purified by FLAG affinity chromatography as described. The eluted M2β-HMM-eGFP or M2β-S1-eGFP was then ammonium sulfate precipitated and dialyzed into MOPS20 buffer overnight at 4°C. M2β-HMM-eGFP and M2β-S1-eGFP was assessed for purity by coomassie stained SDS-polyacrylamide gels and concentrations were determined by eGFP absorbance (ε_{488} = 55,000 $M^{-1}{\cdot}cm^{-1}$) or Bradford assay using BSA as a standard.

Actin and Reconstituted Regulated Thin Filament Preparation:

For assays with F-actin, actin was purified from rabbit skeletal muscle using an acetone powder method (Pardee and Spudich 1982). The actin concentration was determined by absorbance at 290 nm (ε290= 2.66 x 104 M-1·cm-1). A molar equivalent

of tetramethylrhodamine (TRITC) phalloidin (MilliporeSigma, Burlington, MA) was added to stabilize and fluorescently label the F-actin. Calcium-regulated native thin filaments were prepared from mouse ventricular tissue and TRITC-labeled as described previously (Mun et al. 2014).

Standard In Vitro Motility Surface Assay:

Flow chambers were created using tape placed ~3 mm apart on a glass slide to adhere coverslips coated with 0.1% collodion in amyl acetate (Electron Microscopy Sciences, Hatfield, PA). For standard gliding assays with β-cardiac myosin eGFP, myosin was attached to coated coverslips through GFP nanobody with an encoded SNAP protein bound to oligonucleotides annealed to single-stranded DNA nanotube handles (Sommese et al. 2016). Briefly, GFP nanobody SNAP was incubated in flow chambers at ~0.5-1 μM for 4 minutes. Excess GFP nanobody SNAP was washed out, and the surface was incubated with assay buffer (AB: 20 mM Imidazole, pH 7.5, 25 mM KCl, 4 mM MgCl2, 1 mM EGTA, 1 mM DTT) and BSA (AB.BSA: AB + 1 mg/mL BSA) for 2 minutes. Finally, human β cardiac myosin at ~0.6-0.8 μM was incubated on the surface for 4 minutes and washed out with AB.BSA (for experiments with regulated thin filaments, flow cell was washed with pCa 5 buffer containing an appropriate $CaCl_2$ concentration calculated using Max Chelator from UC-Davis). The final actin imaging solution was added containing tetramethylrhodamine (TRITC) phalloidin-labeled (Invitrogen, Waltham, MA) F-actin (or regulated thin filaments in pCa 5 buffer), 0.1% methylcellulose, 2 mM ATP, 1 mM phosphocreatine, 0.1 mg/mL creatine-phosphokinase, 45 μg/mL catalase, 25 μg/mL glucose oxidase, and 1% glucose. Flow cells were imaged at 1000x magnification on a Nikon (Tokyo, Japan) TiE microscope equipped with a 100x 1.4 NA Plan-Apo oil-immersion objective, 1.5x magnifier, Nikon Perfect Focus System, mercury arc lamp, Evolve EMCCD camera (512 pixel x 512 pixel;

Photometrics), and Nikon NIS-Elements software. All *in-vitro* motility assays were performed at room temperature (20-23°C).

Standard Nanotube Assay:

The standard nanotube assay, previously reported and characterized (Hariadi et al. 2015), was presented for comparison in Figure 3.2b. At room temperature (20-23°C), nanotubes were attached to the coverslip surface coated with 0.1% collodion in amyl acetate (Electron Microscopy Sciences, Hatfield, PA) using biotinylated-BSA at 0.1 mg/mL in AB (AB: 20 mM Imidazole, pH 7.5, 25 mM KCl, 4 mM MgCl2, 1 mM EGTA, 1 mM DTT) incubated for 4 minutes. Excess biotin-BSA was washed out and the surface was incubated with AB.BSA (AB + 1 mg/mL BSA) for 2 minutes. Next, neutravidin at 0.1 mg/mL in AB.BSA was incubated for 4 minutes. AB.BSA was added to wash out excess neutravidin. Nanotubes were added at 2–5 nM concentration in AB.BSA.nt (AB.BSA + 5–10 nM random DNA nucleotide mix to reduce non-specific interactions) and incubated for 4 minutes. Excess nanotubes were washed out of the chamber with AB.BSA.nt. For attachment of β-cardiac myosin with eGFP, GFP nanobody SNAP at ~0.5-1 μM in AB.BSA.nt was incubated in flow chambers for 4 minutes. Excess GFP nanobody SNAP was washed out, and the surface was incubated with AB.BSA.nt for 2 minutes. Human β-cardiac myosin at ~0.6-0.8 μM was incubated on the surface for 4 minutes and washed out with AB.BSA.nt. The final actin imaging solution was added containing sheared tetramethylrhodamine (TRITC) phalloidin-labeled (Invitrogen, Waltham, MA) F-actin (sheared to ensure actin filament lengths are shorter than ~5 μm nanotubes), 0.1% methylcellulose, 2 mM ATP, 1 mM phosphocreatine, 0.1 mg/mL creatine-phosphokinase, 45 μg/mL catalase, 25 μg/mL glucose oxidase, and 1% glucose. For each flow cell, the actin channel was imaged as above at 0.5-3 second intervals for 2-3

minutes. For each actin video, several nanotube images were acquired of the same field of view for overlay.

Nanosurf Assay:

Flow chambers were created with nitrocellulose-coated coverslips as described above. At room temperature (20-23°C), nanotubes were attached to the coverslip using biotinylated-BSA at 0.1 mg/mL in AB (AB: 20 mM Imidazole, pH 7.5, 25 mM KCl, 4 mM MgCl2, 1 mM EGTA, 1 mM DTT) incubated for 4 minutes. Excess biotin-BSA was washed out, and the surface was incubated with AB for 2 minutes. Neutravidin at 0.1 mg/mL in AB was incubated for 4 minutes. AB was added to wash out excess neutravidin. Nanotubes were added at 2–5 nM concentration in AB.nt (AB + 5–10 nM random DNA nucleotide mix) and incubated for 4 minutes. Excess nanotubes were washed out of the chamber with AB.nt. For attachment of β-cardiac myosin with eGFP, GFP nanobody SNAP at ~0.5-1 μM in AB.nt was incubated in flow chambers for 4 minutes. Excess GFP nanobody SNAP was washed out with AB.BSA.nt (AB.nt + 1 mg/mL BSA), and the surface was incubated with AB.BSA.nt for 2 minutes. For assays with cMyBP-C, N-terminal fragments at ~0.2-0.6 μM in AB.BSA.nt were incubated for 4 minutes, then washed out before the flow cell was incubated with AB.BSA.nt for 2 minutes. Finally, human β-cardiac myosin at ~0.6-0.8 μM was incubated on the surface for 4 minutes and washed out with AB.BSA.nt (for experiments with regulated thin filaments, flow cell was washed with pCa 5 buffer containing an appropriate $CaCl_2$ concentration calculated using Max Chelator from UC-Davis). The final actin imaging solution was added, as described in the standard nanotube assay above. For each flow cell, the actin and nanotube channels were imaged as described above. Nanotubes with Cy3-labeled oligonucleotides incorporated into the annealing protocol and annealed to protein binding sites were imaged and used as a labeling control for Cy3-labeled

cMyBP-C fragments. Nanotubes were imaged and the Cy3 and Cy5 intensities were quantified by manually selecting individual nanotubes using ImageJ and normalizing the Cy3 intensity by the corresponding Cy5 intensity for each detected pixel.

Actin Trajectory Analysis:

Actin trajectories were analyzed using the ImageJ MTrackJ plug-in. Actin movies were corrected for any drift with the TurboReg plug-in. Actin and nanotube channels were merged, and movies were analyzed to identify actin-nanotube gliding events with filaments that move along DNA nanotubes for at least 4 frames (~1 sec). For the β-cardiac myosin nanosurf assay, to clearly quantify filaments traveling on the nanotubes, we quantified velocities of the filaments that were first traveling on the coverslip surface, encountered a nanotube, and then turned sharply to glide across the nanotube. We recorded the velocity of the filament while it was on the nanotube surface as the nanotube velocity and the velocity of the filaments traveling on the surrounding coverslip surface in the nanosurf assay as nano-surface velocity.

Statistical Analysis:

Data are represented as mean values of pooled filaments ± SEM using n=82-514 filaments per condition. Experiments were independently conducted at least three times from 3-8 independent protein preparations per condition. Statistical analysis was performed using Origin 9 (OriginLab Corporation, Northampton, MA). Statistical significance was calculated for individual experiments using paired Student's t test. Data were pooled for each condition and paired or unpaired Student's t tests were conducted to evaluate significance. One-way ANOVA with a Tukey's posttest was performed to assess significance when evaluating comparisons between multiple conditions (Figures 3.4d, 3.6c, and 3.6d) with P values *$P \leq 0.05$ and ***$P \leq 0.001$.

CHAPTER 4: Conclusions

4.1. Project Summary

4.1.1. Impact of G-peptides on Canonical GPCR Signaling:

In conclusion, we have used protein engineering techniques, including SPASM and the incorporation of ER/K α-helices, to characterize the impact of weak, transient interactions in the G-protein environment on canonical GPCR signaling. GPCR priming appears to be another layer of regulation to the classic GPCR ternary-complex model, with impacts on signaling multiplicity and functional selectivity. Previous work from our lab has demonstrated this priming effect between non-cognate Gq protein and β2-adrenergic and Dopamine receptors, resulting in increased cAMP corresponding to increased signaling through the cognate Gs pathway (Gupte et al. 2017, 2019). This phenomenon has also been demonstrated for non-cognate Gs protein on the canonical Gq-coupled receptor, vasopressin. However, the α_1-adrenergic receptor did not exhibit priming, suggesting it is receptor-specific (Gupte et al. 2017). This study investigating the impact of the G-protein environment in CB_1 and A_1R receptors provides a framework for how priming occurs in promiscuous Gi and Gq-coupled receptors. These results have implications for the development of functionally selective ligands for A_1R and CB_1. The ability to develop functionally selective therapies would be particularly pertinent for CB_1, which signals through the Gi pathway producing euphoria and analgesia upon THC binding (Agarwal et al. 2007; Ibsen, Connor, and Glass 2017). The physiological effects of CB_1 signaling through Gs, Gq, and non-G-protein mediated pathways are unclear due to the lack of biased ligands targeting these pathways. The development of functionally

selective ligands would allow for the exploration of any therapeutic benefit of these pathways while potentially mitigating the euphoric effects.

Further studies will be needed to characterize priming in other receptors and to resolve the mechanism of priming. Our group has previously shown that non-cognate Gα peptides exhibit more shallow binding compared to cognate interactions (Semack et al. 2016). Additionally, we contributed data to a complementary study which suggests non-cognate G-proteins interface with latent intracellular GPCR cavities but dissociate due to weak and unstable interactions. Further, we found that these cavities could be tuned by mutagenesis or evolved to alter G-protein selectivity (Sandhu et al. 2019). Priming may be particularly significant with the emerging concept of signal compartmentalization where the signal output can vary based on the cellular context (Calebiro et al. 2021). Interestingly, studies on intact cells and tissues have noted the existence of spatial compartmentalization in receptor signaling with the possibility of locally higher concentrations of signaling molecules, including G-protein signaling at intracellular sites (Calebiro et al. 2021).

While these non-cognate interactions may be weak, transient interactions that do not precipitate G-protein activation, our study confirms these interactions can have a significant impact on canonical signaling in multiple G-protein pathways (Gupte et al. 2017, 2019; Touma et al. 2020). The mechanism of priming is still being understood, however data from our lab supports a sequential mechanism of interaction at the cognate site. Using SPASM FRET sensors, our group found that Gα C-terminal peptides altered the conformation of the prototypical Gs-coupled β2-AR receptor (Gupte et al. 2019). We found that this primed conformation persisted for approximately 90 seconds and led to enhanced cognate G-protein activation and downstream signaling. Our studies provide evidence that the GPCR-G-protein interaction may be a valuable target for functionally selective drugs to tune therapeutic response to target specific GPCR signaling pathways.

4.1.2. Characterizing Sarcomeric Interactions with the Nanosurf Assay:

We have established a nanosurf assay for the characterization of β-cardiac myosin ensembles. The synthetic thick filament mimics the protein interactions in the native sarcomere, allowing us to probe the cMyBP-C interactions essential for contractile regulation. We had previously used a nanotube assay to characterize myosin V and VI, which spend a large portion of their ATPase cycles bound to actin (Hariadi et al. 2015). β-cardiac myosin, however, operates in muscle ensembles, and therefore individual motors spend only a small percentage of the ATPase cycle bound to actin (Uyeda, Kron, and Spudich 1990; D. E. Harris and Warshaw 1993). To improve the poor actin-landing rate associated with β-cardiac myosin in the traditional nanotube assay, we created the nanosurf assay by combining traditional surface gliding assays with nanotube assays. With β-cardiac myosin loaded on both the nanotube and the surrounding surface, an enhanced actin landing rate also increased the probability of motile events on nanotubes. We characterized the nanosurf assay and found that increasing the spacing of β-cardiac myosin on synthetic thick filaments from 14 nm to 28 nm intervals did not impact thin filament motility. We could therefore increase β-cardiac myosin spacing and incorporate cMyBP-C.

The structure of the β-cardiac myosin nanosurf assay creates the ideal architecture to mimic cMyBP-C interactions with actin and/or myosin in the sarcomere. For the first time, we incorporated cMyBP-C N-terminal fragments with β-cardiac myosin on a DNA nanotube. We recapitulated inhibition by cMyBP-C N-terminal fragments, C0-C2 and C1-C2, with both β-cardiac myosin S1 and HMM. Myosin HMM contains the myosin S2 region that is thought to interact with the myosin S1 motor domain, forming an auto-inhibited super-relaxed (SRX) state (Nag et al. 2017). cMyBP-C is thought to interact with the

myosin S2, stabilizing the SRX. Therefore, inhibition of β-cardiac myosin HMM nanotube motility by cMyBP-C fragments may be due to interaction with actin or the myosin S2, by stabilizing the auto-inhibited SRX. Myosin S1, however, lacks this S2 region and therefore cannot form the SRX. Yet, myosin S1 nanotube motility is also inhibited by cMyBP-C fragments. This suggests that inhibition of β-cardiac myosin nanotube motility by C0-C2 and C1-C2 fragments in our nanosurf assay may be due to cMyBP-C interaction with actin rather than myosin. This agrees with recent *in vivo* super-resolution data suggesting the N-terminus of cMyBP-C is positioned predominantly near the thin filament (Rahmanseresht et al. 2021). These results are consistent with many other studies suggesting the cMyBP-C inhibitory effect *in vitro* may be due in large part to its interaction with actin (M.J. Previs et al. 2012; Mun et al. 2014; Luther et al. 2011; Kensler, Shaffer, and Harris 2011; S. P. Harris et al. 2016; M. Previs et al. 2015; Risi et al. 2021; Michael J. Previs et al. 2016; Shaffer, Kensler, and Harris 2009).

To determine which cMyBP-C domains are critical for this inhibition, we utilized a shorter C0-C1f N-terminal fragment which was previously characterized as the minimally sufficient fragment required for actomyosin inhibition in a standard surface gliding assay (A. Weith et al. 2012). The C0-C1f fragment contains the first 17 amino acids of the M domain, including several C-terminal arginine residues. However, the C0-C1f fragment does not include the four phosphorylatable serines present in the full M-domain. A previous study concluded that the C-terminal arginine residues in C0-C1f were likely sufficient and responsible for actomyosin inhibition (A. Weith et al. 2012). In our nanosurf assay, however, we did not observe inhibition of β-cardiac myosin nanotube motility by C0-C1f. This may be due to the precise positioning of the C0-C1f fragment and orientation of the C-terminal arginine residues on the nanotube. However, it appears that the entire M-domain is crucial for β-cardiac myosin inhibition in our nanosurf assay. Partial release

of cMyBP-C inhibition by phosphomimetic fragments also highlights the regulatory capability of the phosphorylatable serines in the M-domain. In summary, the nanosurf assay is an effective tool to mimic and dissect cMyBP-C interactions on a β-cardiac myosin synthetic thick filament. These transient interactions present a unique challenge, and this approach can be readily used to dissect numerous other weak, transient protein interactions.

4.2. Future Directions

4.2.1. G-Peptides in GPCR Signaling:

While our studies demonstrate modulation of signaling through G-peptides, in many cases the impacts of the G-peptides were modest. Future studies can design mutations in G-peptides to improve selectivity and efficacy of GPCR signaling. Generation of mutations would initially focus on the C-terminus of the G-peptides. It has been established that the last three residues of this C-terminus are important for G-protein selectivity (Conklin et al. 1993). Our group has previously identified three hot spot residues in Gαs and Gαq peptides that contribute to selective interactions in the β2-AR and vasopressin V_{1A}R receptors (Semack et al. 2016). In addition, we have found that the intracellular β2-AR cavity can be tuned by mutagenesis to alter G-protein selectivity (Sandhu et al. 2019), further highlighting our ability to enhance selectivity at the GPCR-G-protein interface. However, potential hot spot residues for selectivity may be different

for CB_1 and A_1R compared to β2-AR. Mutant G-peptides can be screened with CB_1 and A_1R using multiple downstream assays (i.e. cAMP, IP_1). This approach would help identify which peptides enhance or eliminate priming in these promiscuous Gi-coupled receptors, and which features or residues in these G-peptides may be key determinants for selectivity and efficacy. Peptidomimetics could also be screened alongside G-peptides. Peptidomimetics mimic the G-peptides but are unnatural so they cross the cell membrane and can be potentially used directly as therapeutics. Identifying G-peptides or peptidomimetics with impacts on one particular G-protein pathway would be particularly useful for identifying mechanisms of selectivity.

In addition to screening G-peptides, future studies could also screen CB_1 ligands for differential effects. Finding ligands that selectively enhance Gi or Gq, or selectively impact priming, could help us understand how functionally selective ligands impact this mechanism. Understanding the characteristics of selective CB_1 ligands, and their impact on priming, could aid in the development of functionally selective therapeutics targeting CB_1. Screening peptides, peptidomimetics, and ligands for selectivity will help us understand the basis for G-protein selectivity, which is a crucial component to resolving the mechanisms of GPCR priming (Gupte et al. 2017, 2019). Our long-term goal is to elucidate the mechanisms by which GPCR interactions with non-cognate G-proteins modulate signaling through cognate G-proteins, which will be a critical step toward understanding how the cellular environment contributes to drug efficacy. The ability to enhance the selectivity of therapeutics would be a powerful tool to reduce harmful side effects from signaling through multiple G-protein pathways.

4.2.2. Characterizing β-cardiac myosin and cMyBP-C with Nanosurf Assay:

Future work can continue to optimize aspects of the nanosurf assay. Our characterization of the nanosurf assay revealed a reduced nano-surface velocity which we attributed to the BSA-biotin and neutravidin used to attach nanotubes to the motility surface. It is unclear if the presence of these elements on the coverslip surface impacts motility on the nanotubes. The nanosurf assay does not currently have the optical resolution to determine if actin filaments are traveling exclusively on nanotubes, on the motility surface parallel to nanotubes, or if filaments traveling on nanotubes are interacting with surface elements. Significant slowing of filaments on C0-C2 and C1-C2 decorated nanotubes compared to the surrounding nano-surface suggests the interaction is specific to the nanotube. Nonetheless, the similar nanotube and nano-surface velocities observed in the cardiac myosin-only nanosurf assay make it difficult to resolve. Future studies and enhanced technology will be required to ensure filaments are traveling on the nanotube in the nanosurf assay.

Our nanosurf data suggests cMyBP-C interactions with actin are the dominant contribution towards inhibition of β-cardiac myosin nanotube motility by cMyBP-C fragments. Given the many studies reporting myosin-cMyBP-C interactions, it is surprising that there is apparently no significant contribution from the myosin S2 interaction with cMyBP-C on nanotube motility inhibition (Gruen and Gautel 1999; Howarth et al. 2012; S. P. Harris et al. 2004; Ratti et al. 2011; Pfuhl and Gautel 2012; Nag et al. 2017). The role of myosin-cMyBP-C interactions in our assay is therefore unclear and can be a topic for future study. The current format of the assay lacks the resolution to observe interactions between cMyBP-C and myosin. Hence, this limits interpretation of the relative contributions of actin and myosin interactions in cMyBP-C regulation. A potential approach

to address this challenge would be the use of FRET to directly visualize interactions on the nanotube and correlate them to the effects on motility. FRET sensors can be placed between C0-C2 and myosin S2 on the nanotube. While the reach and conformational flexibility enabled by the DNA linkers and ER/K α-helices should enable interactions between cMyBP-C and β-cardiac myosin, a FRET assay would provide direct evidence for potential S2-cMyBP-C interactions.

To further characterize the S2-cMyBP-C interaction, we can generate mutations in β-cardiac myosin that are implicated in HCM and have been hypothesized to disrupt this interaction. E924K and R870H are two HCM mutations in the β-cardiac myosin S2 that have been shown to abolish or reduce the interaction with the cMyBP-C fragment, C1-C2 (Gruen and Gautel 1999). By investigating the impact of these mutations in our nanosurf assay, we can further clarify the role of the S2-cMyBP-C interaction. Although less likely, there is some evidence that cMyBP-C may also interact with another part of the myosin, for example the RLC (Ratti et al. 2011) or the S1 motor domain (Nag et al. 2017). HCM mutations in β-cardiac myosin S1 that lie along the putative 'myosin mesa' binding interface with cMyBP-C, such as R453C, R249Q, or H251N, substantially weaken the auto-inhibitory SRX interaction between the myosin S1 motor domain and the myosin S2 proximal tail (Nag et al. 2017). We could investigate how these HCM mutations may also disrupt the myosin-cMyBP-C interaction and the impacts on ensemble function, leading to hyper-contractility. As a negative control for the myosin-cMyBP-C interaction, protein spacing on the nanotube can be increased from 14 to 28 nm to ablate the myosin-cMyBP-C interaction. Further investigation of the 'myosin mesa' may support a unified mechanism by which mutations in both β-cardiac myosin and cMyBP-C result in the HCM phenotype, affirming the importance of this protein interface as an emerging target for small molecule therapeutics.

In addition to HCM mutations in the myosin mesa, future studies can also utilize the nanosurf assay to investigate the structural mechanisms and impact of HCM mutations in other parts of the β-cardiac myosin motor. Using the nanosurf assay, we have recapitulated many elements of the native sarcomere without the high cost of animal model design. With the relative ease of expressing recombinant human β-cardiac myosin, we can incorporate β-cardiac myosin HCM mutants on synthetic thick filaments. Many currently unresolved questions in HCM would benefit from ensemble studies, including the question of how allelic imbalance in HCM contributes to disease phenotype. The existence of mixed mutant and wild type motor populations in most HCM cases has made the correlation between genotype and disease phenotype more difficult (Tripathi et al. 2011). The majority of HCM mutations in β-cardiac myosin are missense mutations, resulting in incorporation into the sarcomere and disruption of normal sarcomeric function (Marsiglia and Pereira 2014). Most HCM patients are heterozygous for these mutations, which should result in about 50% incorporation of mutant protein in the sarcomere (Tyska et al. 2000). However due to allelic imbalance, the relative ratio of mutant to wild-type (WT) myosin can range from less than 20% to upwards of 70% of motors. Studies have shown the fraction of mutated protein varies depending on the specific HCM mutant, and that it correlates with both disease severity and the extent of functional changes at the sarcomeric level (Tripathi et al. 2011; Witjas-Paalberends et al. 2014). DNA nanotubes uniquely enable the precise manipulation of defined motor populations. To understand how WT and mutant motor populations contribute to altered sarcomeric function in allelic balance, different ratios of mutant to WT motors can be patterned onto a synthetic thick filament. Increasing the population of mutant motors may have a non-linear, disproportional impact on ensemble velocity. Initially, this effect could be examined with the well-characterized HCM mutation, R403Q, near the actin-binding interface. However, there are numerous other β-cardiac HCM mutations that

would be good candidates for investigation of allelic imbalance. We can also dissect the effects of altering other parameters including stiffness of connection, load, and spacing of myosin on the nanotube. Overall, this approach would provide insight as to how allelic imbalance may be contributing to pathogenicity in HCM and would help establish connections between genotype and disease phenotype.

The nanosurf assay is also the ideal approach to investigate the impact of HCM mutations in cMyBP-C, and haploinsufficiency, on contractile function. The majority of HCM mutations in *MYBPC3* are frameshift mutations resulting from deletions or insertions, leading to a truncated protein with no function. Therefore the HCM disease mechanism in cMyBP-C may be the result of haploinsufficiency, where the protein is not incorporated into the sarcomere (Marsiglia and Pereira 2014). Loss of wild-type cMyBP-C in haploinsufficiency may result in loss of the high calcium “brake pedal” effect, leading to hypercontractility (Michael J. Previs, Michalek, and Warshaw 2014). Using the nanosurf assay, we could investigate how alterations in cMyBP-C density and pattern, mimicking cMyBP-C HCM-associated haploinsufficiency, impacts ensemble function. Experiments could also be performed at a range of calcium concentrations with regulated thin filaments to better understand how alterations in cMyBP-C density impact thin filament activation. Our current assays have focused on the role of cMyBP-C N-terminal domains C0-C2, however additional cMyBP-C domains could also be incorporated to potentially alter cMyBP-C interactions. Overall, the controlled environment of the synthetic thick filament will uniquely enable the characterization of HCM mutations, particularly in the context of allelic imbalance and cMyBP-C haploinsufficiency. Our long-term goal will be to elucidate the mechanisms by which HCM mutations modulate sarcomeric function, which will be a crucial step toward the development of small molecule therapeutics.

BIBLIOGRAPHY

Acuner Ozbabacan, SE, HB Engin, A Gursoy, and O Keskin. 2011. “Transient Protein-Protein Interactions.” *Protein Engineering, Design & Selection : PEDS* 24 (9): 635–48. https://doi.org/10.1093/PROTEIN/GZR025.

Agarwal, Nitin, Pal Pacher, Irmgard Tegeder, Fumimasa Amaya, Cristina E. Constantin, Gary J. Brenner, Tiziana Rubino, et al. 2007. “Cannabinoids Mediate Analgesia Largely via Peripheral Type 1 Cannabinoid Receptors in Nociceptors.” *Nature Neuroscience* 10 (7): 870–79. https://doi.org/10.1038/nn1916.

Alyonycheva, Tatiana N., Takashi Mikawa, Fernando C. Reinach, and Donald A. Fischman. 1997. “Isoform-Specific Interaction of the Myosin-Binding Proteins (MyBPs) with Skeletal and Cardiac Myosin Is a Property of the C-Terminal Immunoglobulin Domain.” *Journal of Biological Chemistry* 272 (33): 20866–72. https://doi.org/10.1074/JBC.272.33.20866.

Barefield, David, and Sakthivel Sadayappan. 2010. “Phosphorylation and Function of Cardiac Myosin Binding Protein-C in Health and Disease.” *Journal of Molecular and Cellular Cardiology* 48 (5): 866–75. https://doi.org/10.1016/J.YJMCC.2009.11.014.

Bhuiyan, Md Shenuarin, James Gulick, Hanna Osinska, Manish Gupta, and Jeffrey Robbins. 2012. “Determination of the Critical Residues Responsible for Cardiac Myosin Binding Protein C’s Interactions.” *Journal of Molecular and Cellular Cardiology* 53 (6): 838–47. https://doi.org/10.1016/J.YJMCC.2012.08.028.

Bonhaus, D. W., L. K. Chang, J. Kwan, and G. R. Martin. 1998. “Dual Activation and Inhibition of Adenylyl Cyclase by Cannabinoid Receptor Agonists: Evidence for Agonist-Specific Trafficking of Intracellular Responses.” *Journal of Pharmacology*

and Experimental Therapeutics 287 (3): 884–88.

Bonne, Gisèle, Lucie Carrier, Josiane Bercovici, Corinne Cruaud, Pascale Richard, Bernard Hainque, Mathias Gautel, et al. 1995. “Cardiac Myosin Binding Protein–C Gene Splice Acceptor Site Mutation Is Associated with Familial Hypertrophic Cardiomyopathy.” *Nature Genetics 1995 11:4* 11 (4): 438–40. https://doi.org/10.1038/ng1295-438.

Calebiro, D, Z Koszegi, Y Lanoiselée, T Miljus, and S O’Brien. 2021. “G Protein-Coupled Receptor-G Protein Interactions: A Single-Molecule Perspective.” *Physiological Reviews* 101 (3): 857–906. https://doi.org/10.1152/PHYSREV.00021.2020.

Carrier, Lucie, Giulia Mearini, Konstantina Stathopoulou, and Friederike Cuello. 2015. “Cardiac Myosin-Binding Protein C (MYBPC3) in Cardiac Pathophysiology.” *Gene* 573 (2): 188–97. https://doi.org/10.1016/J.GENE.2015.09.008.

Chen, XP, W. Yang, Y. Fan, JS Luo, K. Hong, Z. Wang, JF Yan, et al. 2010. “Structural Determinants in the Second Intracellular Loop of the Human Cannabinoid CB 1 Receptor Mediate Selective Coupling to G s and G I.” *British Journal of Pharmacology* 161 (8): 1817–34. https://doi.org/10.1111/j.1476-5381.2010.01006.x.

Cherezov, Vadim, Enrique Abola, and Raymond C. Stevens. 2010. “Recent Progress in the Structure Determination of GPCRs, a Membrane Protein Family with High Potential as Pharmaceutical Targets.” *Methods in Molecular Biology (Clifton, N.J.)* 654: 141–68. https://doi.org/10.1007/978-1-60761-762-4_8.

Cherezov, Vadim, Daniel M. Rosenbaum, Michael A. Hanson, Søren G.F. Rasmussen, Sun Thian Foon, Tong Sun Kobilka, Hee Jung Choi, et al. 2007. “High-Resolution Crystal Structure of an Engineered Human B2-Adrenergic G Protein-Coupled Receptor.” *Science* 318 (5854): 1258–65.

https://doi.org/10.1126/SCIENCE.1150577.

Chung, Ka Young. 2013. “Structural Aspects of GPCR-G Protein Coupling.” *Toxicological Research* 29 (3): 149–55. https://doi.org/10.5487/TR.2013.29.3.149.

Colson, Brett A. 2019. “What a Drag!: Skeletal Myosin Binding Protein-C Affects Sarcomeric Shortening.” *Journal of General Physiology* 151 (5): 614–18. https://doi.org/10.1085/JGP.201912326.

Conklin, Bruce R., Zvi Farfel, Kevin D. Lustig, David Julius, and Henry R. Bourne. 1993. “Substitution of Three Amino Acids Switches Receptor Specificity of Gqα to That of Giα.” *Nature 1993 363:6426* 363 (6426): 274–76. https://doi.org/10.1038/363274a0.

Conn, P. Jeffrey, Arthur Christopoulos, and Craig W. Lindsley. 2009. “Allosteric Modulators of GPCRs: A Novel Approach for the Treatment of CNS Disorders.” *Nature Reviews Drug Discovery* 8 (1): 41–54. https://doi.org/10.1038/nrd2760.

Cordeaux, Yolande, Adriaan P. Ijzerman, and Stephen J. Hill. 2004. “Coupling of the Human A 1 Adenosine Receptor to Different Heterotrimeric G Proteins: Evidence for Agonist-Specific G Protein Activation.” *British Journal of Pharmacology* 143 (6): 705–14. https://doi.org/10.1038/sj.bjp.0705925.

Eschenhagen, T, U Mende, M Diederich, M Nose, W Schmitz, H Scholz, J Schulte am Esch, A Warnholtz, and H Schäfer. 1992. “Long Term Beta-Adrenoceptor-Mediated up-Regulation of Gi Alpha and G(o) Alpha MRNA Levels and Pertussis Toxin-Sensitive Guanine Nucleotide-Binding Proteins in Rat Heart.” *Molecular Pharmacology* 42 (5).

Feldman, AM, AE Cates, WB Veazey, RE Hershberger, MR Bristow, KL Baughman, WA Baumgartner, and C Van Dop. 1988. “Increase of the 40,000-Mol Wt Pertussis

Toxin Substrate (G Protein) in the Failing Human Heart." *The Journal of Clinical Investigation* 82 (1): 189–97. https://doi.org/10.1172/JCI113569.

Flashman, Emily, Charles Redwood, Johanna Moolman-Smook, and Hugh Watkins. 2004. "Cardiac Myosin Binding Protein C: Its Role in Physiology and Disease." *Circulation Research* 94 (10): 1279–89. https://doi.org/10.1161/01.RES.0000127175.21818.C2.

Foster, Daniel J., and P. Jeffrey Conn. 2017. "Allosteric Modulation of GPCRs: New Insights and Potential Utility for Treatment of Schizophrenia and Other CNS Disorders." *Neuron* 94 (3): 431–46. https://doi.org/10.1016/j.neuron.2017.03.016.

Foster, Simon R., Eugeni Roura, Peter Molenaar, and Walter G. Thomas. 2015. "G Protein-Coupled Receptors in Cardiac Biology: Old and New Receptors." *Biophysical Reviews* 7 (1): 77. https://doi.org/10.1007/S12551-014-0154-2.

Fraser, Iain D.C., and Steven B. Marston. 1995. "In Vitro Motility Analysis of Actin-Tropomyosin Regulation by Troponin and Calcium: The Thin Filament Is Switched as a Single Cooperative Unit." *Journal of Biological Chemistry* 270 (14): 7836–41. https://doi.org/10.1074/JBC.270.14.7836.

Freissmuth, M., W. Schutz, and M. E. Linder. 1991. "Interactions of the Bovine Brain A1-Adenosine Receptor with Recombinant G Protein α-Subunits: Selectivity for RG(Iα-3)." *Journal of Biological Chemistry* 275: (Pt 3): 651-656. https://doi.org/10.1042/bj2750651.

Geeves, Michael A. 2016. "Review: The ATPase Mechanism of Myosin and Actomyosin." *Biopolymers* 105 (8): 483–91. https://doi.org/10.1002/BIP.22853.

Gibson, TJ. 2009. "Cell Regulation: Determined to Signal Discrete Cooperation." *Trends*

in Biochemical Sciences 34 (10): 471–82. https://doi.org/10.1016/J.TIBS.2009.06.007.

Gilchrist, Annette, Moritz Bünemann, Anli Li, M. Marlene Hosey, and Heidi E. Hamm. 1999. “A Dominant-Negative Strategy for Studying Roles of G Proteins in Vivo.” *Journal of Biological Chemistry* 274 (10): 6610–16. https://doi.org/10.1074/jbc.274.10.6610.

Gilchrist, Annette, Anli Li, and Heidi E. Hamm. 2002. “G Alpha COOH-Terminal Minigene Vectors Dissect Heterotrimeric G Protein Signaling.” *Science’s STKE : Signal Transduction Knowledge Environment*. https://doi.org/10.1126/scisignal.1182002pl1.

Gilchrist, Annette, Jurgen F. Vanhauwe, Anli Li, Tarita O. Thomas, Tatyana Voyno-Yasenetskaya, and Heidi E. Hamm. 2001. “Gα Minigenes Expressing C-Terminal Peptides Serve as Specific Inhibitors of Thrombin-Mediated Endothelial Activation.” *Journal of Biological Chemistry* 276: 25672–79. https://doi.org/10.1074/jbc.M100914200.

Greenberg, Michael J., Henry Shuman, and E. Michael Ostap. 2014. “Inherent Force-Dependent Properties of β-Cardiac Myosin Contribute to the Force-Velocity Relationship of Cardiac Muscle.” *Biophysical Journal* 107 (12): L41–44. https://doi.org/10.1016/J.BPJ.2014.11.005.

Gruen, Mathias, and Mathias Gautel. 1999. “Mutations in β-Myosin S2 That Cause Familial Hypertrophic Cardiomyopathy (FHC) Abolish the Interaction with the Regulatory Domain of Myosin-Binding Protein-C.” *Journal of Molecular Biology* 286 (3): 933–49. https://doi.org/10.1006/JMBI.1998.2522.

Gruen, Mathias, Heino Prinz, and Mathias Gautel. 1999. “CAPK-Phosphorylation

Controls the Interaction of the Regulatory Domain of Cardiac Myosin Binding Protein C with Myosin-S2 in an on-off Fashion." *FEBS Letters* 453 (3): 254–59. https://doi.org/10.1016/S0014-5793(99)00727-9.

Gupte, Tejas M., Rabia U. Malik, Ruth F. Sommese, Michael Ritt, and Sivaraj Sivaramakrishnan. 2017. "Priming GPCR Signaling through the Synergistic Effect of Two G Proteins." *Proceedings of the National Academy of Sciences of the United States of America* 114 (14): 3756–61. https://doi.org/10.1073/pnas.1617232114.

Gupte, Tejas M., Michael Ritt, Matthew Dysthe, Rabia U. Malik, and Sivaraj Sivaramakrishnan. 2019. "Minute-Scale Persistence of a GPCR Conformation State Triggered by Non-Cognate G Protein Interactions Primes Signaling." *Nature Communications* 10: 4836. https://doi.org/10.1038/s41467-019-12755-9.

Hamm, Heidi E., Dusanka Deretic, Anatol Arendt, Pal A. Hargrave, Bernd Koenig, and Klaus P. Hofmann. 1988. "Site of G Protein Binding to Rhodopsin Mapped with Synthetic Peptides from the α Subunit." *Science* 241 (4867): 832–35. https://doi.org/10.1126/science.3136547.

Hariadi, R. F., R. F. Sommese, A. S. Adhikari, R. E. Taylor, S. Sutton, J. A. Spudich, and S. Sivaramakrishnan. 2015. "Mechanical Coordination in Motor Ensembles Revealed Using Engineered Artificial Myosin Filaments." *Nature Nanotechnology* 10 (8): 696–700. https://doi.org/10.1038/nnano.2015.132.

Harris, D.E., and D.M. Warshaw. 1993. "Smooth and Skeletal Muscle Myosin Both Exhibit Low Duty Cycles at Zero Load in Vitro." *Journal of Biological Chemistry* 268 (20): 14764–68. https://doi.org/10.1016/S0021-9258(18)82398-5.

Harris, Samantha P. 2021. "Making Waves: A Proposed New Role for Myosin-Binding Protein C in Regulating Oscillatory Contractions in Vertebrate Striated Muscle."

Journal of General Physiology 153 (3). https://doi.org/10.1085/JGP.202012729.

Harris, Samantha P., Betty Belknap, Robert E. Van Sciver, Howard D. White, and Vitold E. Galkin. 2016. “C0 and C1 N-Terminal Ig Domains of Myosin Binding Protein C Exert Different Effects on Thin Filament Activation.” *Proceedings of the National Academy of Sciences* 113 (6): 1558–63. https://doi.org/10.1073/PNAS.1518891113.

Harris, Samantha P., Ross G. Lyons, and Kristina L. Bezold. 2011. “In the Thick of It: HCM-Causing Mutations in Myosin Binding Proteins of the Thick Filament.” *Circulation Research* 108 (6): 751–64. https://doi.org/10.1161/CIRCRESAHA.110.231670.

Harris, Samantha P., Elena Rostkova, Mathias Gautel, and Richard L. Moss. 2004. “Binding of Myosin Binding Protein-C to Myosin Subfragment S2 Affects Contractility Independent of a Tether Mechanism.” *Circulation Research* 95 (9): 930–36. https://doi.org/10.1161/01.RES.0000147312.02673.56.

Heling, LWHJ, MA Geeves, and NM Kad. 2020. “MyBP-C: One Protein to Govern Them All.” *Journal of Muscle Research and Cell Motility* 41 (1): 91–101. https://doi.org/10.1007/s10974-019-09567-1.

Hermans, E. 2003. “Biochemical and Pharmacological Control of the Multiplicity of Coupling at G-Protein-Coupled Receptors.” *Pharmacology & Therapeutics* 99 (1): 25–44. https://doi.org/10.1016/S0163-7258(03)00051-2.

Hilser, Vincent J., Jeremy A. Anderson, and Hesam N. Motlagh. 2015. “Allostery vs. ‘Allokairy.’” *Proceedings of the National Academy of Sciences of the United States of America* 112 (37): 11430–31. https://doi.org/10.1073/pnas.1515239112.

Hooijman, Pleuni, Melanie A. Stewart, and Roger Cooke. 2011. “A New State of Cardiac Myosin with Very Slow ATP Turnover: A Potential Cardioprotective Mechanism in the Heart.” *Biophysical Journal* 100 (8): 1969–76. https://doi.org/10.1016/J.BPJ.2011.02.061.

Howarth, Jack W., Srinivas Ramisetti, Kristof Nolan, Sakthivel Sadayappan, and Paul R. Rosevear. 2012. “Structural Insight into Unique Cardiac Myosin-Binding Protein-C Motif: A Partially Folded Domain.” *Journal of Biological Chemistry* 287 (11): 8254–62. https://doi.org/10.1074/JBC.M111.309591.

Ibsen, Mikkel Søes, Mark Connor, and Michelle Glass. 2017. *Cannabinoid CB 1 and CB 2 Receptor Signaling and Bias*. *Cannabis and Cannabinoid Research*. https://doi.org/10.1089/can.2016.0037.

Inchingolo, Alessio V., Samantha Beck Previs, Michael J. Previs, David M. Warshaw, and Neil M. Kad. 2019. “Revealing the Mechanism of How Cardiac Myosin-Binding Protein C N-Terminal Fragments Sensitize Thin Filaments for Myosin Binding.” *Proceedings of the National Academy of Sciences* 116 (14): 6828–35. https://doi.org/10.1073/PNAS.1816480116.

Insel, Paul A, Chih-Min Tang, Ines Hahntow, and Martin C Michel. 2007. “Impact of GPCRs in Clinical Medicine: Monogenic Diseases, Genetic Variants and Drug Targets.” *Biochimica et Biophysica Acta* 1768 (4): 994–1005. https://doi.org/10.1016/j.bbamem.2006.09.029.

Jacobson, Kenneth A., and Zhan Guo Gao. 2006. “Adenosine Receptors as Therapeutic Targets.” *Nature Reviews Drug Discovery* 5 (3): 247–64. https://doi.org/10.1038/nrd1983.

Jockers, R., M. E. Linder, M. Hohenegger, C. Nanoff, B. Bertin, A. D. Strosberg, S.

Marullo, and M. Freissmuth. 1994. “Species Difference in the G Protein Selectivity of the Human and Bovine A1-Adenosine Receptor.” *Journal of Biological Chemistry* 269 (51): 32077–84.

Kachur, Torah M., and David B. Pilgrim. 2008. “Myosin Assembly, Maintenance and Degradation in Muscle: Role of the Chaperone UNC-45 in Myosin Thick Filament Dynamics.” *International Journal of Molecular Sciences*. https://doi.org/10.3390/ijms9091863.

Kensler, Robert W., Justin F. Shaffer, and Samantha P. Harris. 2011. “Binding of the N-Terminal Fragment C0–C2 of Cardiac MyBP-C to Cardiac F-Actin.” *Journal of Structural Biology* 174 (1): 44–51. https://doi.org/10.1016/J.JSB.2010.12.003.

Lambright, David G., Joseph P. Noel, Heidi E. Hamm, and Paul B. Sigler. 1994. “Structural Determinants for Activation of the α-Subunit of a Heterotrimeric G Protein.” *Nature* 369 (6482): 621–28. https://doi.org/10.1038/369621a0.

Lauckner, Jane E., Bertil Hille, and Ken Mackie. 2005. “The Cannabinoid Agonist WIN55,212-2 Increases Intracellular Calcium via CB1 Receptor Coupling to Gq/11 G Proteins.” *Proceedings of the National Academy of Sciences of the United States of America* 102 (52): 19144–49. https://doi.org/10.1073/pnas.0509588102.

Lee, Kyounghwan, Samantha P. Harris, Sakthivel Sadayappan, and Roger Craig. 2015. “Orientation of Myosin Binding Protein C in the Cardiac Muscle Sarcomere Determined by Domain-Specific Immuno-EM.” *Journal of Molecular Biology* 427 (2): 274–86. https://doi.org/10.1016/J.JMB.2014.10.023.

Liu, Y, HD White, B Belknap, DA Winkelmann, and E Forgacs. 2015. “Omecamtiv Mecarbil Modulates the Kinetic and Motile Properties of Porcine β-Cardiac Myosin.” *Biochemistry* 54 (10): 1963–75. https://doi.org/10.1021/BI5015166.

Lowey, Susan, Leanne M. Lesko, Arthur S. Rovner, Alex R. Hodges, Sheryl L. White, Robert B. Low, Mercedes Rincon, James Gulick, and Jeffrey Robbins. 2008. “Functional Effects of the Hypertrophic Cardiomyopathy R403Q Mutation Are Different in an α- or β-Myosin Heavy Chain Backbone.” *Journal of Biological Chemistry* 283 (29): 20579–89. https://doi.org/10.1074/jbc.M800554200.

Luther, Pradeep K., Pauline M. Bennett, Carlo Knupp, Roger Craig, Raúl Padrón, Samantha P. Harris, Jitendrakumar Patel, and Richard L. Moss. 2008. “Understanding the Organisation and Role of Myosin Binding Protein C in Normal Striated Muscle by Comparison with MyBP-C Knockout Cardiac Muscle.” *Journal of Molecular Biology* 384 (1): 60–72. https://doi.org/10.1016/J.JMB.2008.09.013.

Luther, Pradeep K., Hanspeter Winkler, Kenneth Taylor, Maria E. Zoghbi, Roger Craig, Raúl Padrón, John M. Squire, and Jun Liu. 2011. “Direct Visualization of Myosin-Binding Protein C Bridging Myosin and Actin Filaments in Intact Muscle.” *Proceedings of the National Academy of Sciences* 108 (28): 11423–28. https://doi.org/10.1073/PNAS.1103216108.

Machackova, Jarmila, Judit Barta, and Naranjan S Dhalla. 2006. “Myofibrillar Remodeling in Cardiac Hypertrophy, Heart Failure and Cardiomyopathies.” *The Canadian Journal of Cardiology* 22 (11): 953–68.

Malik, R., M Dysthe, M Ritt, RK Sunahara, and S Sivaramakrishnan. 2017. “ER/K Linked GPCR-G Protein Fusions Systematically Modulate Second Messenger Response in Cells.” *Scientific Reports* 7 (1). https://doi.org/10.1038/S41598-017-08029-3.

Malik, R., Michael Ritt, Brian T. DeVree, Richard R. Neubig, Roger K. Sunahara, and Sivaraj Sivaramakrishnan. 2013. “Detection of G Protein-Selective G Protein-Coupled Receptor (GPCR) Conformations in Live Cells.” *Journal of Biological*

Chemistry 288 (24): 17167–78. https://doi.org/10.1074/jbc.M113.464065.

Maneuf, Yannick P., and Jonathan M. Brotchie. 1997. “Paradoxical Action of the Cannabinoid WIN 55,212-2 in Stimulated and Basal Cyclic AMP Accumulation in Rat Globus Pallidus Slices.” *British Journal of Pharmacology* 120 (8): 1397–98. https://doi.org/10.1038/sj.bjp.0701101.

Manglik, Aashish, and Brian Kobilka. 2014. “The Role of Protein Dynamics in GPCR Function: Insights from the B2AR and Rhodopsin.” *Current Opinion in Cell Biology* 0 (1): 136. https://doi.org/10.1016/J.CEB.2014.01.008.

Mangmool, Supachoke, and Hitoshi Kurose. 2011. “Gi/o Protein-Dependent and -Independent Actions of Pertussis Toxin (Ptx).” *Toxins* 3 (7): 884–99. https://doi.org/10.3390/toxins3070884.

Maron, BJ, JM Gardin, JM Flack, SS Gidding, TT Kurosaki, and DE Bild. 1995. “Prevalence of Hypertrophic Cardiomyopathy in a General Population of Young Adults. Echocardiographic Analysis of 4111 Subjects in the CARDIA Study. Coronary Artery Risk Development in (Young) Adults.” *Circulation* 92 (4): 785–89. https://doi.org/10.1161/01.CIR.92.4.785.

Marsiglia, Júlia Daher Carneiro, and Alexandre Costa Pereira. 2014. “Hypertrophic Cardiomyopathy: How Do Mutations Lead to Disease?” *Arquivos Brasileiros de Cardiologia* 102 (3): 295–304. https://doi.org/10.5935/ABC.20140022.

McNamara, James W., Rohit R. Singh, and Sakthivel Sadayappan. 2019. “Cardiac Myosin Binding Protein-C Phosphorylation Regulates the Super-Relaxed State of Myosin.” *Proceedings of the National Academy of Sciences* 116 (24): 11731–36. https://doi.org/10.1073/PNAS.1821660116.

Moss, Richard L., Daniel P. Fitzsimons, and J. Carter Ralphe. 2015. “Cardiac MyBP-C Regulates the Rate and Force of Contraction in Mammalian Myocardium.” *Circulation Research* 116 (1): 183–92. https://doi.org/10.1161/CIRCRESAHA.116.300561.

Mun, Ji Young, Michael J. Previs, Hope Y. Yu, James Gulick, Larry S. Tobacman, Samantha Beck Previs, Jeffrey Robbins, David M. Warshaw, and Roger Craig. 2014. “Myosin-Binding Protein C Displaces Tropomyosin to Activate Cardiac Thin Filaments and Governs Their Speed by an Independent Mechanism.” *Proceedings of the National Academy of Sciences* 111 (6): 2170–75. https://doi.org/10.1073/PNAS.1316001111.

Nag, Suman, and Darshan V. Trivedi. 2021. “To Lie or Not to Lie: Super-Relaxing with Myosins.” *ELife* 10 (February): 1–21. https://doi.org/10.7554/ELIFE.63703.

Nag, Suman, Darshan V Trivedi, Saswata S Sarkar, Arjun S Adhikari, Margaret S Sunitha, Shirley Sutton, Kathleen M Ruppel, and James A Spudich. 2017. “The Myosin Mesa and the Basis of Hypercontractility Caused by Hypertrophic Cardiomyopathy Mutations.” *Nature Structural & Molecular Biology* 24 (6): 525–33. https://doi.org/10.1038/nsmb.3408.

Nag, Suman, Darshan V Trivedi, Saswata S Sarkar, Shirley Sutton, Kathleen M Ruppel, and James A Spudich. 2016. “Beyond the Myosin Mesa: A Potential Unifying Hypothesis on the Underlying Molecular Basis of Hyper-Contractility Caused by a Majority of Hypertrophic Cardiomyopathy Mutations.” *BioRxiv*, July, 065508. https://doi.org/10.1101/065508.

Neumann, J, W Schmitz, H Scholz, L von Meyerinck, V Döring, and P Kalmar. 1988. “Increase in Myocardial Gi-Proteins in Heart Failure.” *Lancet (London, England)* 2

(8617): 936–37. https://doi.org/10.1016/S0140-6736(88)92601-3.

Nygaard, Rie, Yaozhong Zou, Ron O. Dror, Thomas J. Mildorf, Daniel H. Arlow, Aashish Manglik, Albert C. Pan, et al. 2013. “The Dynamic Process of B2-Adrenergic Receptor Activation.” *Cell* 152 (3): 532–42. https://doi.org/10.1016/j.cell.2013.01.008.

Offer, Gebald, Cabl Moos, and Roger Starr. 1973. “A New Protein of the Thick Filaments of Vertebrate Skeletal Myofibrils: Extraction, Purification and Characterization.” *Journal of Molecular Biology* 74 (4): 653–76. https://doi.org/10.1016/0022-2836(73)90055-7.

Ojima, Koichi, Mika Oe, Ikuyo Nakajima, Masahiro Shibata, Susumu Muroya, Koichi Chikuni, Akihito Hattori, and Takanori Nishimura. 2015. “The Importance of Subfragment 2 and C-Terminus of Myosin Heavy Chain for Thick Filament Assembly in Skeletal Muscle Cells.” *Animal Science Journal* 86 (4): 459–67. https://doi.org/10.1111/asj.12310.

Okagaki, T, F E Weber, D A Fischman, K T Vaughan, T Mikawa, and F C Reinach. 1993. “The Major Myosin-Binding Domain of Skeletal Muscle MyBP-C (C Protein) Resides in the COOH-Terminal, Immunoglobulin C2 Motif.” *Journal of Cell Biology* 123 (3): 619–26. https://doi.org/10.1083/JCB.123.3.619.

Okashah, Najeah, Qingwen Wan, Soumadwip Ghosh, Manbir Sandhu, Asuka Inoue, Nagarajan Vaidehi, and Nevin A. Lambert. 2019. “Variable G Protein Determinants of GPCR Coupling Selectivity.” *Proceedings of the National Academy of Sciences of the United States of America* 116 (24): 12054–59. https://doi.org/10.1073/pnas.1905993116.

Oldham, William M., and Heidi E. Hamm. 2008. “Heterotrimeric G Protein Activation by

G-Protein-Coupled Receptors.” *Nature Reviews Molecular Cell Biology* 9 (1): 60–71. https://doi.org/10.1038/nrm2299.

Palczewski, K, T Kumasaka, T Hori, CA Behnke, H Motoshima, BA Fox, I Le Trong, et al. 2000. “Crystal Structure of Rhodopsin: A G Protein-Coupled Receptor.” *Science (New York, N.Y.)* 289 (5480): 739–45. https://doi.org/10.1126/SCIENCE.289.5480.739.

Palmiter, K a, M J Tyska, J R Haeberle, and N R Alpert. 2000. “R403Q and L908V Mutant β-Cardiac Myosin from Patients with Familial Hypertrophic Cardiomyopathy Exhibit Enhanced Mechanical Performance at the Single Molecule …” *Journal of Muscle Research and Cell Motility* 21: 609–20.

Pardee, JD, and JA Spudich. 1982. “Purification of Muscle Actin.” *Methods in Enzymology* 85 Pt B (C): 164–81. https://doi.org/10.1016/0076-6879(82)85020-9.

Perkins, JR, I Diboun, BH Dessailly, JG Lees, and C Orengo. 2010. “Transient Protein-Protein Interactions: Structural, Functional, and Network Properties.” *Structure (London, England : 1993)* 18 (10): 1233–43. https://doi.org/10.1016/J.STR.2010.08.007.

Pfuhl, Mark, and Mathias Gautel. 2012. “Structure, Interactions and Function of the N-Terminus of Cardiac Myosin Binding Protein C (MyBP-C): Who Does What, with What, and to Whom?” *Journal of Muscle Research and Cell Motility 2012 33:1* 33 (1): 83–94. https://doi.org/10.1007/S10974-012-9291-Z.

Pierce, Kristen L., Richard T. Premont, and Robert J. Lefkowitz. 2002. “Seven-Transmembrane Receptors.” *Nature Reviews Molecular Cell Biology 2002 3:9* 3 (9): 639–50. https://doi.org/10.1038/nrm908.

Ping, P, and HK Hammond. 1994. “Diverse G Protein and Beta-Adrenergic Receptor MRNA Expression in Normal and Failing Porcine Hearts.” *The American Journal of Physiology* 267 (5 Pt 2). https://doi.org/10.1152/AJPHEART.1994.267.5.H2079.

Previs, M.J., S.B. Previs, J. Gulick, J. Robbins, and D.M. Warshaw. 2012. “Molecular Mechanics of Cardiac Myosin Binding Protein-C in Native Thick Filaments.” *Science (New York, N.Y.)* 337 (6099): 1215. https://doi.org/10.1126/SCIENCE.1223602.

Previs, Michael J., Arthur J. Michalek, and David M. Warshaw. 2014. “Molecular Modulation of Actomyosin Function by Cardiac Myosin-Binding Protein C.” *Pflugers Archiv European Journal of Physiology*. https://doi.org/10.1007/s00424-013-1433-7.

Previs, Michael J., Ji Young Mun, Arthur J. Michalek, Samantha Beck Previs, James Gulick, Jeffrey Robbins, David M. Warshaw, and Roger Craig. 2016. “Phosphorylation and Calcium Antagonistically Tune Myosin-Binding Protein C’s Structure and Function.” *Proceedings of the National Academy of Sciences* 113 (12): 3239–44. https://doi.org/10.1073/PNAS.1522236113.

Previs, MJ, BL Prosser, JY Mun, SB Previs, J Gulick, K Lee, J Robbins, R Craig, WJ Lederer, and DM Warshaw. 2015. “Myosin-Binding Protein C Corrects an Intrinsic Inhomogeneity in Cardiac Excitation-Contraction Coupling.” *Science Advances* 1 (1). https://doi.org/10.1126/SCIADV.1400205.

Qin, Kou, Chunmin Dong, Guangyu Wu, and Nevin A. Lambert. 2011. “Inactive-State Preassembly of Gq-Coupled Receptors and Gq Heterotrimers.” *Nature Chemical Biology* 7 (10): 740. https://doi.org/10.1038/NCHEMBIO.642.

Rahmanseresht, Sheema, Kyoung H. Lee, Thomas S. O’Leary, James W. McNamara, Sakthivel Sadayappan, Jeffrey Robbins, David M. Warshaw, Roger Craig, and Michael J. Previs. 2021. “The N Terminus of Myosin-Binding Protein C Extends

toward Actin Filaments in Intact Cardiac Muscle." *Journal of General Physiology* 153 (3). https://doi.org/10.1085/JGP.202012726.

Rai, A, D Vang, M Ritt, and S Sivaramakrishnan. 2021. "Dynamic Multimerization of Dab2-Myosin VI Complexes Regulates Cargo Processivity While Minimizing Cortical Actin Reorganization." *The Journal of Biological Chemistry* 296 (January): 100232. https://doi.org/10.1074/JBC.RA120.012703.

Rasenick, Mark M., Masayuki Watanabe, Milenko B. Lazarevic, Shinichi Hatta, and Heidi E. Hamm. 1994. "Synthetic Peptides as Probes for G Protein Function: Carboxyl-Terminal Gαs Peptides Mimic Gs and Evoke High Affinity Agonist Binding to β-Adrenergic Receptors." *Journal of Biological Chemistry* 269 (34): 21519–25.

Rasmussen, Søren G. F., Brian T. DeVree, Yaozhong Zou, Andrew C. Kruse, Ka Young Chung, Tong Sun Kobilka, Foon Sun Thian, et al. 2011. "Crystal Structure of the B2 Adrenergic Receptor–Gs Protein Complex." *Nature 2011 477:7366* 477 (7366): 549–55. https://doi.org/10.1038/nature10361.

Ratti, Joyce, Elena Rostkova, Mathias Gautel, and Mark Pfuhl. 2011. "Structure and Interactions of Myosin-Binding Protein C Domain C0: Cardiac-Specific Regulation of Myosin at Its Neck?" *Journal of Biological Chemistry* 286 (14): 12650–58. https://doi.org/10.1074/JBC.M110.156646.

Razumova, MV, JF Shaffer, AY Tu, GV Flint, M Regnier, and SP Harris. 2006. "Effects of the N-Terminal Domains of Myosin Binding Protein-C in an in Vitro Motility Assay: Evidence for Long-Lived Cross-Bridges." *The Journal of Biological Chemistry* 281 (47): 35846–54. https://doi.org/10.1074/JBC.M606949200.

Risi, CM, M Patra, B Belknap, SP Harris, HD White, and VE Galkin. 2021. "Interaction of the C2 Ig-like Domain of Cardiac Myosin Binding Protein-C with F-Actin." *Journal of*

Molecular Biology 433 (19): 167178. https://doi.org/10.1016/J.JMB.2021.167178.

Saber, Walid, Kelly J. Begin, David M. Warshaw, and Peter VanBuren. 2008. “Cardiac Myosin Binding Protein-C Modulates Actomyosin Binding and Kinetics in the in Vitro Motility Assay.” *Journal of Molecular and Cellular Cardiology* 44 (6): 1053–61. https://doi.org/10.1016/J.YJMCC.2008.03.012.

Sandhu, Manbir, Anja M. Touma, Matthew Dysthe, Fredrik Sadler, Sivaraj Sivaramakrishnan, and Nagarajan Vaidehi. 2019. “Conformational Plasticity of the Intracellular Cavity of GPCR−G-Protein Complexes Leads to G-Protein Promiscuity and Selectivity.” *Proceedings of the National Academy of Sciences of the United States of America* 116 (24): 11956–65. https://doi.org/10.1073/pnas.1820944116.

Schlossarek, Saskia, Giulia Mearini, and Lucie Carrier. 2011. “Cardiac Myosin-Binding Protein C in Hypertrophic Cardiomyopathy: Mechanisms and Therapeutic Opportunities.” *Journal of Molecular and Cellular Cardiology*. https://doi.org/10.1016/j.yjmcc.2011.01.014.

Semack, Ansley, Manbir Sandhu, Rabia U. Malik, Nagarajan Vaidehi, and Sivaraj Sivaramakrishnan. 2016. “Structural Elements in the Gαs and Gβq C Termini That Mediate Selective G Protein-Coupled Receptor (GPCR) Signaling.” *Journal of Biological Chemistry* 291 (34): 17929–40. https://doi.org/10.1074/jbc.M116.735720.

Shaffer, Justin F., Robert W. Kensler, and Samantha P. Harris. 2009. “The Myosin-Binding Protein C Motif Binds to F-Actin in a Phosphorylation-Sensitive Manner.” *Journal of Biological Chemistry* 284 (18): 12318–27. https://doi.org/10.1074/JBC.M808850200.

Sivaramakrishnan, S, and JA Spudich. 2011. “Systematic Control of Protein Interaction Using a Modular ER/K α-Helix Linker.” *Proceedings of the National Academy of*

Sciences of the United States of America 108 (51): 20467–72. https://doi.org/10.1073/PNAS.1116066108.

Sommese, RF, RF Hariadi, K Kim, M Liu, MJ Tyska, and S Sivaramakrishnan. 2016. "Patterning Protein Complexes on DNA Nanostructures Using a GFP Nanobody." *Protein Science : A Publication of the Protein Society* 25 (11): 2089–94. https://doi.org/10.1002/PRO.3020.

Spudich, James A. 2015. "The Myosin Mesa and a Possible Unifying Hypothesis for the Molecular Basis of Human Hypertrophic Cardiomyopathy." *Biochemical Society Transactions* 43 (1): 64–72. https://doi.org/10.1042/BST20140324.

Starr, Roger, and Gerald Offer. 1971. "Polypeptide Chains of Intermediate Molecular Weight in Myosin Preparations." *FEBS Letters* 15 (1): 40–44. https://doi.org/10.1016/0014-5793(71)80075-3.

Sung, Jongmin, Suman Nag, Kim I. Mortensen, Christian L. Vestergaard, Shirley Sutton, Kathleen Ruppel, Henrik Flyvbjerg, and James A. Spudich. 2015. "Harmonic Force Spectroscopy Measures Load-Dependent Kinetics of Individual Human β-Cardiac Myosin Molecules." *Nature Communications 2015 6:1* 6 (1): 1–9. https://doi.org/10.1038/ncomms8931.

Swanson, Carter J., and Sivaraj Sivaramakrishnan. 2014. "Harnessing the Unique Structural Properties of Isolated α-Helices." *Journal of Biological Chemistry* 289 (37): 25460–67. https://doi.org/10.1074/jbc.R114.583906.

Swenson, Anja M., Wanjian Tang, Cheavar A. Blair, Christopher M. Fetrow, William C. Unrath, Michael J. Previs, Kenneth S. Campbell, and Christopher M. Yengo. 2017. "Omecamtiv Mecarbil Enhances the Duty Ratio of Human β-Cardiac Myosin Resulting in Increased Calcium Sensitivity and Slowed Force Development in

Cardiac Muscle." *Journal of Biological Chemistry* 292 (9): 3768–78. https://doi.org/10.1074/JBC.M116.748780.

Touma, Anja M., Rabia U. Malik, Tejas Gupte, and Sivaraj Sivaramakrishnan. 2020. "Allosteric Modulation of Adenosine A1 and Cannabinoid 1 Receptor Signaling by G-peptides." *Pharmacology Research & Perspectives* 8 (6). https://doi.org/10.1002/PRP2.673.

Tripathi, Snigdha, Imke Schultz, Edgar Becker, Judith Montag, Bianca Borchert, Antonio Francino, Francisco Navarro-Lopez, et al. 2011. "Unequal Allelic Expression of Wild-Type and Mutated β-Myosin in Familial Hypertrophic Cardiomyopathy." *Basic Research in Cardiology* 106 (6): 1041–55. https://doi.org/10.1007/s00395-011-0205-9.

Trivedi, Darshan V., Arjun S. Adhikari, Saswata S. Sarkar, Kathleen M. Ruppel, and James A. Spudich. 2018. "Hypertrophic Cardiomyopathy and the Myosin Mesa: Viewing an Old Disease in a New Light." *Biophysical Reviews*. https://doi.org/10.1007/s12551-017-0274-6.

Tyska, M. J., E. Hayes, M. Giewat, C. E. Seidman, J. G. Seidman, and D. M. Warshaw. 2000. "Single-Molecule Mechanics of R403Q Cardiac Myosin Isolated from the Mouse Model of Familial Hypertrophic Cardiomyopathy." *Circulation Research* 86 (7): 737–44. https://doi.org/10.1161/01.RES.86.7.737.

Uyeda, Taro Q.P., Stephen J. Kron, and James A. Spudich. 1990. "Myosin Step Size: Estimation from Slow Sliding Movement of Actin over Low Densities of Heavy Meromyosin." *Journal of Molecular Biology* 214 (3): 699–710. https://doi.org/10.1016/0022-2836(90)90287-V.

Vaynberg, Julia, Tomohiko Fukuda, Ka Chen, Olga Vinogradova, Algirdas Velyvis,

Yizeng Tu, Lily Ng, Chuanyue Wu, and Jun Qin. 2005. “Structure of an Ultraweak Protein-Protein Complex and Its Crucial Role in Regulation of Cell Morphology and Motility to the Limitations of Most of the Conventional Techniques, Such as Coimmunoprecipitation, Pull-down Assay, and X-Ray Crystallography, Which Become Ambiguous or in-Effective When Analyzing Weak Binary PPIs, Especially Those with K D 10 4 M. On the Other Hand, Because.” *Molecular Cell* 17: 513–23. https://doi.org/10.1016/j.molcel.2004.12.031.

Wakefield, Amanda E., Jonathan S. Mason, Sandor Vajda, and György M. Keserű. 2019. “Analysis of Tractable Allosteric Sites in G Protein-Coupled Receptors.” *Scientific Reports* 9 (1): 6180. https://doi.org/10.1038/s41598-019-42618-8.

Walcott, S, DM Warshaw, and EP Debold. 2012. “Mechanical Coupling between Myosin Molecules Causes Differences between Ensemble and Single-Molecule Measurements.” *Biophysical Journal* 103 (3): 501–10. https://doi.org/10.1016/J.BPJ.2012.06.031.

Walcott, Sam, Steffen Docken, and Samantha P. Harris. 2015. “Effects of Cardiac Myosin Binding Protein-C on Actin Motility Are Explained with a Drag-Activation-Competition Model.” *Biophysical Journal* 108 (1): 10–13. https://doi.org/10.1016/J.BPJ.2014.11.1852.

Waldhoer, Maria, Alan Wise, Graeme Milligan, Michael Freissmuth, and Christian Nanoff. 1999. “Kinetics of Ternary Complex Formation with Fusion Proteins Composed of the A1-Adenosine Receptor and G Protein α-Subunits.” *Journal of Biological Chemistry* 274 (43): 30571–79. https://doi.org/10.1074/jbc.274.43.30571.

Wang, Jialu, Clarice Gareri, and Howard A. Rockman. 2018. “G Protein-Coupled Receptors in Heart Disease.” *Circulation Research* 123 (6): 716.

https://doi.org/10.1161/CIRCRESAHA.118.311403.

Wang, Q, CL Moncman, and DA Winkelmann. 2003. “Mutations in the Motor Domain Modulate Myosin Activity and Myofibril Organization.” *Journal of Cell Science* 116 (Pt 20): 4227–38. https://doi.org/10.1242/JCS.00709.

Watkins, Hugh, David Conner, Ludwig Thierfelder, John A. Jarcho, Calum MacRae, William J. McKenna, Barry J. Maron, J.G. Seidman, and Christine E. Seidman. 1995. “Mutations in the Cardiac Myosin Binding Protein–C Gene on Chromosome 11 Cause Familial Hypertrophic Cardiomyopathy.” *Nature Genetics 1995 11:4* 11 (4): 434–37. https://doi.org/10.1038/ng1295-434.

Weith, Abbey E, Michael J Previs, Gregory J Hoeprich, Samantha Beck Previs, James Gulick, Jeffrey Robbins, and David M Warshaw. 2012. “The Extent of Cardiac Myosin Binding Protein-C Phosphorylation Modulates Actomyosin Function in a Graded Manner.” *Journal of Muscle Research and Cell Motility* 33 (6): 449–59. https://doi.org/10.1007/s10974-012-9312-y.

Weith, Abbey, Sakthivel Sadayappan, James Gulick, Michael J. Previs, Peter VanBuren, Jeffrey Robbins, and David M. Warshaw. 2012. “Unique Single Molecule Binding of Cardiac Myosin Binding Protein-C to Actin and Phosphorylation-Dependent Inhibition of Actomyosin Motility Requires 17 Amino Acids of the Motif Domain.” *Journal of Molecular and Cellular Cardiology* 52 (1): 219–27. https://doi.org/10.1016/J.YJMCC.2011.09.019.

Winkelmann, Donald A., Eva Forgacs, Matthew T. Miller, and Ann M. Stock. 2015. “Structural Basis for Drug-Induced Allosteric Changes to Human β-Cardiac Myosin Motor Activity.” *Nature Communications 2015 6:1* 6 (1): 1–10. https://doi.org/10.1038/ncomms8974.

Witjas-Paalberends, E. Rosalie, Claudia Ferrara, Beatrice Scellini, Nicoletta Piroddi, Judith Montag, Chiara Tesi, Ger J M Stienen, et al. 2014. “Faster Cross-Bridge Detachment and Increased Tension Cost in Human Hypertrophic Cardiomyopathy with the R403Q MYH7 Mutation.” *Journal of Physiology* 592 (15): 3257–72. https://doi.org/10.1113/jphysiol.2014.274571.

Yang, Chii Shen, Nikolai P. Skiba, Maria R. Mazzoni, and Heidi E. Hamm. 1999. “Conformational Changes at the Carboxyl Terminus of Gα Occur during G Protein Activation.” *Journal of Biological Chemistry* 274: 2379–85. https://doi.org/10.1074/jbc.274.4.2379.

Zadran, S, S Standley, K Wong, E Otiniano, A Amighi, and M Baudry. 2012. “Fluorescence Resonance Energy Transfer (FRET)-Based Biosensors: Visualizing Cellular Dynamics and Bioenergetics.” *Applied Microbiology and Biotechnology* 96 (4): 895–902. https://doi.org/10.1007/S00253-012-4449-6.